

Final Report to



ADVANCED HYDRAULIC FRACTURING TECHNOLOGY FOR
UNCONVENTIONAL TIGHT GAS RESERVOIRS
07122-33.Final

1st August 2012

Dr. Ding Zhu

Petroleum Engineering Department, Texas A&M University

979-458-4522

ding.zhu@pe.tamu.edu

LEGAL NOTICE


This report was prepared by Dr. Ding Zhu as an account of work sponsored by the Research Partnership to Secure Energy for America, RPSEA. Neither RPSEA members of RPSEA, the National Energy Technology Laboratory, the U.S. Department of Energy, nor any person acting on behalf of any of the entities:

- a. MAKES ANY WARRANTY OR REPRESENTATION, EXPRESS OR IMPLIED WITH RESPECT TO ACCURACY, COMPLETENESS, OR USEFULNESS OF THE INFORMATION CONTAINED IN THIS DOCUMENT, OR THAT THE USE OF ANY INFORMATION, APPARATUS, METHOD, OR PROCESS DISCLOSED IN THIS DOCUMENT MAY NOT INFRINGE PRIVATELY OWNED RIGHTS, OR
- b. ASSUMES ANY LIABILITY WITH RESPECT TO THE USE OF, OR FOR ANY AND ALL DAMAGES RESULTING FROM THE USE OF, ANY INFORMATION, APPARATUS, METHOD, OR PROCESS DISCLOSED IN THIS DOCUMENT.

THIS IS A FINAL REPORT. THE DATA, CALCULATIONS, INFORMATION, CONCLUSIONS, AND/OR RECOMMENDATIONS REPORTED HEREIN ARE THE PROPERTY OF THE U.S. DEPARTMENT OF ENERGY.

REFERENCE TO TRADE NAMES OR SPECIFIC COMMERCIAL PRODUCTS, COMMODITIES, OR SERVICES IN THIS REPORT DOES NOT REPRESENT OR CONSTITUTE AN ENDORSEMENT, RECOMMENDATION, OR FAVORING BY RPSEA OR ITS CONTRACTORS OF THE SPECIFIC COMMERCIAL PRODUCT, COMMODITY, OR SERVICE.

Principal Investigator: Dr. Ding Zhu

Signature: _____  _____

Date: 1st August 2012

Abstract

This report summarizes the investigation of gel damage in hydraulic fracturing and its effect on fracture conductivity. The findings of this project will help engineers to optimize hydraulic fracturing treatment design in tight gas.

To achieve this objective, several experimental and theoretical studies were carried out. Yield stress measurements were made with and without breaker and these measurements were related to the damage potential of fracturing fluids. Experiments to measure filter-cake thickness were carried out and correlations were obtained between filter-cake thickness and leak-off under both static and dynamic conditions. The analytical model developed for the displacement of gel/filter-cake in a laboratory fracture was validated with experimental work. A systematic experimental investigation was undertaken to consider in a holistic sense most of the factors that determine the final conductivity of a hydraulic fracture. These factors include reservoir properties, fracture fluid/proppant characteristics, and operational considerations (proppant schedule and flow-back rate). The effect of two-phase flow, proppant crushing, gel damage, yield stress and fracture length on long term gas productivity was investigated using a 3-D, 3-phase reservoir simulator. Also, the flow of Herschel Bulkley fluids through a proppant pack was studied. Results from this part of the study can be incorporated into commercial reservoir simulators. Lastly, a tight gas advisor was developed to improve hydraulic fracture design practices.

All the studies agree that the yield stress of the broken fracture fluid is a key indicator of the optimal productivity or otherwise of a hydraulic fracture. It was noted that when breaker is added to the fracture fluid, the yield stress decreases to a near-zero value, hereby aiding cleanup. In static experiments, filter-cake thickness has a direct relationship with the leak-off volume. In dynamic experiments, the shear rate impedes the growth of the filter-cake and there is a quadratic relationship between the filter-cake thickness and leak-off volume.

Dynamic fracture conductivity tests were used to test the impact of some factors on conductivity. Based on the log transformed dataset, the effects of investigated factors arranged in order of decreasing impact on conductivity are closure stress, polymer loading, flow back rate, presence of breaker, reservoir temperature and proppant concentration. Increases in closure stress, flow back rate, temperature and polymer loading were observed to have deleterious effects on fracture conductivity. In particular, at high closure stresses and high temperatures, fracture conductivity was severely reduced due to the formation of a dense proppant-polymer cake. Dehydration of the residual gel in the fracture appears to cause severe damage to the proppant conductivity at higher temperatures. Also, at low proppant concentrations, there is the increased likelihood of the formation of channels resulting in high fracture conductivities.

Simulation runs made to test the important factors that affect cleanup in tight gas reservoirs reached similar conclusions regarding the high importance of proppant crushing (effect of closure stress) and gel damage. It was also concluded that if the fracture fluid does not break completely and retains yield stress of 3-100Pa, then the fracture fluid will either cleanup slowly or will never cleanup when the dimensionless fracture conductivity is 10 or less.

Table of Contents

Table of Contents

Executive Summary

A. INTRODUCTION

- A.1 Statement and Significance of Problem
- A.2 Background and Existing Technologies/Methodologies
- A.3 Objectives

B. EXPERIMENTAL AND THEORETICAL METHODS

- B.1 Experimental Methods
 - B.1.1 Yield Stress Measurement
 - B.1.2 Filter-Cake Thickness and Cleanup Experiments
 - B.1.3 Dynamic Fracture Conductivity Experiments
 - B.1.4 Experimental Strategy and Design
- B.2 Theoretical Methods
 - B.2.1 Modeling Filter-cake Cleanup in Parallel Plates
 - B.2.2 Modeling Fracture Cleanup in Tight gas wells using a 3D, Three-Phase Simulator
 - B.2.3 Modeling flow of Herschel-Bulkley fluid in Proppant Pack

C. RESULTS AND DISCUSSION—EXPERIMENTAL METHODS

- C.1 Yield Stress Measurement
 - C.1.1 Polymer Yield Stress Test Results without Breaker
 - C.1.2 Polymer Yield Stress Test Results with Breaker
 - C.1.3 Flow Initiation Gradient (FIG) Estimated from Yield Stress
- C.2 Filter-cake thickness measurement/filter-cake cleanup
 - C.2.1 Relationship between Leak-off Volume and Filter-cake Thickness
 - C.2.2 Cleanup as a function of Flow Rate
- C.3 Dynamic Fracture Conductivity Tests
 - C.3.1 Initial Results Summary
 - C.3.2 Effects of Outliers
 - C.3.3 Tests of Effect Significance
 - C.3.4 Effect of Closure Stress
 - C.3.5 Effect of Temperature
 - C.3.6 Effect of Nitrogen (Flow-back) Rate
 - C.3.7 Effect of Polymer Loading

- C.3.8 Effect of Breaker
- C.3.9 Effect of Proppant Concentration
- C.3.10 Using Proppant Concentration as a Blocking Variable
- C.3.11 Interaction Effects
- C.3.12 Summary

D. RESULTS AND DISCUSSION—THEORETICAL METHODS

- D.1 Modeling Fracture Fluid Cleanup in Tight Gas Wells
 - D.1.1 Effect of Two-Phase Flow
 - D.1.2 Effect of Proppant Crushing
 - D.1.3 Effect of Polymer Filter Cake
 - D.1.4 Effect of Gel Damage
 - D.1.5 Effect of Yield Stress
 - D.1.6 Effect of Fracture length
- D.2 Modeling flow of Herschel-Bulkley Fluid in Proppant Pack
 - D.2.1 Description of Geometry of the Computational Domain
 - D.2.2 Choosing the Optimal Grid Size
 - D.2.3 Effect of Yield Stress on Pressure Gradient
 - D.2.4 Effect of Power-law Index
 - D.2.5 Effect of Proppant Diameter

E. TIGHT GAS ADVISOR FOR COMPLETION AND STIMULATION

- E.1 Background
- E.2 Approach
- E.3 Applications
- E.4 Program Installation Instructions

F. SUMMARY OF FINDINGS

G. IMPACT TO PRODUCERS

H. TECHNOLOGY TRANSFER EFFORTS

I. CONCLUSIONS / RECOMMENDATIONS

References

List of Figures

Figure		Page
1	Discrete gas inflows in naturally fractured reservoirs retard gel cleanup.	22
2	Diagram of slotted-plate setup.	23
3	Picture of slotted-plate instrument.	23
4	Laser Profilometer and thickness measurement.	26
5	Diagrammatic representation of the pumping process during dynamic placement of slurry during dynamic fracture conductivity measurement.	28
6	Diagrammatic representation of the pressure drop measurement process during dynamic fracture conductivity measurement.	29
7	Core Sample Preparation	30
8	Pressure Transducers	31
9	Analog Input Menu	32
10	Calibration Data Input Screen	33
11	T-140 Pressure Calibrator	33
12	Final Assembly of the Conductivity Cell	35
13	Forcheimer's Conductivity Data Fit Example	40
14	Flowchart describing the experimental workflow.	42
15	Result from hypothetical factorial experiment (no interaction), '-1' represents low setting of factor X and '+1' represents high setting of factor X.	44
16	Result from hypothetical factorial experiment (interaction between X and Y), '-1' represents low setting of factor X and '+1' represents high setting of factor X.	44
17	The force balance on the fluid element in slot flow.	46
18	Flow patterns identified under imposed pressure gradients.	48
19	a) Geometry for proppant package (b) Geometry of flow channel	49
20	Yield stress with different polymer concentrations.	53
21	Yield stress with different breaker concentrations.	55
22	Relationship between guar concentration and the breaker concentration needed to obtain zero yield stress.	55

Figure		Page
23	FIG with different breaker concentrations.	56
24	Profilometer-scanned filter-cake at 0.025-in. resolution.	57
25	Micrometer- and profilometer-thickness comparison.	57
26	Correlation of leakoff volume vs. filter-cake thickness.	59
27	Thickness profiles and correlations at different shear rates.	61
28	Thickness profiles at static conditions and at different shear rates.	61
29	Cleanup test result for experiment 1 before cleanup (a). After cleanup (b).	62
30	Cleanup test result for experiment 2 at 25 ml/s (a). At 40 ml/s (b). At 50 ml/s (c). At 62 ml/s (d).	63
31	Core surfaces after erosion (cleanup) test.	64
32	Proppant distribution on the core surfaces for three replications of the same treatment, proppant distributed uniformly on the surface of the core (a). Proppant distributed with less uniformity on the surface of the core (b). Proppant not uniformly distributed on the surface of the core (c).	67
33	Effects of investigated factors using mean and median estimates.	68
34	Factorial effects based on log transformed data.	71
35	Factorial effects based on rank transformed data	71
36	Half-Normal plot of the factorial effects using raw data.	73
37	Normal plots for raw, logarithm and rank transformed conductivity data.	77
38	Dependence of fracture conductivity on closure stress.	78
39	Dehydrated polymer-proppant cake.	79
40	Dependence of fracture conductivity on temperature.	79
41	Boiling point of water vs. pressure.	80
42	Equilibrium water content of methane gas vs. pressure.	81
43	Dependence of fracture conductivity on nitrogen flow rate.	82
44	Representation of fracture with potential mechanisms that can affect	82

Figure		Page
	cleanup.	
45	Dependence of fracture conductivity on polymer loading.	84
46	Dependence of fracture conductivity on the presence or absence of breaker.	85
47	Dependence of fracture conductivity on proppant concentration using raw conductivity data	85
48	No channels, high closure stress and temperature, conductivity ~ 60 md-ft, 2ppa (a). No channels, high closure stress and temperature, conductivity ~ 10 md-ft, 0.5 ppg (b). Void spaces present, high closure stress and temperature, conductivity ~ 2500 md-ft, 0.5 ppg (c).	86
49	Dependence of fracture conductivity on proppant concentration using log transformed data.	86
50	Effect of investigated factors at high proppant concentration.	88
51	Effect of investigated factors at low proppant concentration.	89
52	Interaction effect between polymer loading and closure stress	90
53	Gas-production rate at different fracture conductivity, where $L_f = 528$ ft, $p_r = 3,720$ psi, $k = 0.1$ md, $S_{wi} = 0.4$, and $h = 25$ ft.	94
54	Cumulative gas production at different fracture conductivity, where $L_f = 528$ ft, $p_r = 3,720$ psi, $k = 0.1$ md, $S_{wi} = 0.4$, and $h = 25$ ft.	95
55	Gas-production rate at different fracture conductivity, where $L_f = 528$ ft, $p_r = 1,860$ psi, $k = 0.1$ md, $S_{wi} = 0.4$, and $h = 25$ ft.	95
56	Gas-production rate at different fracture conductivity, where $L_f = 528$ ft, $p_r = 3,720$ psi, $k = 0.1$ md, $S_{wi} = 0.4$, and $h = 25$ ft-effect of proppant crushing.	97
57	Cumulative gas production at different fracture conductivity, where $L_f = 528$ ft, $p_r = 3,720$ psi, $k = 0.1$ md, $S_{wi} = 0.4$, and $h = 25$ ft-effect of proppant crushing.	97
58	Gas-production rate for different cases for $C_r = 1$, where $L_f = 528$ ft, $p_r = 3,720$ psi, $k = 0.1$ md, $S_{wi} = 0.4$, and $h = 25$ ft-effect of polymer filter cake.	99
59	Gas-production rate at different fracture conductivity, where $L_f = 528$ ft, $p_r = 3,720$ psi, $k = 0.1$ md, $S_{wi} = 0.4$, and $h = 25$ ft-effect of polymer filter cake.	99

Figure		Page
60	Cumulative gas production for different fracture conductivities, where $L_f = 528$ ft, $p_r = 3,720$ psi, $k = 0.1$ md, $S_{wi} = 0.4$, and $h = 25$ ft-effect of polymer filter cake.	100
61	Cumulative gas production for different cases for $C_r = 1$, where $L_f = 528$ ft, $p_r = 3,720$ psi, $k = 0.1$ md, $S_{wi} = 0.4$, and $h = 25$ ft-effect of gel damage.	101
62	Cumulative gas production for different cases for $C_r = 1$, where $L_f = 528$ ft, $p_r = 3,720$ psi, $k = 0.1$ md, $S_{wi} = 0.4$, and $h = 100$ ft-effect of varying yield stress.	102
63	Percentage of fracture that cleans up 1 year after a fracture treatment vs. different yield stress at different L_f , where $p_r = 3,720$ psi, $k = 0.1$ md, $C_r = 10$, $S_{wi} = 0.4$, and $h = 25$ ft.	103
64	Percentage of fracture that cleans up 1 year after a fracture treatment vs. yield stress at different reservoir pressures, where $L_f = 528$ ft, $k = 0.1$ md, $C_r = 0.1$, $S_{wi} = 0.4$, and $h = 25$ ft.	103
65	Percentage of fracture that cleans up 1 year after a fracture treatment vs. yield stress at different reservoir pressures, where $L_f = 528$ ft, $k = 0.1$ md, $C_r = 10$, $S_{wi} = 0.4$, and $h = 25$ ft.	104
66	Representation of gridding on proppant surfaces using different grid sizes, grid size = 0.03mm (a). Grid size = 0.025mm (b). Grid size = 0.02mm (c). Grid size = 0.015mm (d).	106
67	Pressure gradient vs. superficial velocity for Bingham fluids.	107
68	Flow initiation gradient vs. yield stress for Bingham fluids.	107
69	Dimensionless velocity profiles for different yield stress fluids.	108
70	Pressure gradient vs. superficial velocity for power-law fluids at high velocities.	109
71	Pressure gradient vs. superficial velocity for power-law fluids at low velocities.	109
72	Dimensionless velocity profiles for power-law indices.	110
73	Permeability vs. Mesh Size.	111
74	Flow initiation pressure gradient vs. yield stress for varying proppant mesh sizes.	111
75	Major decision points in the completion and stimulation of tight gas	114

Figure		Page
	sands. Every independent level requires making a critical decision that affects all levels below it.	
76	Starting window for the UGR advisory system. Red arrow points to the TGS application.	115

List of Tables

Table		Page
1	Fracturing-fluid recipe in filter-cake measurements	26
2	Typical composition of fracturing fluid	28
3	Conductivity parameters	41
4	Factor levels in experimental space	42
5	Reservoir and fracture parameters for parametric simulation study	49
6	Herschel-Bulkley fluid and proppant parameters for parametric simulation study	51
7	Experimental results without breaker	52
8	Experimental design with breaker	54
9	Experimental results with breaker	54
10	Filter-cake-thickness measurement results	59
11	Cleanup test data	62
12	Factor levels in experimental space	65
13	Design table with orthogonal columns	65
14	Planning table (presence or otherwise of breaker is a qualitative variable)	66
15	Screening experiment results with number of replications in each experiment	67
16	Main and interaction effects	68
17	Raw, log and rank transformed data	69
18	Main and interaction effects based on logarithmic and rank transformed data	70
19	Test statistic for ordered effects (raw data)	73
20	Factorial effects at varying levels of significance (raw data)	74
21	Test statistic for ordered effects (log transformed data)	75
22	Factorial effects at varying levels of significance (log transformed data)	75

Table		Page
23	Test statistic for ordered effects (rank transformed data)	75
24	Factorial effects at varying levels of significance (rank transformed data)	76
25	Comparison of results for analysis on raw and transformed data	76
26	Variation of laboratory fracture width with closure stress	78
27	Variation of proppant mass in conductivity cell	86
28	Results for experiments run at low proppant concentration	87
29	Results for experiments run at high proppant concentration	88
30	Criteria for ignoring interaction effects	90
31	Maximum grid edge size and total number of grids	106

Executive Summary

The objective of this project was to develop modern technologies to understand the fundamentals and to optimize design of fracturing process in tight gas formations. Specific tasks include developing new methods for creating extensive, conductive hydraulic fractures in unconventional tight gas reservoirs by developing a practical guideline for fracturing in tight gas formations based on statistical assessment of the productivity achieved in hundreds of field treatments with a variety of current fracturing practices ranging from “water fracs” to conventional gel fracture treatments; by laboratory measurements of the conductivity created with high rate proppant fracturing using an entirely new conductivity test – the “dynamic fracture conductivity test”; and by developing design models to implement the optimal fracture treatments determined from the field assessment and the laboratory measurements. The accomplishments from this project are grouped under the following subjects:

1. The advisory system for tight gas well fracturing
2. Yield stress and filter-cake investigations
3. Dynamic fracture conductivity investigations
4. Modeling of fracture fluid clean up in tight gas reservoirs
5. Modeling flow of Herschel-Bulkley fluids in proppant packs

Advisory system for tight gas sand fracturing

We conducted a thorough literature review to extract knowledge and experience about completion and stimulation technologies used in Tight Gas Sand (TGS) reservoirs. We developed the principal design and several modules of a computer program called Tight Gas Sand Advisor (TGS Advisor), which can be used to assist engineers in making decisions while stimulating TGS reservoirs. The modules include perforation selection and proppant selection. Based on input well/reservoir parameters these subroutines provide unambiguous recommendations concerning which perforation strategy(s) and what proppant(s) are applicable for a given well. Also, the advisory system can be used for fracturing fluid selection, slurry pumping schedule recommendation, estimates of the optimal fracture half-length and prediction of optimal casing and production tubing sizes. The most crucial parameters from completion best-practices analyses and consultations with experts are built into TGS Advisor’s logic, which mimics human expert’s decision-making process.

Yield stress and filter-cake investigations

In this part of work, we experimentally evaluated two important aspects of the gel damage process—the thickness of the polymer-gel filter cake that is created as fracture-fluid filtrate leaks off into the formation, and the yield stress of the concentrated polymer gel that accumulates in the fracture. The thickness of the filter cake created during the leakoff process was measured as a function of the polymer loading and the volume of leakoff. We created the filter cake following the procedure described by Ayoub et al. (2006) and then measured the filter-cake thickness with a precise laser profilometer. We found that the filter-cake thickness varied linearly with leakoff volume, meaning that the gel concentration factor is constant for this guar polymer fluid. The concentrated polymer filter cakes created by leakoff behave rheologically as Herschel-Bulkley fluids having a

yield stress. The yield stress of this material is a critical parameter influencing whether the gel can be removed from the fracture. We measured the yield stress of borate-crosslinked guar polymer fracture fluids at concentrations up to 200 lbm/1,000 gals by use of a unique flat-plate device. The yield stresses of the polymer filter cakes were found to depend strongly on the concentration of both polymer and breaker.

The experimental results provided the base for the modeling work in this project. From the finding of the experimental study, we developed a model to describe the flow behavior of residual polymer gel being displaced by gas in parallel plates. We developed analytical models for gas-liquid two-phase stratified flow of Newtonian gas and non-Newtonian residual gel in order to investigate gel cleanup under different conditions. The concentrated gel in the filter cake was modeled as a Herschel-Buckley fluid, a shear-thinning fluid following a power law relationship, but also having a yield stress. The model developed shows that three flow regimes may exist in a slot, depending on the gas flow rate and the filter cake yield stress. The parameters for the gel displacement model were evaluated by experiments. We examined the filter cake formation by pumping the fracture fluid through a conductivity cell, allowing leakoff to build the filter cake, measuring the cake thickness, and flowing gas through the cell to simulate the cleanup process. The results show that the yield stress of the residual gel plays a critical role in gel cleanup.

Dynamic fracture conductivity investigations

In this part of the study, we undertook a systematic investigation of the interactive effects of the key parameters that affect the final conductivity of a propped fracture, including flow back rate, proppant loading, polymer loading in the fracture fluid, the presence or absence of breaker, closure stress, and reservoir temperature. We used a fractional factorial design methodology to determine the relative importance of the fracturing parameters varied. The fractional factorial design method examines the combined effects on conductivity of potentially interacting parameters, while minimizing the number of experimental runs required. The effects of the investigated factors arranged in order of decreasing impact on conductivity are closure stress, temperature, flow back rate, polymer loading, proppant concentration and presence of breaker. Increases in closure stress, flow back rate, temperature and polymer loading were observed to have deleterious effects on fracture conductivity. In particular, at high closure stresses and high temperatures, fracture conductivity was severely reduced due to the formation of a dense proppant-polymer cake. Dehydration of the residual gel in the fracture appears to cause severe damage to the proppant conductivity at higher temperatures. Also, at low proppant concentrations, there is the increased likelihood of the formation of channels resulting in high fracture conductivities.

Modeling of fracture fluid clean up in tight gas reservoirs

We developed a comprehensive data set for typical tight gas reservoirs and then ran single-phase-flow cases for each reservoir and fracture scenario to establish the idealized base-case gas recovery. We then systematically evaluated the following factors: multiphase gas and water flow, proppant crushing, polymer filter cake, and, finally, yield stress of concentrated gel in the fracture. The gel in the fracture is concentrated because of fluid leakoff during the fracture treatment. We evaluated these factors additively in the

order listed. We found that the most important factor that reduces fracture-fluid cleanup and gas recovery is the gel strength of the fluid that remains in the fracture at the end of the treatment.

Modeling flow of Herschel-Bulkley fluids in proppant packs

We developed a mathematical model, and then corrected the model based on numerical simulation results. In the simulations, we developed a micro pore-scale model to mimic the real porous structure in a proppant pack. The relationship between pressure gradient and superficial velocity was investigated under the influence of primary parameters such as yield stress, power-law index, consistency index, and the proppant diameter. The Herschel-Bulkley model was used with an appropriate modification proposed by Papanastasiou (1987) to mitigate numerical difficulties.

A. Introduction

A.1 Statement and Significance of the Problem

Unconventional gas reservoirs have two distinct features that drive the optimal use of hydraulic fracturing – very low matrix permeability, which demands additional extensive flow paths to produce; and the presence of natural fractures, which may fundamentally alter the fracturing process. The key to producing gas from tight gas reservoirs is to create a long, highly conductive hydraulic fracture to stimulate flow from the reservoir to the wellbore. To maintain conductivity in the fracture, it is important to pump sufficient quantities of propping agent into the fracture. In fracturing treatments, high concentration proppants are carried deep into the fracture by viscous fluids. However, these same viscous fluids need to break back to a thin fluid after the treatment is over so that the fracture fluid can be cleaned up.

Tight gas reservoirs are found at all depths. In deep, high temperature (above 270°F) reservoirs, we have to pump high concentrations of high strength proppant to keep the fracture open. The polymers used to create viscosity will break down and the fluid will clean up after the treatment at high temperature. Thus, the use of ‘gel fracs’ has proved to be optimum in deep, high temperature reservoirs.

In shallower, lower temperature (less than 250°F) reservoirs, the choice of fracture fluids is very critical to the success of the treatment. We still need viscosity to carry proppant deeply into the fracture. However, unless the proper breakers are used, the viscous fracture fluids will not break correctly and the ‘gel’ causes significant damage in the fracture. “Water frac” becomes an option. Driven as much by economics (cost-savings) as by technical benefits, operators have increasingly used so-called “water fracs” instead of more conventional gel fracs over the last fifteen years in many unconventional reservoirs. A “water frac” is a fracturing treatment using low concentrations of polymer in the fracturing fluid, less than 20 lb_m/1000 gallons, and low proppant concentrations, less than an average of 0.5 lb_m/gal. The smaller amounts of proppant and polymer used in these treatments reduce the costs considerably; however, they also result in much less proppant being placed in the created fractures. Yet, there is substantial evidence that the productivity of unconventional gas wells increases proportionately to the amount of

proppant placed, even with water fracs, such as are being applied in the Barnett shale (Coulter et al., 2004). There is also strong evidence in many tight gas provinces where conventional hydraulic fracture treatments are widely applied that the well productivity created increases proportionately to the amount of proppant placed (Coulter et al., 2004; Holditch and Ely, 1973).

In summary, current hydraulic fracturing methods in unconventional tight gas reservoirs have been developed largely through ad-hoc application of low-cost water fracs, with little optimization of the process. It seems clear that some of the standard tests and models are missing the basic physics of the fracturing process in low-permeability, naturally fractured porous media. This work is aimed at developing modern technologies to understand the fundamentals and to optimize design of fracturing process in tight gas formations.

A.2 Background and Existing Technologies/Methodologies

Research on gel damage control in tight gas formation fracturing has been carried out over last 15 years, and one practical solution to the problem is water frac. From the very early applications of water fracs, the explanation of the success of these treatments relative to conventional gel fractures has had two parts (Mayerhofer et al., 1997). The first explanation is that sufficient conductivity can be created in a fracture in a tight gas reservoir without the amount of proppant pack in the fracture that would be presumed based on the usual laboratory measurements of fracture conductivity. Speculation about the created conductivity with very low proppant amounts includes displacement of the fracture walls, so that the rough walls of the fracture do not match up when the fracture closes, to non-uniform “partial monolayer propping”, which could presumably maintain adequate overall conductivity in the fracture. There is also considerable speculation about the development of multiple fractures and the opening of natural fractures to explain the performance of water fracs (Grieser et al., 2003; Coulter et al., 2004).

The second explanation offered for the success of water fracs relative to gel fracs is that the gel fracs have such high residual damage from unbroken gel in the fracture that the residual conductivity is no better than that which can be created with a water frac with considerably less proppant. Even some of the strongest proponents of water fracs

(Mayerhofer et al., 1997; Walker et al. 1998) attributed the relative success of water fracs to the failure of gel fracs because of residual damage to the proppant packs.

Gel damage is a complex problem combining proppant pack damage inside fracture, filter cake deposition at the fracture walls, and fracture fluid invasion in the near-fracture formation. To understand the mechanism of gel damage, lab experiments have focused on identifying the critical factors that result in low productivity after treatment, such as chemicals, treatment conditions and flow back rates. So far, most lab studies are conducted on a standard static conductivity cell, which pack the proppant at a defined concentration before pumping the fracture fluid. This conventional conductivity experimental procedure does not simulate the dynamic flow phenomena that may play an important role in gel damage.

We adopted a three-part approach to develop a fresh understanding of the hydraulic fracturing process as applied in these types of unconventional gas reservoirs. We expected this new understanding to lead to improved designs of hydraulic fracturing treatments, with changes possible in the proppant loading and schedule, proppant type and size, and fluid type and polymer loading. First, we conducted a thorough data-driven study of current field practices in hydraulic fracturing of tight gas reservoirs. Second, we applied a newly developed fracture conductivity testing procedure to more closely simulate the process occurring in high-rate, low proppant concentration fracturing. This testing methodology includes pumping slurry (actual fracture fluid with proppant as used in the field) through a modified conductivity cell. Finally, we implemented the findings of the field treatment analysis and the laboratory studies in fractured well models to design optimized hydraulic fracture treatments.

A.3 Objectives

The objectives of this project were to develop new methods for creating extensive, conductive hydraulic fractures in unconventional tight gas reservoirs by statistically assessing the productivity achieved in hundreds of field treatments with a variety of current fracturing practices ranging from “water fracs” to conventional gel fracture treatments; by laboratory measurements of the conductivity created with high rate proppant fracturing using an entirely new conductivity test – the “dynamic fracture

conductivity test”; and by developing design models to implement the optimal fracture treatments determined from the field assessment and the laboratory measurements. By applying a fresh approach to determining the manner in which proppant is placed and fracture conductivity created in low-permeability gas well fracturing, we aimed to develop novel systematic treatment design procedures to develop the next generation of hydraulic fracturing technology for these reservoirs.

We proposed three main subjects to achieve our objectives of the project; developing an advisory based on extensive literature study of the industry practice to date, conducting extensive experiments to investigate gel damage problems and implementing the findings of the field treatment analysis and the laboratory studies in fractured well models to design optimized hydraulic fracture treatments.

In the first part of the research, we used production data from thousands of wells to evaluate the effect of the volume of proppant and the type of fluid used in the long term behavior of tight gas wells where water fracs have been compared to gel fracs. We worked with industry to gain access to well records to learn more about the formation properties, especially formation permeability and formation temperature, and to obtain details on the type of fracture fluids used and the volume of the fluid and proppant for specific treatments.

We thereafter used publicly available production data and software developed in previous work to analyze the production data in order to determine the effect of the fracture treatment size and type of fluid on the performance of the tight gas well. We used this information and our laboratory results to determine optimum design parameters for a variety of reservoirs where water fracs are currently used by operators.

The second part of the project consists of intensive laboratory evaluation of the mechanisms of proppant interaction with the fracture faces and the creation of fracture conductivity in water fracs using the dynamic fracture conductivity testing procedure. In these experiments, fracture fluid with proppant was injected into a fracture conductivity cell at injection rates representative of conditions in an actual fracture. Leakoff conditions were set to mimic actual field rates. After flowing the frac fluid slurry a short time (about 1 minute), the cell was shut in, then gas flowed through the cell to represent the flowback period. Finally, fracture conductivity was measured, with the residual proppant trapped in

the fracture after the simulated treatment in place. Test conditions were varied to determine the effects of injection rate, fluid rheology, proppant loading and size, and gel loading on resulting fracture conductivity.

A special focus was on gel damage of the proppant pack, with some of the tests using conventional gel frac conditions to assess the damage occurring with higher polymer concentrations. In all conductivity measurements, we measured non-Darcy flow effects in addition to the conventional low-rate conductivity. The detrimental effects of gel damage are proportionately greater to effective conductivity under non-Darcy flow conditions than with Darcy flow, so the use of gas in our conductivity measurements provided a more realistic assessment of the effects of gel damage than is normally obtained. There is also evidence that before unbroken gel in a fracture can flow, a yield stress must be exceeded. Because the stress on the gel created by gas flow diminishes with gas flow rate, at some point along a fracture, the gas flow will not be sufficient to initiate movement of the gel. Consequently, from this point in the fracture to the fracture tip, gel cleanup is incomplete, leaving an effective fracture length that can be much shorter than the created length (**Figure 1**).

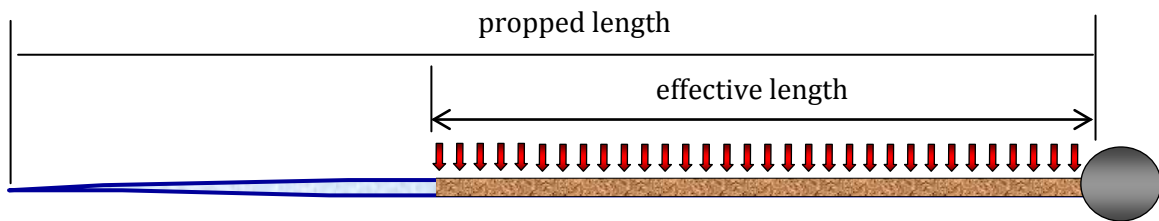


Figure 1—Discrete gas inflows in naturally fractured reservoirs retard gel cleanup.

B. Experimental and Theoretical Methods

B.1 Experimental Methods

There are three main parts in experimental study in this project; yield stress characterization, filter cake investigation and dynamic conductivity measurements.

B.1.1 Yield Stress Measurement

Detailed treatment of the experimental setup required to measure the yield stress of polymer fluids (slotted-plate method) can be found in the work by Xu et al. (2011). A simple device was built for this measurement. **Figure 2** is a schematic diagram of the slotted plate illustrating how the device works, and **Figure 3** is a picture of the actual device. A typical experimental procedure starts with heating the fluid if breaker is used. The gel was mixed at room temperature and then placed in a water bath having a temperature of 200°F and left at this temperature for 2 hours.

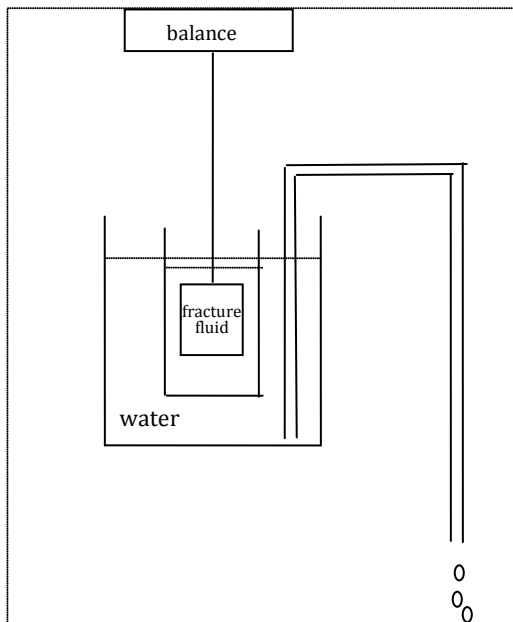


Figure 2—Diagram of slotted-plate setup.



Figure 3—Picture of slotted-plate instrument.

Although the sample was in an open beaker, the humidity in the water bath minimized evaporation from the gel. The plate is coated with the fracturing fluid first, then vertically inserted into the small beaker filled with fracturing fluid for approximately

10 hours for stabilization. The small beaker is placed carefully in the big beaker, which is filled with water. The water can be drained through a tube. The water-draining rate is regulated to approximately 1 drop/second steadily for 1 hour and the force is recorded by the balance. The total volume of water drained is also measured and the displacement of the small beaker is calculated using Equations 1 through 4 shown below.

During the test, water flows from the large glass beaker through a pipe, causing the small glass beaker to move down. A force will act on the balance through a metal wire. As the water flows out, the volume of the water and the force on the wire are recorded. The end point of this procedure is to calculate the yield stress. The yield stress can be calculation as follows:

$$S_1 = \frac{V}{\pi R^2} \quad (1)$$

$$S_2 = \frac{F}{\rho g \pi r^2} \quad (2)$$

$$S_3 = S_2 - \frac{S_2 \pi (R^2 - r^2)}{\pi R^2} = \frac{S_2 r^2}{R^2} = \frac{r^2 F}{R^2 \rho g \pi r^2} = \frac{F}{\rho g \pi R^2} \quad (3)$$

$$S = S_1 - S_2 + S_3 = \frac{V}{\pi R^2} - \frac{F}{\rho g \pi r^2} + \frac{F}{\rho g \pi R^2} = \frac{V}{\pi R^2} - \frac{F}{\rho g \pi} \left(\frac{1}{r^2} - \frac{1}{R^2} \right) \quad (4)$$

$$\tau_o = \frac{F_o}{2LH} \quad (5)$$

where V is volume of water that flowed out from the big beaker, F is the force on the metal wire, S_1 is the displacement of the small beaker moving downward because of water flowing out, S_2 is the displacement of the small beaker moving upward because of the force F through the wire, S_3 is the displacement of the water surface moving downward, R and r are the radii of the big beaker and the small beaker respectively, S is the actual displacement of the small beaker moving downward, L and H are the length and height of the plate, F_0 is the force at the yield point, and τ_o is yield stress. During a test, we measure the displacement of the beaker, the volume of the water flowing out, and the force on the wire. The yield point is identified by a change in slope of the force versus displacement plots. We thereafter calculated the yield stress using Equation 5.

Experimental Procedures. We tested a crosslinked guar polymer solution with and without breakers at temperatures ranging from 150 to 250°F. A typical experimental

procedure starts with heating the fluid if breaker is used. The fluid is maintained at this temperature for 2 hours. The plate is coated with the fracturing fluid first, then vertically inserted into the small beaker filled with fracturing fluid for about 10 hours for stabilization. The small beaker is carefully placed in the bigger beaker which is filled with water. The water can be drained through a tube. We regulated the water draining rate to about 1drip/sec steadily for one hour, and then measured the water draining rate, and the force recorded by a balance. The total volume of the water drained is also measured, and the displacement of the small beaker is calculated by equations 2-4. The displacement is linearly related to the force before the fluid yields.

B.1.2 Filter-Cake Thickness and Cleanup Experiments

We need to know the polymer concentration in the filter cake created by leakoff in order to apply the yield stress results. To determine the concentration of polymer in the fracture fluid filter cakes, we created filter cakes in a fracture conductivity cell and then carefully measured the thickness of the filter cake created.

Measurement Procedure. The conductivity cell was used to build a filter cake, and then the filter cake thickness was measured using a laser profilometer. The filter cake was created using the static procedures described by Ayoub et al. (2006a). A modified API fracture conductivity cell was set up with the core sample on one side separated by about one inch from a steel plate on the other side of the cell. The space between the core sample and the plate was filled with fracture fluid gel, and then stress was applied in a load frame to initiate leakoff through the core.

The filter cake thickness was measured using a laser profilometer. This was done by first scanning the surface of the filter cake, and then scanning the surface of the core after remove the filter cake. The difference between the two surfaces is the filter cake thickness. We also used micrometer measurements of the filter cake thickness to confirm the profilometer results. **Table 1** shows the typical fluid recipe used in the filter cake experiments. **Figure 4** shows the laser profilometer used in the thickness measurement procedure.

TABLE 1—FRACTURING-FLUID RECIPE IN FILTER-CAKE MEASUREMENTS	
Chemical	Concentration
Guar (lb/mgal)	40
pH Buffer 1	Variable
pH Buffer 2	Variable
Breaker (gal/mgal)	10
Breaker activator (gal/mgal)	1.0
Borate crosslinker (gal/mgal)	0.9
Crosslink accelerator (gal/mgal)	0.2

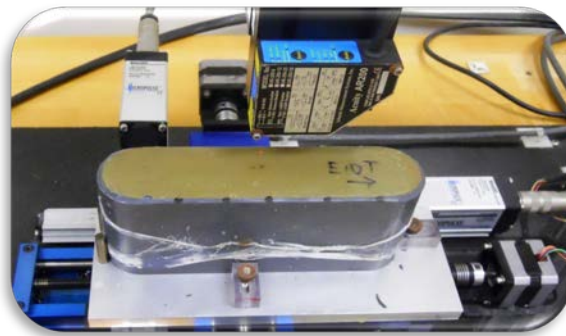


Figure 4—Laser Profilometer and thickness measurement.

B.1.3 Dynamic Fracture Conductivity Experiments

The objective of performing a dynamic conductivity test is to be able to mimic actual field conditions in a fracturing job by pumping the slurry fluid instead of loading the proppant manually in the fracture (static testing). The experimental dynamic conductivity setup is divided into three different units; the pad/slurry pumping unit to simulate fracturing, the gas flow-back unit to simulate flow-back and production, and the proppant pack conductivity measurement unit.

A detailed breakdown of the polymer fluid components is shown in **Table 2**. The schematic for the fracturing fluid pumping unit is shown in **Figure 5**. To start each experiment, two pieces of core samples are assembled in the conductivity cell with a fracture width of 6.5mm. A heating jacket is used to heat the conductivity cell for two hours before pumping to ensure that the desired temperature for the experimental condition is reached. Approximately 12 gallons of pad are prepared for each experiment; the pad is mixed in 4 gallon batches to ensure proper mixing. The mixer contains the

fluid with proppant (slurry) and the plastic drum contains the base gel (pad). The two jet pumps are used to displace the base gel and slurry mixture from the tanks to the line where the inlet of the multistage centrifugal pump is located. The base fluid is pumped first to recreate the effect of the pad injection into the formation. Meanwhile, 4 gallons of slurry fluid is mixed in the bucket with the paddle mixer by adding the desired amount of proppant (based on proppant loading) and cross-linker. After the base gel is pumped through the conductivity cell, the slurry was then pumped. Both fluids are pumped through the conductivity cell for 1-2 minutes with a pumping back-pressure of 200 psi. After pumping, the inlet and outlet of the conductivity cell are closed; trapping the slurry within the conductivity cell. A desired closure stress is then applied through the load frame. Finally, the system is flushed with base fluid and water to prevent blockage of the pump by the cross-linked propped slurry.

When the pumping procedure is concluded, the gel is allowed to break for approximately 12 hours and then the next procedure of conductivity measurement is initiated. The schematic for the pressure drop conductivity measurement is shown in **Figure 6**. Nitrogen flow is initiated through the water chamber before reaching the conductivity cell to wet the gas before it reaches the propped fracture. The fracture conductivity cell consists of two side pistons that ensure that the cores inside the cell stay in place while stress is applied, and three pressure ports where the pressure transducers are connected. The middle transducer measures absolute pressure inside the conductivity cell and the other two transducers measure the pressure drop across the conductivity cell. Finally, these pressures are measured by the GCTS C.A.T.S data acquisition system at regular time intervals through the pressure transducers. Fracture conductivity is calculated with either Forchheimer's equation or Darcy's law. The equation used depends on whether the Non-Darcy flow effect is significant or not.

TABLE 2—TYPICAL COMPOSITION OF FRACTURING FLUID

<u>Constituent</u>	<u>Loading</u>
Polymer	10—30 pounds per thousand gallons of fracture fluid
Buffer 1- reduce pH to allow for proper hydration	Variable
Buffer 2 – raise pH to allow for proper cross-linking	Variable
High temperature buffer	Variable
Gel stabilizer	1.5—3 gallons per thousand gallons of fracture fluid
Breaker	5—10 gallons per thousand gallons of fracture fluid
Breaker activator	0—1 gallons per thousand gallons of fracture fluid
Cross-linker	0.9—1.2 gallons per thousand gallons of fracture fluid
Cross-linker accelerator	0.1—0.4 gallons per thousand gallons of fracture fluid

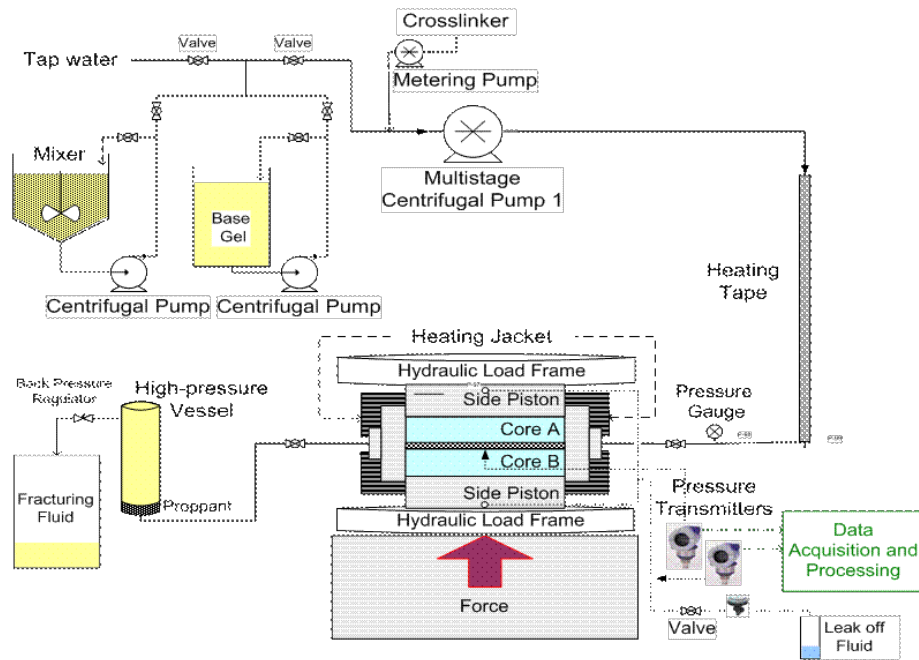


Figure 5—Diagrammatic representation of the pumping process during dynamic placement of slurry during dynamic fracture conductivity measurement.

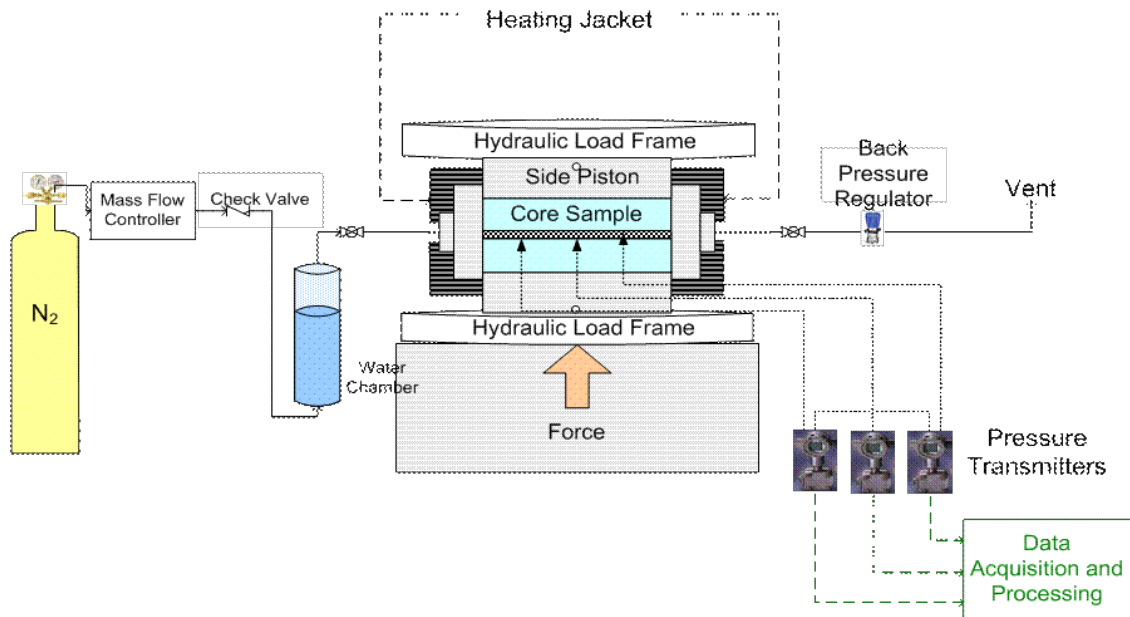


Figure 6—Diagrammatic representation of the pressure drop measurement process during dynamic fracture conductivity measurement.

Experimental Procedures

Fracture conductivities representing field conditions in tight gas reservoirs were determined via a series of experiments using the dynamic conductivity test. This experimental procedure is divided into a series of steps:

- Core sample preparation
- Pressure transducers calibration
- Fracturing conductivity cell setup
- Pad and slurry fluid preparation
- Fracturing fluid pumping
- Closure stress shut-in
- Proppant pack conductivity measurement

Core Sample Preparation

The core samples used for these experiments are the low permeability Ohio Scioto Sandstone with dimensions of 7-in. in length, 1.7-in. in width, and 3-in. in height. The purpose of the core sample preparation is to cover the sides of the cores with a silicon

mixture to provide a perfect seal between the rock sample and the conductivity cell. It is very important to create a perfect seal inside the conductivity cell to avoid any type of leakage that might lead to an erroneous reading of the pressure drop in the propped fracture. **Figure 7** shows a comparison of the rock samples before and after the preparation procedure.

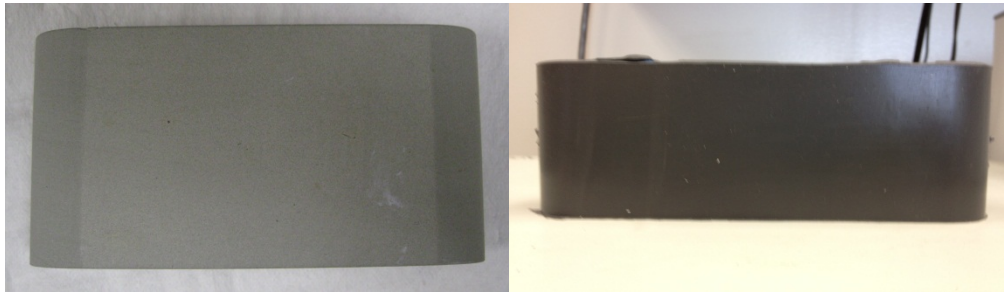


Figure 7—Core Sample Preparation

Core Sample Preparation Procedure:

- Place tape on the top and the bottom surfaces of the core sample, edges should be removed with a razor cutter.
- Use a brush to apply 3 layers of silicon primer (SS415501P), allowing 15-minute time intervals between layers.
- Clean the metal molds and the bottom plastic piece with acetone and a cloth.
- Spray 3 layers of Sprayon S000315 (silicon mold release) on the molds, allowing 5-minute time intervals between layers.
- Assemble the mold with 3 bolts on the side and 4 on the bottom. Make sure all the bolts are properly tightened to avoid silicon leakage.
- Place the core sample in the mold, making sure that is properly centered.
- Weight 60 grams of silicone potting compound and 60 grams of silicon curing agent. Mix and stir thoroughly.
- Pour the silicon mixture into the void space between the mold and the core sample until it reaches the surface of the core sample.
- Let the mold dry at room temperature for 3 hours.
- Place the mold in the oven at 200°F for 3 hours.

- Take the mold out of the oven and wait for the temperature to decrease to room temperature.
- Unscrew all the bolts from the mold and disassemble it to remove the core sample.
- Cut off the extra silicon on the edges with a razor cutter.
- Label the core sample

Pressure Transducer Calibration

Pressure measurements inside the conductivity cell are crucial in calculating the final conductivity of the propped fracture. The pressure transducers used for these experiments, shown in **Figure 8**, need to be calibrated and tested before each experiment. A T-140 Pressure Calibrator and the GCTS C.A.T.S software are used to calibrate the transducers.

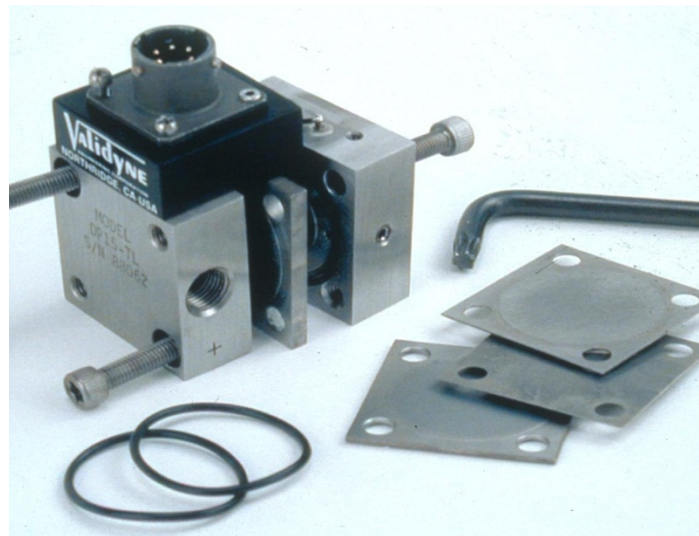


Figure 8—Pressure Transducers

Pressure Transducer Calibration Procedure:

- Start the GCTS C.A.T.S software.
- In the upper panel, proceed to System/Inputs/Analog.
- **Figure 9** shows the Analog Input Menu. Select the desired transducer to calibrate (Absolute/Differential).
- After selecting the transducer to calibrate. Click on Edit and the Editing Analog Input AI-4 screen will appear. Select Calibrate option (**Figure 10**).

- Select 2 point calibration from the Calibration Type selection menu.
- Connect the pressure transducer to the T-140 Pressure Calibrator (**Figure 11**).
- Set the pressure manometer to 0 psi pressure by selecting the vacuum mode.
- Set the “First Calibration” point to 0 psi and click “Next”.
- Switch the pressure calibrator to pressure mode and apply the desired calibration pressure for the transducer.
- Set the Second Calibration Point equal to the pressure in the calibrator and click Next.
- Repeat First and Second Calibration point if necessary for accuracy.
- Click Close and then OK. Make sure that the pressure values from the calibrator are equal to the measured values in the C.A.T.S software.

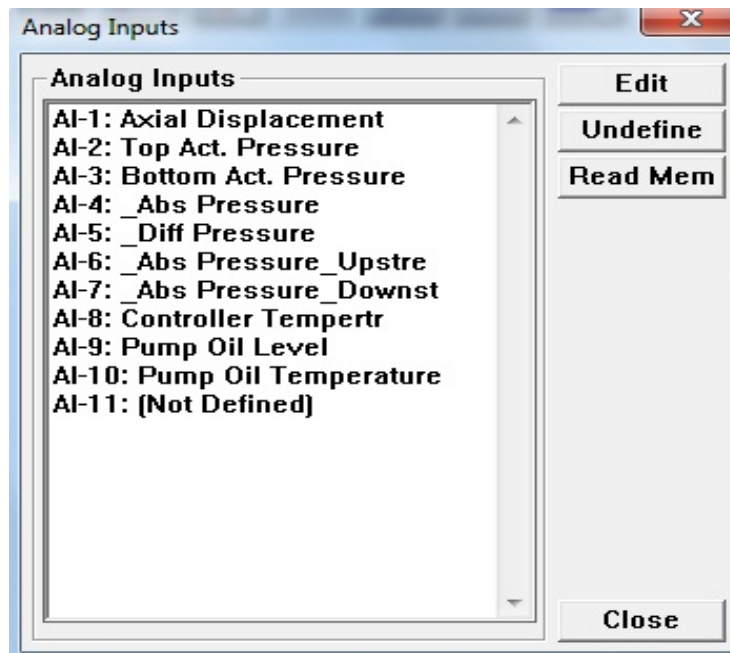


Figure 9—Analog Input Menu

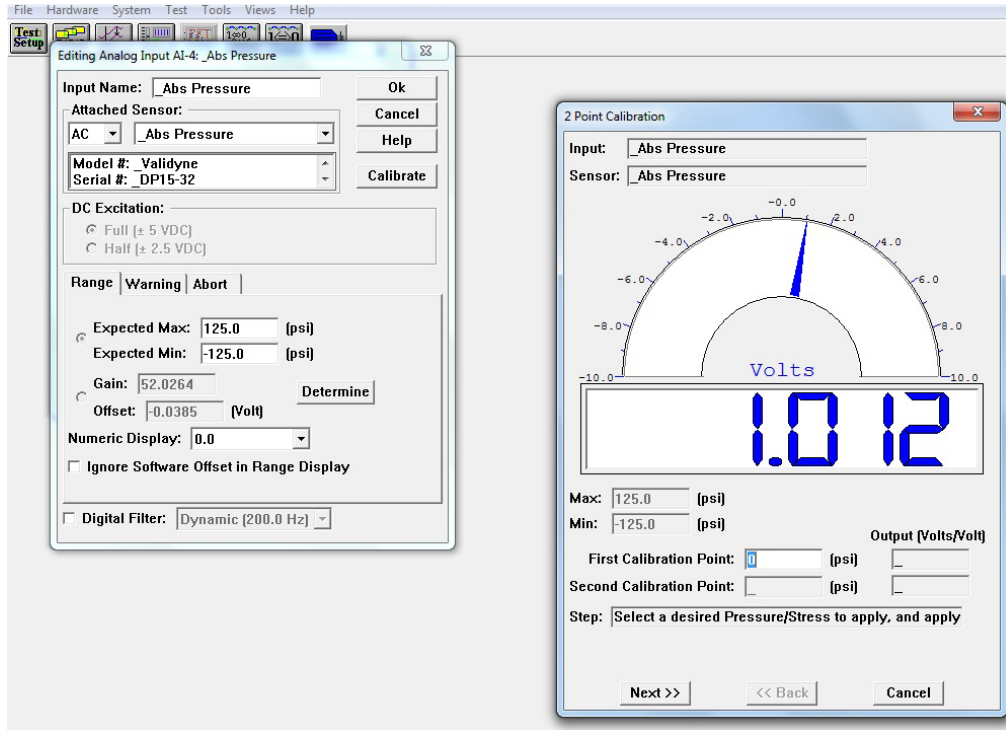


Figure 10—Calibration Data Input Screen

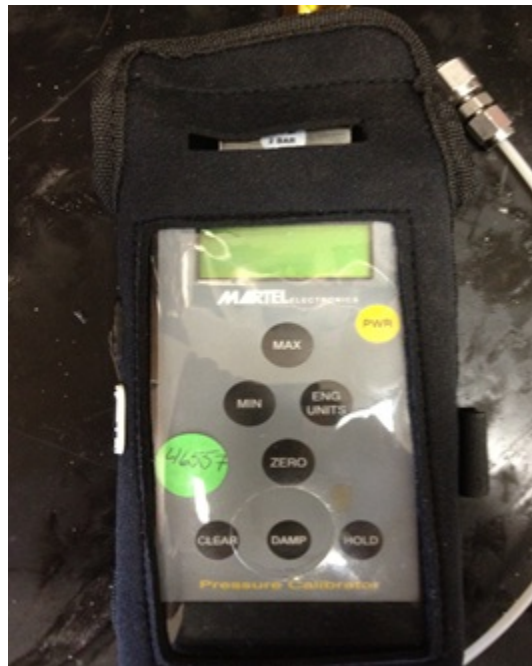


Figure 11—T-140 Pressure Calibrator

Fracture Conductivity Cell Setup

To start each experiment, two pieces of core sample are assembled in the conductivity cell with a preset fracture width of 6.5 mm. The following procedure shows how to assemble the conductivity cell with a fracture width of 6.5 mm.

Fracture Conductivity Cell Setup Procedure:

- Select a pair of cores prepared following the Core Sample Preparation guideline.
- Wrap each core with Teflon tape to prevent leakage inside the conductivity cell.
- Apply vacuum grease to each layer placed around the core sample.
- Make sure that the conductivity cell is properly cleaned before starting the loading process.
- Insert the bottom core sample into the bottom opening of the fracture conductivity cell with help of hydraulic press.
- Insert the bottom piston with the support pushing the bottom core sample until it reaches the end of the pressure reading ports. This will ensure that the fracture is placed in the middle of the conductivity cell.
- Plug the lower leak off port of the piston with a cap.
- Insert the top core sample into the top opening of the fracture conductivity cell with help of hydraulic press.
- Push the top core sample until there is enough room to place the top piston.
- Using the C.A.T.S software, activate the output function tool and select the Axial Displacement option.
- Displace the load frame upwards to a distance of -45 mm.
- Place the conductivity cell in the center of the load frame.
- Insert the top piston into the top of the conductivity cell.
- Once the conductivity cell is placed in the middle of the load frame with the top piston in place, start displacing the frame downwards to a distance of -21 mm. This will ensure that the fracture created has a width of 6.5 mm inside the conductivity cell.
- Plug the top leak off port of the piston with a cap.

- Assemble the inlet and outlet ports of the conductivity cell making sure they match with the number/letter of the conductivity cell. Make sure the bolts are tight enough to avoid leakage.
- Connect the outlet and the inlet pipelines to the ports of the conductivity cell making sure all the connections are tight to avoid leakage.
- Connect the absolute and differential pressure transducers to the conductivity cell.
- Wrap the heating jacket around the conductivity cell and connect it to the temperature controller.
- Turn on the temperature controller and select the desired temperature for the experiment.
- Wait for 2 hours for the conductivity cell to heat up and reach the desired temperature.
- The conductivity cell is now ready for the experiment. **Figure 12** shows the final assembly of the conductivity cell.



Figure 12—Final Assembly of the Conductivity Cell

Pad and Slurry Fluid Preparation

The fracturing fluid used in these experiments is a water-based guar containing polymer, gel stabilizer (necessary for experiments at high temperatures), breaker, buffers, and cross-linker. The recipe used for the mixing of the fracturing fluid resembles the characteristics of those used in field treatments. Approximately 12 gallons of the pad fluid are prepared for each experiment; the pad is mixed in 4 gallon batches to ensure proper mixing.

Pad preparation procedure:

- Use a 5 gallon bucket and a paddle mixer (Caframo ZRZ50).
- Fill the bucket with 4 gallons of water at room temperature.
- Add the buffering agent (BA-20) to decrease the Ph of the water to 6.5, to ensure proper hydration.
- Add desired loading of Guar gelling agent to the mixture.
- Transfer the 4 gallons of base gel to the mixer drum.
- Repeat previous steps until 12 gallons are mixed in the mixing tank.
- Mix thoroughly in the mixing tank for 30 minutes.
- Transfer the 12 gallons of pad from the mixing tank to the plastic drum.

Slurry preparation procedure for low-temperature experiments:

- Use a 5 gallon bucket and a paddle mixer (Caframo ZRZ50).
- Fill the bucket with 4 gallons of high temperature water.
- Add the buffering agent (BA-20) to decrease the Ph of the water to 6.5 to ensure proper hydration.
- Add desired loading of Guar gelling agent to the fluid and mix for 30 minutes.
- Add the buffering agent (BA-40) to increase the Ph of the fluid to 10.
- Add 138.90 ml of ViCon NF, 13.81 ml of CAT-OS1 for breaker and breaker activator.
- Measure the desired proppant weight based on concentration and add it to the mixture.
- Add 12.43 ml of CL-28M (Cross-linker) to the propped mixture.
- After the propped fluid is fully cross-linked, transfer the slurry to the mixing tank.

Slurry preparation procedure for high-temperature experiments:

- Use a 5 gallon bucket and a paddle mixer (Caframo ZRZ50).
- Fill the bucket with 4 gallons of high temperature water.

- Add the buffering agent (BA-20) to decrease the Ph of the water to 6.5 to ensure proper hydration.
- Add desired loading of Guar gelling agent to the fluid and mix for 30 minutes.
- Add the buffering agent (BA-40) to increase the Ph of the fluid to 10.
- Add MO-67 to increase the Ph of the fluid from 10 to 11.5
- Add 41.43 ml of Gelsta-L to stabilize the gel at high temperatures.
- Add 69.05 ml of ViCon NF for breaker.
- Measure the desired proppant weight based on concentration and add it to the mixture.
- Add 16.57 ml of CL-28M (Cross-linker) to the propped mixture.
- After the propped fluid is fully cross-linked, transfer the slurry to the mixing tank.

Fracturing Fluid Pumping

The fracturing fluid pumping unit consists of 2 different jet pumps and a high-pressure centrifugal pump. The main function of the 2 jet pumps is to displace the slurry and the pad to the line connected to the centrifugal pump. After the pad and the slurry are properly mixed, both fluids are pumped with a back-pressure of 200 psi for proper proppant transport and to replicate actual pumping conditions occurring in the field.

Fracturing fluid pumping procedure:

- The 12 gallons of pad and the 4 gallons of slurry need to be stored in the plastic drum and in the mixing tank before starting the pumping procedure.
- The first step is to pump the pad volume from the plastic drum to the conductivity cell, maintaining a pumping pressure of 200 psi by operating the back-pressure valve.
- Leave the remaining 5 gallons of pad to flush the pipelines, clean the system, and extend the operating life of the pump.
- Make the necessary changes by switching the valves to start pumping the slurry volume from the mixing tank to the conductivity cell.
- After pumping the total slurry volume, close the outlet and the inlet valves of the conductivity cell respectively to trap the slurry inside.

- Make the necessary valve changes and start pumping the remaining 5 gallons of pad volume to clean the pipes.
- Fill up the mixing tank with tap water.
- Pump the full tank volume of water to make sure the pipelines and the centrifugal pump are completely clean.

Closure Stress Application Procedure

An 850 kN load frame is used to apply a desired closure stress to the conductivity cell. After finishing the pumping procedure, closure stress is applied to the conductivity cell for a period of time, using the GCTS C.A.T.S software to operate the frame.

Closure stress application procedure:

- Start the GCTS C.A.T.S software.
- In the top menu, go to File/Projects.
- Create a new project schedule.
- Create a new sample for the experiment.
- Click on “new specimen” and input the design parameters for the experiment.
- Select the desired program from the Universal Test Setup Screen (high or low closure stress). Click on New to create a new program if the pressure/rate needs to be changed.
- Click Run to start applying closure stress to the conductivity cell. The GCTS C.A.T.S software saves data automatically.

Propped Pack Conductivity Measurement

After closure stress is applied to the cell, the slurry inside the cell is allowed to break for approximately 12 hours. The next step is to start nitrogen flow at a desired constant flow rate for a time period of at least 6 hours. Finally, pressure and flow rate are measured at regular intervals to calculate fracture conductivity using either Forcheimer’s equation or Darcy’s law. The equation used was selected whether the Non-Darcy flow effect is significant or not.

Proppant pack conductivity measurement procedure:

- Open the inlet of the conductivity cell.
- Turn on the mass flow controller and start flowing nitrogen into the conductivity cell until a cell pressure of 50 psi is reached.
- Make sure to check the pressure lines and conductivity cell for leakage. If leakage is found repair the leak and continue with the procedure.
- Open the valves of the pressure transducers and the outlet of the conductivity cell, while keeping the back-pressure valve closed so the pressure is maintained inside the cell.
- Wait for the system to stabilize for 5 minutes and record the baseline absolute and differential pressure.
- Start varying the nitrogen flow rate from 1 slm to 9 slm to get 9 sets of data, keeping the pressure inside the cell around 50 psi. For each data set, record absolute and differential pressure.
- For every measurement, wait 2 minutes for each flow rate to stabilize before recording the absolute and differential pressure inside the cell.
- To vary the flow rate, operate either the nitrogen flow regulator or the back pressure valve.
- Shut down the nitrogen flow and release the pressure in the system very carefully.
- Disconnect all the lines from the conductivity cell.
- Disassemble the conductivity cell and remove the core samples from the cell with the help of a hydraulic jack.
- Collect and measure the weight of the amount of proppant in the fracture.
- Calculate fracture conductivity by using either Forcheimer's equation (Eq. 6) or Darcy's equation (Eq. 7).

$$\frac{(p_1^2 - p_2^2)Mh}{2ZRTL\mu\rho q} = \frac{1}{k_f w} + \frac{\beta\rho q}{w^2\mu h} \quad (6)$$

$$\frac{(p_1^2 - p_2^2)M}{2ZRTL} = \frac{\rho q \mu}{h} \frac{1}{wk} \quad (7)$$

To calculate the conductivity of the fracture from the experimental data, Eq. 6 and Eq. 7, shown above, were set up as straight line equations of the form $y = mx + c$, where $\frac{\rho q}{\mu h}$ or $\frac{\rho q \mu}{h}$ is the x-axis, and $\frac{(p_1^2 - p_2^2) M h}{2 Z R T L \mu \rho q}$ or $\frac{(p_1^2 - p_2^2) M}{2 Z R T L}$ is the y-axis for Forcheimer's equation and Darcy's law respectively. The y intercept of the straight line represents the inverse of fracture conductivity. The final conductivity used as a result for the experiment depends whether Non-Darcy flow effects are significant or not. **Figure 13** shows an example of a good data fit for an accurate measurement of fracture conductivity.

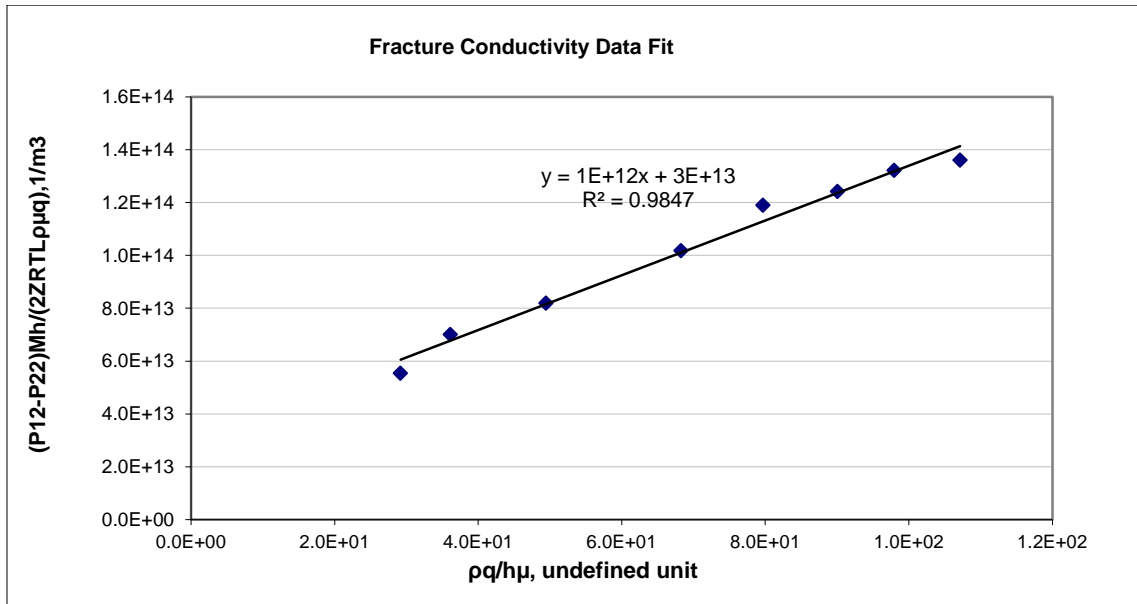


Figure 13—Forcheimer's Conductivity Data Fit Example

The parameters used in the conductivity calculation in this study are listed in **Table 3**.

TABLE 3— CONDUCTIVITY PARAMETERS		
Parameter	Value	Units
Length, L	5.25	In
Compressibility Factor, Z	1	
Universal Constant, R	8.3144	J/mol K
Temperature, T	293.15	K
RMM of Nitrogen, M	0.028	Kg / kg mole
Viscosity of Nitrogen, μ	1.795E-05	Pa.s
Density of Nitrogen, ρ	1.16085	Kg/m ³
Height of fracture face, h	1.61	In

B.1.4 Experimental Strategy and Design

There are at least 6 parameters that are identified as important factors that will affect the conductivity behavior in tight sand fracturing. The objective of the first set of experiments was to determine the ‘vital fewer’ factors out of the 6 factors that were investigated. The most efficient way to attain this objective is by using fractional factorial designs to construct the table of experimental conditions. The objective for the subsequent set of experiments would then be to clarify interesting observations or to further investigate counter-intuitive conclusions reached during the first (screening) phase of this study. The general approach to the planning and implementation of experiments is as shown in **Figure 14**. It is a summary of the workflow suggested by Wu and Hamada (2000) in a flow chart format. The six factors that we investigated are as shown in **Table 4**.

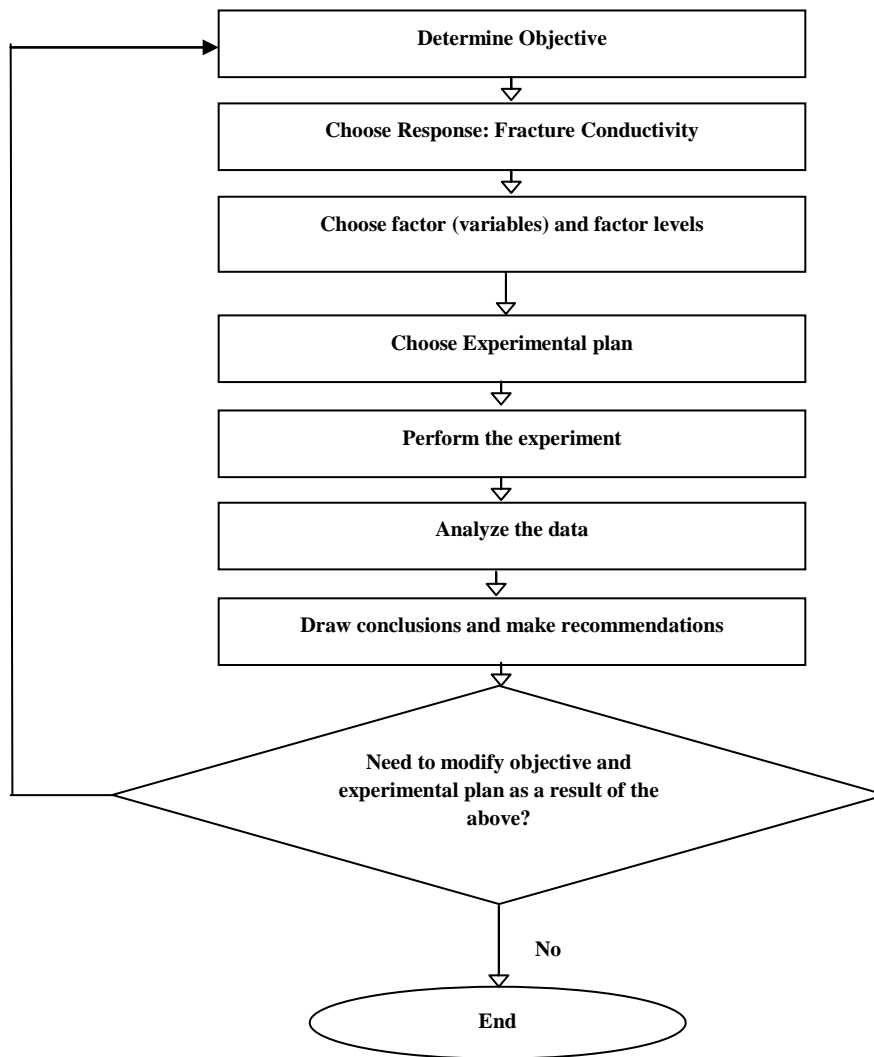


Figure 14—Flowchart describing the experimental workflow

TABLE 4—FACTOR LEVELS IN EXPERIMENTAL SPACE		
Factor	Factor Setting	
	Low Setting	High Setting
Temperature, degF	150	250
Flow back rate, standard liter per minute	1*	3**
Presence of breaker	none	Standard loading
Closure Stress, psi	2000	6000
Polymer concentration, pounds per thousand gallons	10	30
Proppant concentration, ppg	0.5	2

* Equivalent to field rates of about 0.35 MMscf/D assuming height of fracture is 100 ft. and width is 0.073 in.

** Equivalent to field rates of about 2 MMscf/D assuming height of fracture is 100 ft. and width is 0.073 in.

At this juncture, it is necessary to discuss some terms and concepts that are essential to understanding the experimental approach. A **factorial experiment** is one in which all possible combinations of the levels of the factors are investigated. The most common design is the 2^k design where each factor is tested at 2 levels and k is the number of factors to be tested. A **fractional factorial** experiment is one in which a carefully selected subset of all the possible combinations of the levels of the factors are investigated. It can also be referred to as a 2^{k-p} experiment, where k is as defined for the full factorial experiment and p is an integer less than k. For example, in a 2^{k-p} experiment, we make at least $(1/2^p)*2^k$ experimental runs. The main reason for using fractional factorial experiments is that we can obtain information about the main and lower-order interaction effects with reduced experimental load.

Main effect. Consider that we have made some experimental runs and we want to determine the main effect of a variable (factor), say temperature, tested at two levels: the low setting (ex. 150°F) and high setting(ex. 250°F), as shown in Table 4. The main effect is determined by computing the difference between the average response (fracture conductivity) of all runs of the experiment at the high level of the factor and the average response of all runs of the experiment at the low level of the factor. For example, the main effect of a factor, say temperature (T), ME (T), is calculated as the following, where \bar{z} represents the average of the observations at a given factor setting:

$$ME(T) = \bar{z}(T+) - \bar{z}(T-) \quad (8)$$

Interaction effect. When the difference in response between the levels of one factor is not similar at all levels of the other factors, these factors are said to interact. This is important because in some scenarios, a significant interaction can mask the significance of the main effect. It is important to note that the use of factorial experiments is the effective way to determine if two factors interact. **Figures 15 and 16** plot the levels of a hypothetical factor X for both levels of factor Y. In Figure 15, it is seen that the Y_{low} and Y_{high} values are parallel lines. This is a qualitative indication that X and Y do not interact. In Figure 16, the Y lines are not parallel, indicating that X and Y interact. To estimate the interaction effect quantitatively, we use the following illustration. Consider two factors; say temperature (T) and closure stress (σ_c). The interaction effect between T

and σ_c , $INT(T, \sigma_c)$ is computed as follows, where $\bar{z}(\sigma_c + | T +)$ means the average of all observations at the high level of closure stress given that the temperature is at the high level:

$$INT(T, \sigma_c) = \frac{1}{2} \left\{ \bar{z}(\sigma_c + | T +) - \bar{z}(\sigma_c - | T +) \right\} - \frac{1}{2} \left\{ \bar{z}(\sigma_c + | T -) - \bar{z}(\sigma_c - | T -) \right\} \quad (9)$$

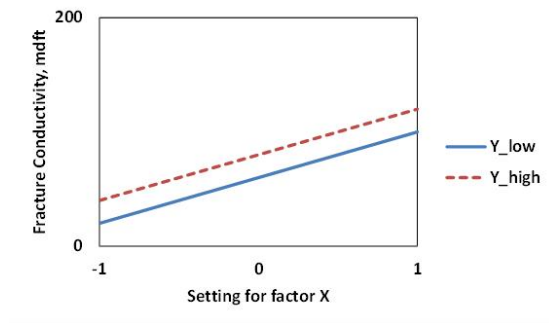


Figure 15—Result from hypothetical factorial experiment (no interaction), ‘-1’ represents low setting of factor X and ‘+1’ represents high setting of factor X.

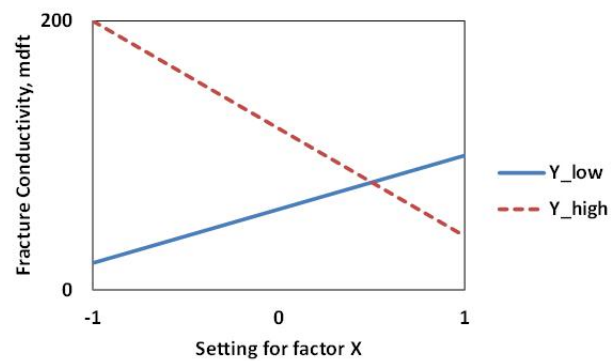


Figure 16—Result from hypothetical factorial experiment (interaction between X and Y), ‘-1’ represents low setting of factor X and ‘+1’ represents high setting of factor X.

The concept of experimental design was used in this study to eliminate the number of experiments and quickly reach the conclusions of which parameters deserve more attention. This approach also allows us to study the interactive effect of combined parameters. The experimental design ensured successes of this project.

B.2 Theoretical Methods

B.2.1 Modeling Filter-cake Clean-up between Parallel Plates

Theoretical modeling of filter cake cleanup is an important step to fully understand gel damage problem. We consider the following scenario as the physical model. The two surfaces of the fracture are represented by two parallel plates. There is a filter cake deposition on the surfaces of the plates and the original gel occupies the center of the slot. Compared to the filter cake, the original gel has a much lower initial yield stress and viscosity. If the pressure drop along the fracture is below a certain value, the original gel will be cleaned up and the filter cake will be left relatively untouched on the surface of the plate. Hence, only gas flows between the plates. In this situation, there is two-phase stratified flow of Newtonian gas and non-Newtonian filter cake. Otherwise, if the pressure drop exceeds a critical value, the filter cake will start to move.

The schematic of the force balance on a small fluid element in slot flow is shown in **Figure 17**. The equation for force balance in the z-direction on a small fluid element located at the distance, r , from the center can be written as:

$$p \cdot 2r = (p + \Delta p)2r + 2\tau L \quad (10)$$

The shear stress distribution can be written as:

$$\tau = \frac{-\Delta p}{L} r \quad (11)$$

This equation can be used for laminar or turbulent flow, and Newtonian or Non-Newtonian fluid, because it is only based on the force balance law and no additional assumptions have been made. The rheology of the filter cake can be described by the Herschel-Bulkley model

$$\begin{cases} \gamma = 0 & |\tau| < \tau_0 \\ \tau = \tau_0 + c\gamma^n & |\tau| \geq \tau_0 \end{cases} \quad (12)$$

where τ_0 is the initial yield stress. The shear rate, γ , is related to the velocity gradient. The Herschel-Bulkley fluid element will have a shear rate only if the applied stress exceeds the yield stress. This means that there will be a solid plug-like core flowing when the shear stress is larger than the yield stress; or stationary when the shear stress is

smaller than the yield stress. The situation of the plug depends on the shear stress distribution.

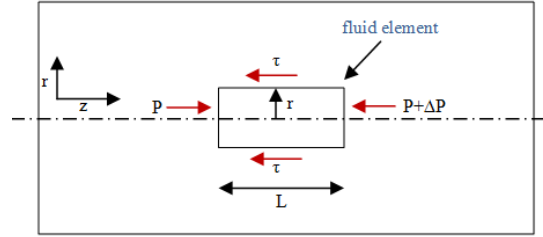


Figure 17—The force balance on the fluid element in slot flow.

Combining the shear stress distribution equation in channel with the Herschel-Bulkley fluid's rheological equation, and the appropriate boundary conditions, we get the expression for the velocity profile. The model developed shows that three flow regimes may exist in a slot, depending on the pressure gradient and the filter cake yield stress.

We distinguish that there may exist three flow patterns in a slot, depending on the shear condition. At low pressure gradients (case 1), the value of the shear stress through the filter-cake region is smaller than the yield stress. The filter cake is completely immobile and gas flows only between the filter cakes, as seen in **Figure 18a**.

At higher pressure gradients (case 2), the shear stress is equal to the yield stress at some position in the filter cake region, R_{ys} , as seen in **Figure 18b**. Because the shear stress increases linearly with increasing distance from the center of the slot, shear stress is larger than initial yield stress in the region $R_{ys} < r < R$. This causes deformation of the filter cake in this area. For the region $R_G < r < R_{ys}$, the shear stress is smaller than the yield stress, so the filter cake has a uniform velocity. Hence, the velocity of the filter cake gradually increases from zero at the surface of the cell to a constant solid-plug velocity near the gas/gel interface. The situation that the shear stress is equal to the initial yield stress, R_{ys} , is determined

$$R_{ys} = \frac{\tau_0 L}{-\Delta p} \quad (13)$$

The filter cake velocity profile within the region $R_{ys} < r < R$ can be obtained by solving Eq. 11 and 12 with the no-slip wall boundary condition. For the region $R_G < r < R_{ys}$,

the constant plug velocity can be obtained by the velocity continuity condition. By integrating the velocity profile within two flow regions, the average velocity of the filter cake through a slot can be obtained, as follows.

$$\bar{u}_{HB} = \frac{(AR - B)^{1+\frac{1}{n}}}{A\left(1+\frac{1}{n}\right)} - \frac{(AR - B)^{2+\frac{1}{n}}}{A^2\left(1+\frac{1}{n}\right)\left(2+\frac{1}{n}\right)(R - R_G)} \quad (14)$$

Similarly, we can get a gas velocity profile by solving the general expression for gas velocity with the velocity continuity condition at the gel/gas interface. And then, mean gas velocity can be obtained by integrating within the domain $0 < r < R_G$.

$$\bar{u}_{GAS} = -\frac{1}{3} \frac{\Delta p}{L} \frac{R_G^2}{\mu_{gas}} + \frac{(AR - B)^{1+\frac{1}{n}}}{A\left(1+\frac{1}{n}\right)} \quad (15)$$

The shear condition for case 2 is

$$\frac{\tau_0}{R} < -\frac{\Delta p}{L} < \frac{\tau_0}{R_G} \quad (16)$$

Finally, in case 3, the shear stress through the filter cake domain is greater than the initial yield stress. The velocity field of the filter cake is fully developed. The mean velocities for filter cake and gas are shown in Eq. 17 and Eq. 18 separately.

$$\bar{u}_{HB} = \frac{(AR - B)^{1+\frac{1}{n}}}{A\left(1+\frac{1}{n}\right)} + \frac{(AR_G - B)^{2+\frac{1}{n}}}{A^2\left(1+\frac{1}{n}\right)\left(2+\frac{1}{n}\right)(R - R_G)} - \frac{(AR - B)^{2+\frac{1}{n}}}{A^2\left(1+\frac{1}{n}\right)\left(2+\frac{1}{n}\right)(R - R_G)} \quad (17)$$

and

$$\bar{u}_{GAS} = -\frac{1}{3} \frac{\Delta p}{L} \frac{R_G^2}{\mu_{gas}} + \frac{(AR - B)^{1+\frac{1}{n}}}{A\left(1+\frac{1}{n}\right)} - \frac{(AR_G - B)^{1+\frac{1}{n}}}{A\left(1+\frac{1}{n}\right)} \quad (18)$$

If the Reynolds number for gas flow is larger than 4000, all equations are not appropriate for calculating the mean gas velocity. We need to use an empirical turbulent flow expression to calculate the average gas velocity.

The shear condition for case 3 is as follows:

$$-\frac{\Delta p}{L} > \frac{\tau_0}{R_G} \quad (19)$$

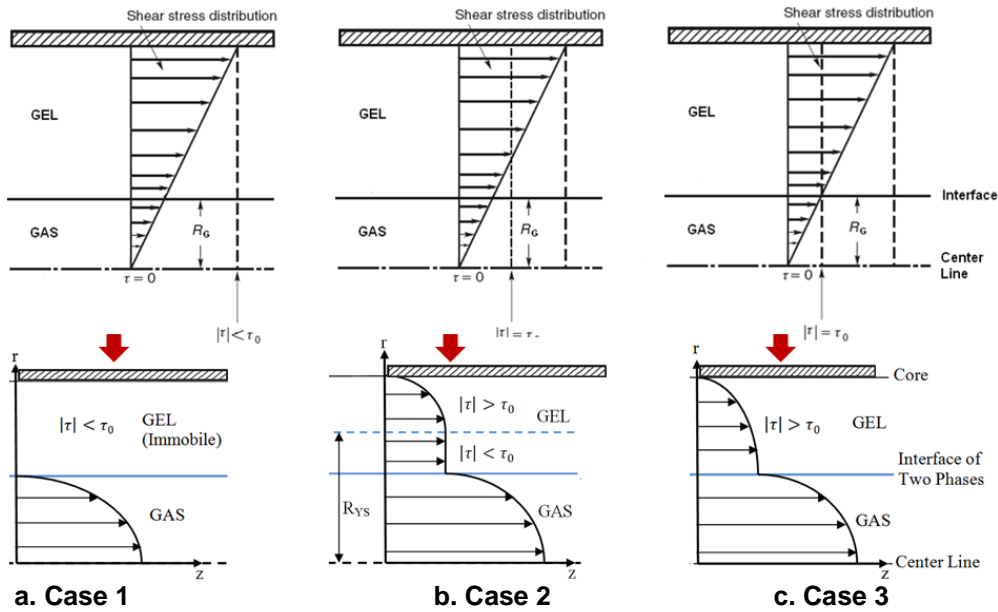


Figure 18—Flow patterns identified under imposed pressure gradients.

B.2.2 Modeling Fracture Cleanup in Tight Gas Wells Using 3D, Three-Phase Simulator

A 3D, three-phase black-oil simulator was used to model fracture-fluid cleanup and long-term gas production in a tight-gas well. We assumed that the fracture extends an equal distance on two sides of the wellbore and fully penetrates the formation. The width of the fracture is assumed to be a constant from the wellbore to the tip, while the porosity of the fracture is 30%. The reservoir is assumed to be homogeneous and isotropic. One quarter of the drainage area of the fractured well was simulated because of symmetry. The dataset for this part of the study is summarized in **Table 5**. This is based on the work of Wang et al. (2008) and Wang (2010).

TABLE 5—RESERVOIR AND FRACTURE PARAMETERS FOR PARAMETRIC SIMULATION STUDY

<u>Parameter</u>	<u>Value</u>
Drainage area, acre	160
Reservoir thickness, ft	25
Formation permeability, md	0.001, 0.01, 0.1
Formation porosity, %	10
Formation depth, ft	4000, 8000, 12000
Reservoir pressure, psi	1860, 3720, 5580
Reservoir Temperature, °F	130, 190, 250
Formation water saturation, fraction	0.4
Water compressibility, psi ⁻¹	3x10 ⁻⁶
Gas specific gravity, fraction	0.6
Fracture half length, ft	264, 528, 924
Dimensionless fracture conductivity	0.1, 1, 10, 100
Bottomhole pressure, psi	10% of reservoir pressure
Fracture fluid, gallon	80,000

B.2.3 Modeling flow of Herschel-Bulkley fluid in Porous Media

After understanding the yield stress behavior in parallel plate system for non-Newtonian, we want to investigate the flow behavior of Herschel-Bulkley fluid in porous media. We studied the impacts of different key parameters such as proppant size, rheology of Herschel-Bulkley fluid and imposed pressure gradients. We assumed the packing arrangement of proppant is simple cubic, as shown in **Figure 19a**. To replicate the porous structure of proppant package, we used a micro pore-scale modeling for the computational domain and micro pore-scale model consisted of a pore-throat which was surrounded by proppant and connected to other pore-throats, as shown in **Figure 19b**.

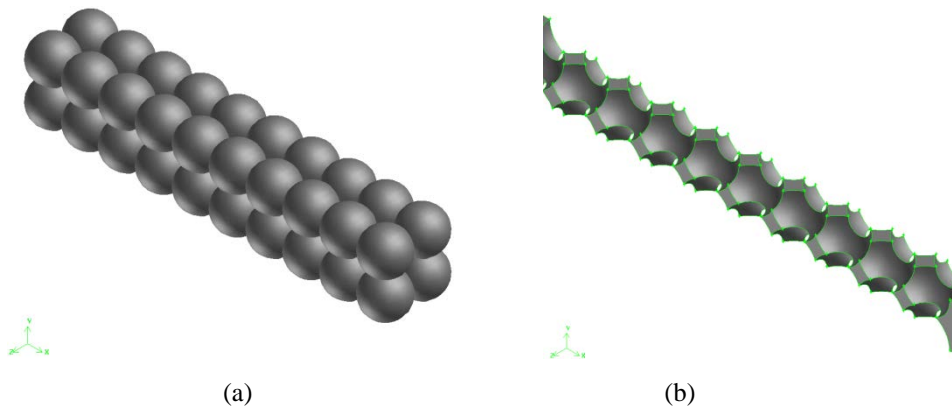


Figure 19— (a) Geometry for proppant package (b) Geometry of flow channel

We numerically simulated the flow behavior of Herschel-Bulkley fluid at the pore scale using FLUENT, a computational fluid dynamics (CFD) software package. FLUENT uses the finite-volume method to solve the Navier-Stokes equations for fluids. For the spatial discretization of flow governing equations, the second-order upwind scheme is adopted to assure the accuracy of results. To avoid pressure-velocity decoupling, we used Semi-Implicit Method for Pressure Linked Equations (SIMPLE) algorithm. For the flow boundary condition, constant pressure boundary conditions are maintained at the inlet and outlet. For wall boundary conditions, the no-slip condition applies at the surface of proppant. Symmetry is assumed in the span-wise and transverse directions. The calculations assume that the flows are three-dimensional, laminar and incompressible due to the short calculation region. The meshes of computation domain are generated by GAMBIT, a preprocessing software package for geometry and meshing. Surrounding computation domain, there are two half proppants in the y- and z-directions and ten proppants in the x-direction. An unstructured grid is adopted. Unstructured grid has irregular shape and is much more flexible in their ability to define complex shapes, which is suitable for our cases.

The Herschel-Bulkley model includes the shear-thinning or shear-thickening behavior of power-law fluids and the yield- stress effect of the Bingham Model. It is given as following:

$$\begin{cases} \gamma = 0, & |\tau| < \tau_o \\ \tau = \tau_o + C\gamma^n, & |\tau| > \tau_o \end{cases} \quad (20)$$

where γ is the shear rate, τ is the shear stress, τ_o is the initial yield stress above which the fluid starts flowing, C is the consistency factor and n is the flow behavior index. To cover all possible condition, we consider a large range of parameter. The dataset for this part of the study is summarized in Table 6.

**TABLE 6—HERSCHEL-BULKLEY FLUID AND PROPPANT PARAMETERS FOR
PARAMETRIC SIMULATION STUDY**

<u>Parameter</u>	<u>Value</u>
Superficial Velocity, m/s	0.5, 0.1, 0.05, 0.01, 0.005, 0.001, 0.0001, 0.00001
Consistency Factor, cP	1, 10, 100
Flow Behavior Index	0.6, 0.7, 0.8, 0.9, 1
Initial Yield Stress, Pa	0.1, 1, 10, 50, 100
Porosity	0.3
Diameter of Proppant, mm	0.84, 0.42, 0.21, 0.149

C. Results and Discussion—Experimental Methods

C.1 Yield Stress Measurement

C.1.1 Polymer Yield Stress Test Results without Breaker

The yield stress of fracturing fluid was measured at different concentrations of polymer without adding breaker to the fluids. Guar concentrations from 40 to 200lbm/1000gal were tested. **Figure 20** and **Table 7** show the results of the tests without breaker. The yield stress is very low at low polymer concentrations. However, the yield stress increases sharply as the guar concentration increases. In an actual fracturing treatment, the polymer concentration in the fracture increases as leak off occurs and the concentration of guar can become very high at the end of a treatment. Such a high yield stress can influence the fracturing-fluid clean-up process and result in serious gel damage.

<u>Guar Conc.(lb/Mgal)</u>	<u>Yield Stress(Pa)</u>
40	0.329
80	5.823
100	18.228
150	45.570
200	63.292

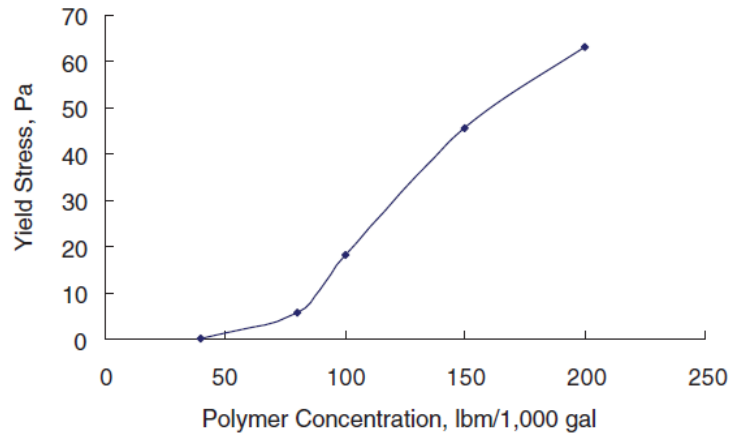


Figure 20—Yield stress with different polymer concentrations.

C.1.2 Polymer Yield Stress Test Results with Breaker

In the next series of tests, breakers were added to the fracturing fluid. The yield stress of fracturing fluid was measured with different concentration of polymer and breaker. The polymer concentration ranged from 80 to 200 lbm/1000gal. At each concentration, the yield stress at different breaker concentrations, from 2 to 15 gal/1000gal, were measured. Higher breaker concentration was used when the polymer concentration was increased. **Table 8** lists the test conditions of the yield stress tests with breakers.

Table 9 shows the results of the tests with the breakers. **Figure 21** plots the yield stress as a function of breaker concentration for different polymer loading. As seen from Figure 21, the yield stress is higher with higher guar concentration for the same concentration of the breaker. Yield stress decreases with increasing breaker concentration at a given concentration of guar. At low polymer concentrations, the concentration of breaker does not affect the value of yield stress significantly. As the polymer concentration increased, the breakers effectively reduced the yield stress of the gel. The yield stress becomes zero when the breaker concentration reaches a certain value. The relationship between guar concentration and needed breaker concentration to reduce the yield stress to zero is shown in **Figure 22**. The relationship is almost linear. The test results show that the use of breakers is extremely important in gel damage and filter-cake cleanup procedures. If breakers are designed properly and function as designed, gel damage should not be a problem in hydraulically fractured tight gas wells. The relationship in Figure 22 can be used as a guideline for breaker design.

TABLE 8—EXPERIMENTAL DESIGN WITH BREAKER	
<u>Guar Concentration</u> (lbm/1000gal)	<u>Breaker Concentration</u> (gal/1000gal)
80	2
80	5
100	2
100	5
100	8
150	2
150	5
150	8
150	10
200	2
200	5
200	8
200	10
200	15

TABLE 9—EXPERIMENTAL RESULTS WITH BREAKER				
	Yield Stress (Pa)			
<u>Breaker</u> <u>Conc.(gal/Mgal)</u>	<u>80lbm/1000gal</u> <u>guar</u>	<u>100lbm/1000gal</u> <u>guar</u>	<u>150lbm/1000gal</u> <u>guar</u>	<u>200lbm/1000gal</u> <u>Guar</u>
0	5.823	18.228	45.570	63.292
2	2.532	10.633	27.848	35.443
5	0	3.797	7.342	19.494
8	-	0	1.418	10.127
10	-	-	0	6.582
15	-	-	-	0

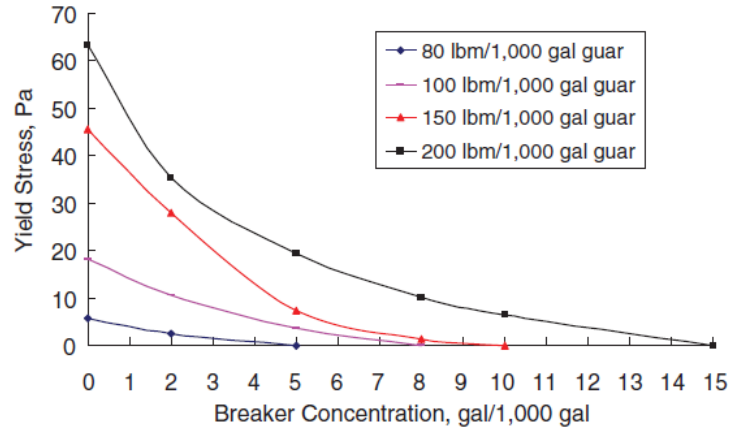


Figure 21—Yield stress with different breaker concentrations.

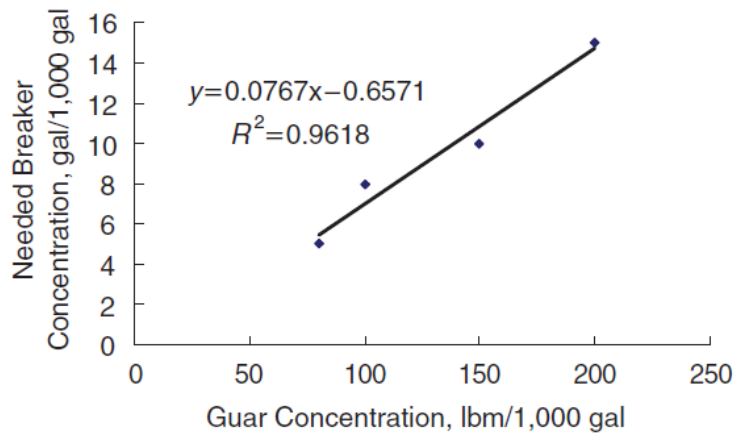


Figure 22—Relationship between guar concentration and the breaker concentration needed to obtain zero yield stress.

C.1.3 Flow Initiation Gradient (FIG) Estimated from Yield Stress

Yield stress is a property of fracturing fluids. After a fractured well is on production, the bottomhole pressure is lower than the reservoir pressure and it creates a pressure gradient inside the fracture, which acts as an external forces to move the fracturing fluid to the well bore. FIG is defined as the minimum pressure gradient needed to make the gel yield.

The relationship between yield stress, τ_0 , and FIG is given by (Ayoub et al. 2006)

$$FIG = 21.8\tau_0\sqrt{\frac{\phi}{k}} \quad (21)$$

where ϕ is porosity and k is permeability in Darcy. The constant 21.8 is a unit conversion factor which results in FIG being calculated in psi/ft if τ_0 is in Pa. Using the above relationship, we calculated FIG from the measured yield stress, and the result is shown in **Figure 23**. The fracture permeability is 80 Darcy and the porosity is 0.2. The results relate the breaker concentration to the minimum pressure gradient required to displace the gel inside the fracture.

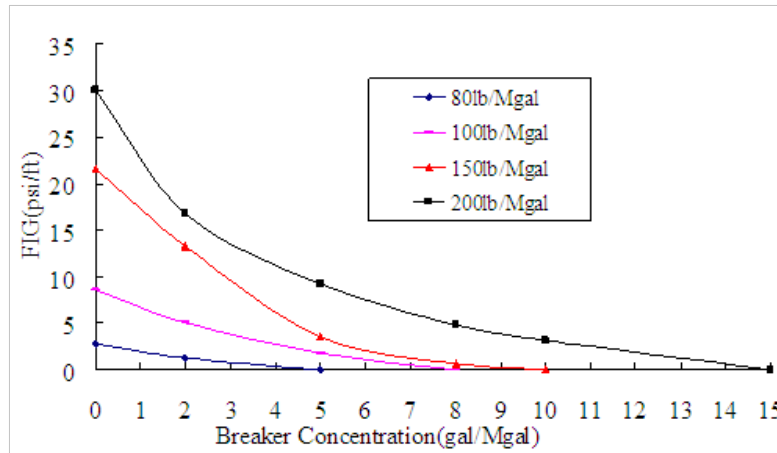


Figure 23—FIG with different breaker concentrations.

C.2 Filter-cake Thickness Measurement and Filter-cake Cleanup

C.2.1 Relationship between Leak-off Volume and Filter-cake Thickness—Static Measurements

The filter cake thickness is measured by first scanning the surface of the filter cake, and thereafter scanning the surface of the core after gel removal. As mentioned previously, the profilometer measures the distance between a given object and the laser sensor. The difference between the two surfaces scanned is the filter cake thickness. We also used micrometer measurements of the filter cake thickness to confirm the profilometer results. The micrometer consists of a 0.1-in.-diameter spindle, which could be carefully lowered onto the gel surface.

Figure 24 shows a picture of a filter cake built during an experiment and the scanned surface profile of the same surface. This scan clearly images the shape of the

filter cake. To verify the thickness data, the arithmetic mean value of the profilometer scan was compared with the micrometer mean value. **Figure 25** shows the comparison of profilometer scanned thickness and micrometer measured thickness. The two measurements are in good agreement.

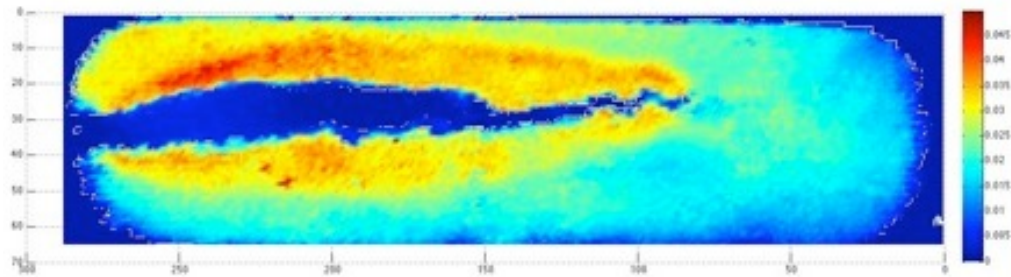


Figure 24—Profilometer-scanned filter-cake at 0.025-in. resolution.

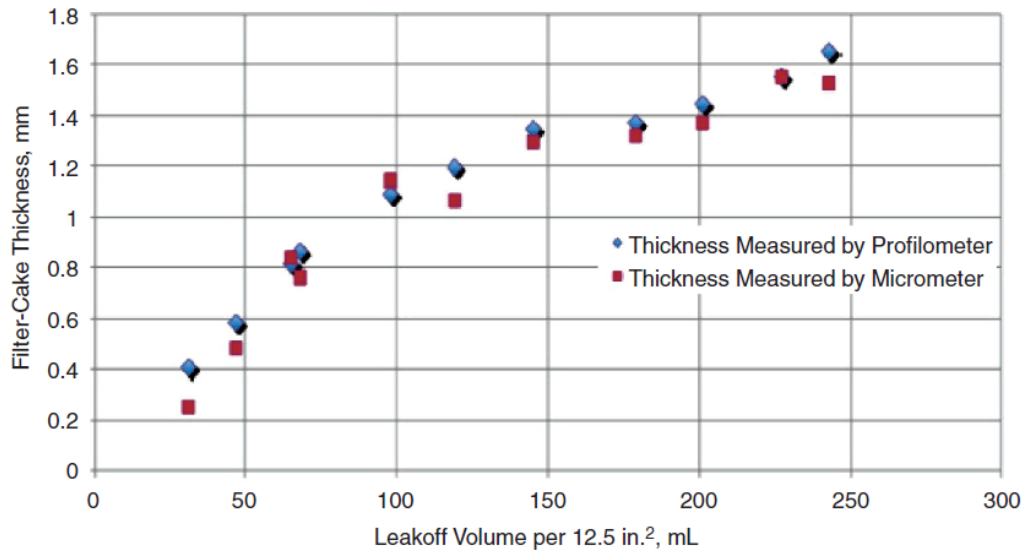


Figure 25—Micrometer- and profilometer-thickness comparison.

If the polymer filter cake created by leakoff has a constant concentration, then the filter cake thickness should increase linearly with the cumulative leakoff volume. **Table 10** shows the results of the filter cake thicknesses measured in this study. Plotting this result, **Figure 26** shows a simple linear relationship between leakoff volume and the filter cake thickness. The concentration factor defined by Ayoub et al. (2006) is also calculated in this work corresponding to the leakoff volume and the measured thickness in Table 10.

$$F_{fc} = \frac{V_{fc} + V_L}{V_{fc}} \quad (22)$$

In equation 22, V_{fc} is the volume of filter cake, and V_L is the leakoff volume. As the leakoff volume increases, more polymer was concentrated in the filter cake. Ayoub et al. (2006b) observed a similar effect. Also, the polymer concentration in the filter cake, C_{fc} , is defined as follows:

$$C_{fc} = C_p F_{fc} \quad (23)$$

where C_p is the polymer loading in the original gel. The original polymer concentration is 40 lbm/1000gal in the measurements. From the concentration factor measured, polymer concentrations in the filter cakes range from about 400 lbm/1000gal to approximately 700 lb/1000gal, more than 10 times higher than the original loading. These concentrations could result in yield stresses higher than those measured in the yield stress experiments.

In Figure 26, based on the definition of the concentration factor, we expect to see a linear fit between the leakoff volume and the filter-cake thickness. Therefore, a linear model was fitted to the data (black line in Figure 26). However, we know that at low leakoff volumes (near the origin of Figure 26); a non-linear relationship exists between leakoff volume and filter-cake thickness. This is due to spurt loss; that is, the volume of fluid lost before the filter cake is established.

TABLE 10—FILTER-CAKE-THICKNESS MEASUREMENT RESULTS

<u>Number</u>	<u>Leakoff Volume (ml)</u>	<u>Filter cake Thickness by Profilometer (ml)</u>	<u>Concentration Factor in Filter cake (dimensionless)</u>
1	31	0.4064	11.6175
2	47	0.5842	10.0018
3	65	0.8128	9.78903
4	68	0.8636	10.7967
5	98	1.0922	11.1549
6	119	1.1938	12.3925
7	145	1.3462	13.3907
8	179	1.3716	16.2244
9	201	1.4478	17.2596
10	227	1.5494	18.2140
11	243	1.651	18.2980
12	182	1.4376	14.6033

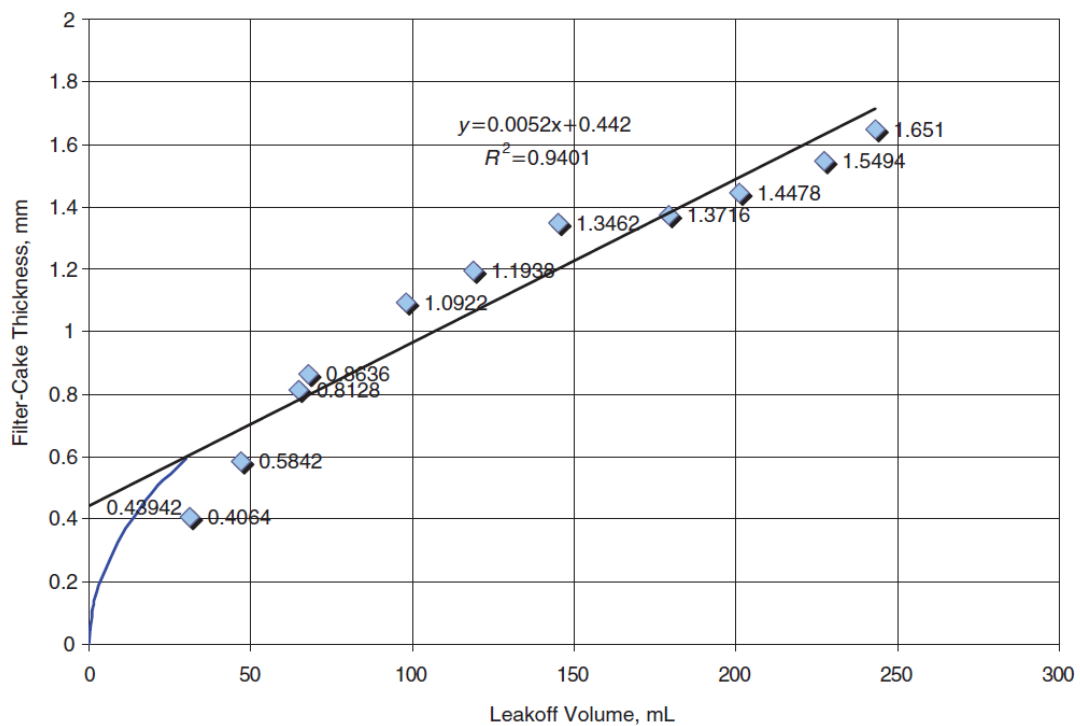


Figure 26—Correlation of leakoff volume vs. filter-cake thickness.

C.2.2 Relationship between Leak-off Volume and Filter-Cake Thickness—Dynamic Measurements

In order to build up filter cake dynamically, we mixed a 40 lb/Mgal guar borate crosslinked gel and pumped it through a modified API RP-61 cell. The cell is preloaded with core samples of 7 in. long by 1.61 in. wide by 3 in. thick. The cores are pre-saturated with water and coated with silicone to provide a primary seal between the core and the conductivity cell. The cores are mounted through the top and bottom of the cell with a gap between them to represent the fracture width. A space bar is used to facilitate setting up the fracture width. Pistons are placed on the top and bottom cores to keep them in place and provide leakoff ports. The 40 lb/Mgal gel is pumped through the cell at high pressure using a Hydra-Cell diaphragm pump. The leakoff ports on the pistons are opened during pumping to allow dynamic fluid leak off under pressure. The leak off fluid is collected through a fraction collector in timed test tubes which are weighed to obtain leakoff volume as a function of time. After the fluid has leaked off for 1 to 2.5 hours, the experiment is stopped and the cores are taken apart. Excess original gel is cleaned up leaving a filter cake on the core surface. The filter cake thickness is then measured using the laser profilometer as discussed in the above section.

For cleanup experiments, the same procedure is repeated, except after leakoff, the cores are not taken out. A cleanup fluid (liquid or gas) is then pumped through the cell during which the filter cake thickness is monitored. The details of the experiments are presented by Yango (2011).

Using the procedures described above, we built up filter cake under dynamic leakoff conditions. The filter cake thickness for each experiment at a given shear rate level is plotted against leakoff volume in **Figure 27**.

Figure 27 shows the filter cake thickness increases as leak off volume increases because more polymer solids are deposited on the core face. The filter cake thickness per unit leak off volume is lower at higher shear rates due to erosion of the filter cake from shear. The filter cake thickness is found to have a quadratic relationship with leak off volume, probably as a result of the interplay between filter cake deposition and erosion. Static build up tests were conducted by placing a guar crosslinked gel in the conductivity cell, capping the inlet and outlet then applying a closure stress, as described in Xu et al.

(2011). The leak off volume was collected and the resulting filter cake thickness was measured using the laser profilometer. It was also observed that there was a direct relationship between filter cake thickness and leak off volume. However, for the same leak off volume, the resulting static filter cake thickness was greater than the thickness from any of the dynamic experiments. This further confirms that shear rate reduces the buildup of a filter cake residue. **Figure 28** illustrates this effect.

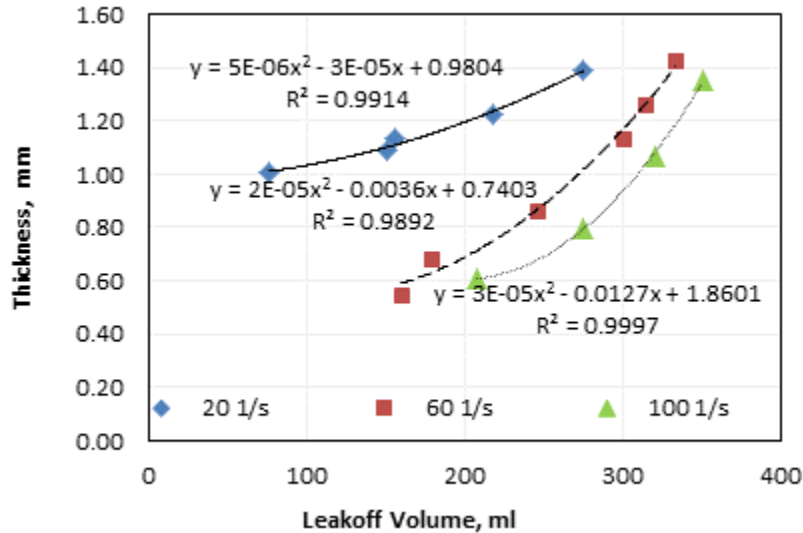


Figure 27— Thickness profiles and correlations at different shear rates. Note that data did not start from the origin because spurt loss data has been removed from the plot.

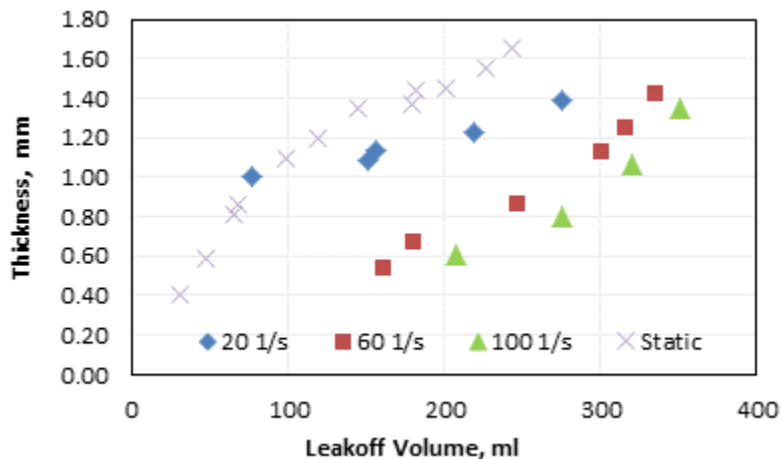


Figure 28— Thickness profiles at static conditions and at different shear rates. Note that data did not start from the origin because spurt loss data has been removed from the plot.

C.2.3 Cleanup as a Function of Flow Rate

In **Section B.2.1** of this report, we briefly considered the modeling of filter-cake cleanup in parallel plates. We tested the models presented using experiments. The filter cake was built as described in the previous section. An experiment of 20 s^{-1} shear rate was conducted with 90 minutes of leakoff time. The filter-cake properties are tabulated in **Table 11**. The values in bold/italic font were obtained from the model discussed in **Section B.2.1**. The rest are results from the experiments.

TABLE 11—CLEANUP TEST DATA								
<u>w</u> (in)	<u>Rate</u> <u>during</u> <u>leakoff</u> (ml/s)	<u>Shear</u> <u>Rate</u> (s^{-1})	<u>Leakoff</u> <u>Time</u> (min)	<u>Leak</u> <u>off Vol</u> (ml)	<u>Filter Cake</u> <u>Thickness</u> (mm)	<u>Filter Cake</u> <u>Conc.</u> (lbm/1000 gal)	<u>Yield</u> <u>Stress</u> (Pa)	<u>Leakoff</u> <u>Coefficient</u> ($\text{ft}/\text{min}^{0.5}$)
0.25	6.08	20.71	94	177.5	1.1474	748	296	0.0032

Water was used as the cleanup fluid. Two experiments were conducted. The water flow rate during the first experiment was 70 ml/s. **Figure 29** displays the cleanup result. **Figure 29a** shows the filter cake buildup after 94 minutes of leakoff time, and **Figure 29b** shows that after water had been flowed at a cleanup rate of 70 ml/s, all the filter cake was removed from the fracture. In order to properly test the concept, the water flow rate was increased in steps from 25 ml/s to 62 ml/s in the second experiment. The duration for each flow rate step was 10 to 15 minutes. The results are shown in **Figure 30**.

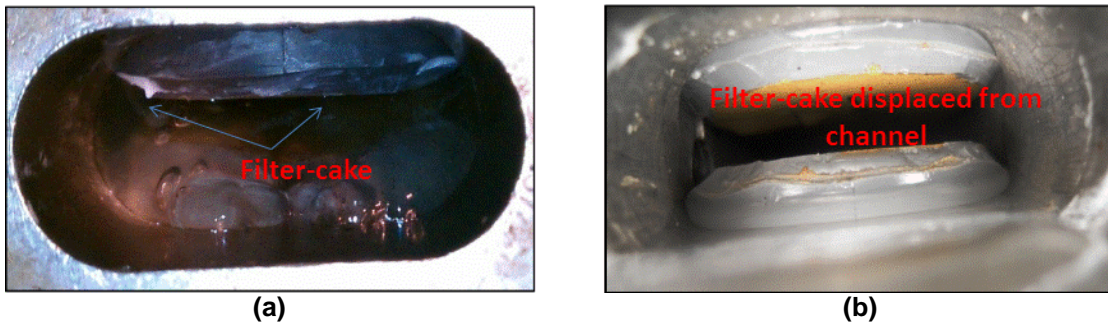


Figure 29—Cleanup test result for experiment 1 before cleanup (a). After cleanup (b).

Before cleanup, the fracture space was full of original gel at the center and filter cake on the core faces for both experiments (as shown in **Figure 29a**). After flowing at 25 ml/s for 10 minutes (**Figure 30a**), the gel was easily displaced by water, and a channel was

created to the right of the fracture. This we attribute to the relatively “lower resistance” in this area. We noticed that the cleanup flux was too low to displace all the original gel. The cleanup rate was increased to 40 ml/s (**Figure 30b**), and more original gel was displaced creating a wider channel. The cleanup rate was further increased to 50 ml/s and all the original gel was displaced, leaving behind the filter cake which is harder to displace or cleanup (**Figure 30c**). The filter cake for this experiment had an estimated concentration of 748 lbm/1000gal and a yield stress of 296 Pa. When the rate was further increased to 62 ml/s, over 85% of the filter cake was eroded (**Figure 30d**). The critical flow rate for this clean up experiment is estimated to be between 55 ml/s to 62 ml/s. **Figure 31** shows the clean surface after flow back for both experiments.

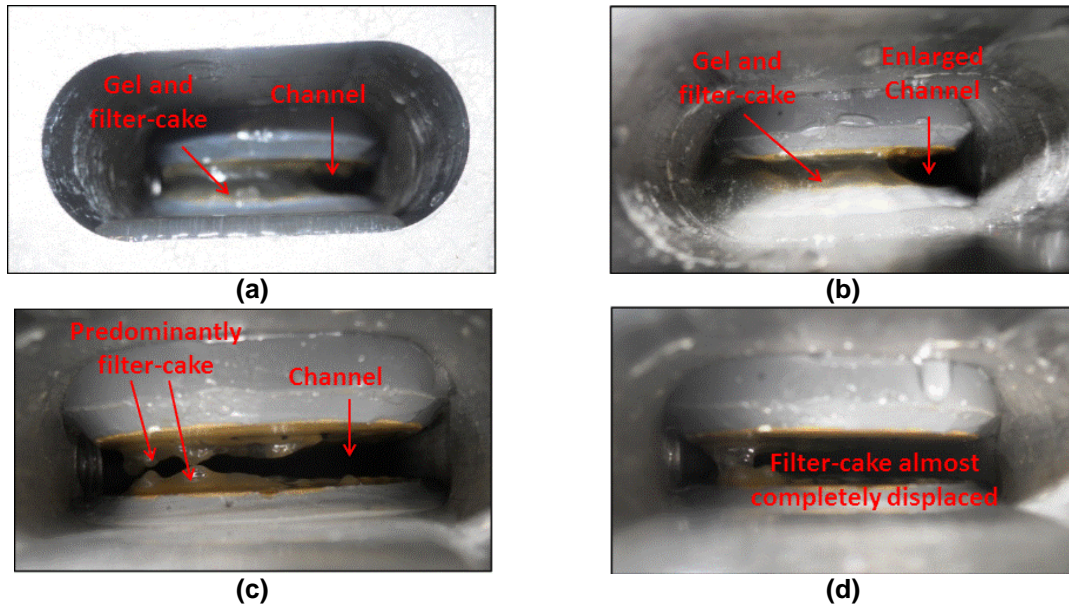


Figure 30—Cleanup test result for experiment 2 at 25 ml/s (a). At 40 ml/s (b). At 50 ml/s (c). At 62 ml/s (d).



Figure 31—Core surfaces after erosion (cleanup) test.

We do not have profilometer images of the core surfaces in Figure 31. For the objective to show that the bulk of the filter-cake was displaced from the laboratory fracture, visual inspection of the core was sufficient.

C.3 Dynamic Fracture Conductivity Tests

In this section, the results from the dynamic conductivity study will be presented.

Design table. The objective of this set of experiments is to rank the six factors in **Table 12** in the order of their potential impact on fracture conductivity. Therefore, we created an experimental table based on a 2^{6-2} fractional factorial design. This type of design would enable us to uniquely determine the main effect of each of the investigated factors. Each row of the design table is called a treatment. Two principal properties of the design table that are important for us to be able to uniquely estimate effects are balance and orthogonality. A balanced design is one in which all treatment combinations have the same number of observations. This affects the relative accuracy of factor effect estimation. A design is said to be orthogonal if the sum of each column is zero or the dot

product of any two columns in the matrix is zero. Orthogonality also helps us to be able to remove non-significant terms in the regression model (if one is developed) without vitiating the model. **Table 13** shows the design table for our screening experiment. Note that '1' and '-1' represents the high and low setting of a factor respectively. The design table is also essentially the planning table in coded variables.

Planning table. The planning table is the representation of the experimental matrix as it is actually executed. It helps avoid any misunderstandings as to what the variables are and the levels they should be set for each run. **Table 14** is the planning table for the screening experiment.

TABLE 12—FACTOR LEVELS IN EXPERIMENTAL SPACE

Factor	Factor Setting	
	Low Setting	High Setting
Temperature, degF	150	250
Flow back rate, standard liter per minute	1*	3**
Presence of breaker	none	Standard loading
Closure Stress, psi	2000	6000
Polymer concentration, pounds per thousand gallons	10	30
Proppant concentration, ppg	0.5	2

* Equivalent to field rates of about 0.7 MMscf/D assuming height of fracture is 100 ft. and width is 0.073 in.

** Equivalent to field rates of about 2 MMscf/D assuming height of fracture is 100 ft. and width is 0.073 in.

TABLE 13—DESIGN TABLE WITH ORTHOGONAL COLUMNS

Treatment #	Nitrogen rate, x_A	Reservoir Temperature, x_B	Polymer loading, x_C	Presence of breaker, x_D	Closure Stress, x_E	Proppant Concentration, x_F
1	-1	-1	-1	-1	1	1
2	-1	-1	1	1	-1	-1
3	-1	1	-1	1	-1	1
4	-1	1	1	-1	1	-1
5	1	-1	-1	1	1	-1
6	1	-1	1	-1	-1	1
7	1	1	-1	-1	-1	-1
8	1	1	1	1	1	1
9	1	1	1	1	-1	-1
10	1	1	-1	-1	1	1
11	1	-1	1	-1	1	-1
12	1	-1	-1	1	-1	1
13	-1	1	1	-1	-1	1
14	-1	1	-1	1	1	-1
15	-1	-1	1	1	1	1
16	-1	-1	-1	-1	-1	-1

TABLE 14—PLANNING TABLE (PRESENCE OR OTHERWISE OF BREAKER IS A QUALITATIVE VARIABLE)

Treatment #	Nitrogen rate, x_A	Reservoir Temperature, x_B	Polymer loading, x_C	Breaker present?, x_D	Closure Stress, x_E	Proppant Concentration, x_F
1	0.5	150	10	No	6000	2
2	0.5	150	30	Yes	2000	0.5
3	0.5	250	10	Yes	2000	2
4	0.5	250	30	No	6000	0.5
5	3	150	10	Yes	6000	0.5
6	3	150	30	No	2000	2
7	3	250	10	No	2000	0.5
8	3	250	30	Yes	6000	2
9	3	250	30	Yes	2000	0.5
10	3	250	10	No	6000	2
11	3	150	30	No	6000	0.5
12	3	150	10	Yes	2000	2
13	0.5	250	30	No	2000	2
14	0.5	250	10	Yes	6000	0.5
15	0.5	150	30	Yes	6000	2
16	0.5	150	10	No	2000	0.5

C.3.1 Initial Results Summary

Experimental results table. Results from the screening experiment are shown in **Table 15**. The treatments at the low setting of polymer loading and proppant concentration were replicated several times because of the stochastic nature of the conductivity measurements. The variability in the results is attributed to the difference in proppant weight/distribution in the core, and to proppant settling at the low polymer concentrations across experiments. **Figures 32a, b & c** show the picture of post-experiment cores for three replications of the same experimental conditions (treatment 14). The factorial effects and aliasing relationships between the experimental variables is shown in **Table 16**. It is beneficial to provide median estimates of the factorial effects. This is because the sensitivity of the results to outliers is reduced. A graphical representation of the data (both mean and median estimates) is shown in **Figure 33**. The conclusions from the figure do not differ significantly using either the mean or the median. We observed that a negative or positive effect means that there is an inverse or direct relationship between the variable and the fracture conductivity respectively. The larger the absolute value of

the effect, the more impact the parameter has on fracture conductivity. Note that concluding (CF,DE) is an alias combination implies that the interaction effect due to (1) polymer loading and proppant concentration and (2) presence of breaker and closure stress cannot be uniquely determined using this design without making further assumptions.

TABLE 15—SCREENING EXPERIMENT RESULTS WITH NUMBER OF REPLICATIONS IN EACH EXPERIMENT

Treatment #	Number of replications	Mean Conductivity, mdft	Standard deviation, mdft
1	2	570	57
2	3	3757	2046
3	4	3521	830
4	1	8	Not Applicable
5	2	868	818
6	2	643	294
7	3	571	569
8	1	66	Not Applicable
9	1	216	Not Applicable
10	1	118	Not Applicable
11	1	7	Not Applicable
12	2	5700	43
13	1	1587	Not Applicable
14	3	1385	1038
15	1	2927	Not Applicable
16	2	11730	2376

*Not Applicable implies treatment had only one replicate

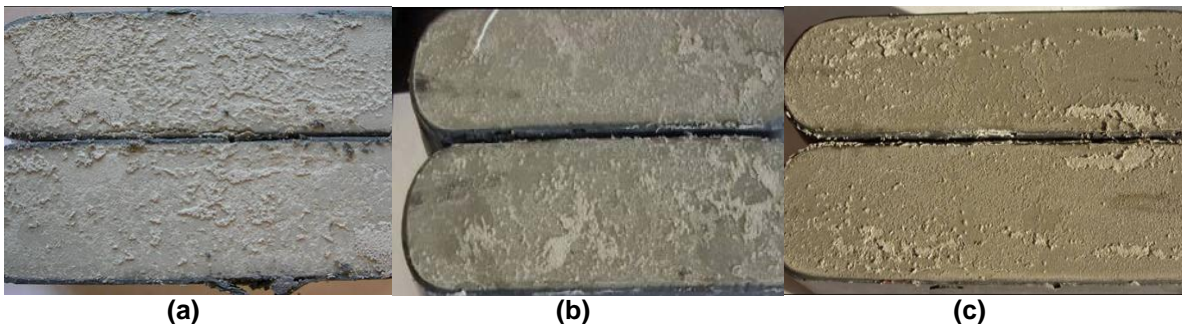


Figure 32—Proppant distribution on the core surfaces for three replications of the same treatment, proppant distributed uniformly on the surface of the core (a). Proppant distributed with less uniformity on the surface of the core (b). Proppant not uniformly distributed on the surface of the core (c).

TABLE 16—MAIN AND INTERACTION EFFECTS

Factor	Factor Effect	Alias Combination	Alias Effects
A (Nitrogen Rate)	-2162	CF, DE	735
B (Temperature)	-2341	CE, DF	1923
C (Polymer Loading)	-1906	AF, BE	1643
D (Presence of Breaker)	401	AE, BF	1204
E (Closure Stress)	-2722	BC, AD	977
F (Proppant Concentration)	-426	AC, BD	325
		AB, CD, EF	780

Before we continue to our explanation of the effect of the various factors, we investigate in the following section the effect of the outliers that might have on the above analysis.

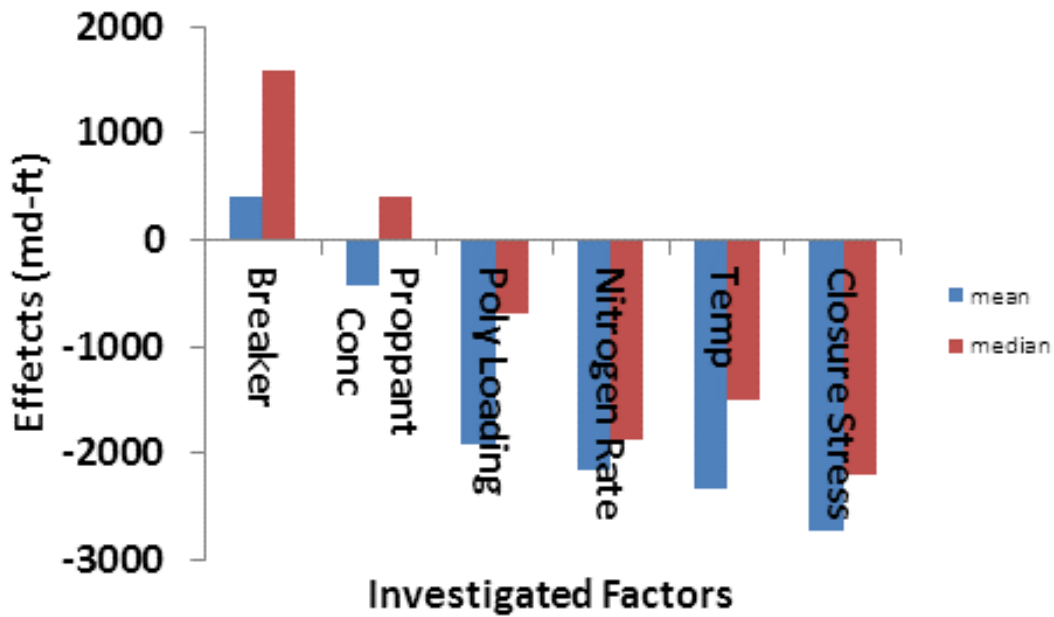


Figure 33—Effects of investigated factors using mean and median estimates.

C.3.2 Effects of Outliers

Outliers have been reported in statistical literature to have the ability to mask the significance of certain factors/experimental variables. The effects of outliers can be minimized by the use of data transformations. We used logarithmic and rank transformation in this study. An examination of the mean conductivity data in **Table 16** shows that the ratio of the maximum to minimum conductivity is $\gg 3$, and we used 3 as the threshold to decide if an observation is likely to be an outlier. In the logarithmic transformation procedure, the log of the conductivity data is computed and the factorial effects are computed thereafter. In the rank transformation procedure described by Aguirre-Torres and Perez-Trejo (2007), the conductivity data is ordered and the rank of each conductivity observation is the index corresponding to its place in the ordered set of conductivity data. If there are tied observations, each observation is assigned the average of the rank that would have been assigned if there were no ties. **Table 17** contains the log and transformed dataset. The 2nd and 3rd columns of **Table 18** show the logarithmic and rank-transformed factorial effects respectively. The ratio of the maximum to minimum observation is 4.82 and 16 respectively for the logarithmic and rank-transformed dataset. This is in comparison to over 1000 for the raw dataset.

TABLE 17—RAW, LOG AND RANK TRANSFORMED DATA

Treatment #	Mean Conductivity, mdft	Logarithm of Conductivity, mdft	Rank Transformed Data
1	570	2.756	6
2	3757	3.575	14
3	3521	3.547	13
4	8	0.903	2
5	868	2.939	9
6	643	2.808	8
7	571	2.757	7
8	66	1.820	3
9	216	2.334	5
10	118	2.072	4
11	7	0.845	1
12	5700	3.756	15
13	1587	3.201	11
14	1385	3.141	10
15	2927	3.466	12
16	11730	4.069	16

Figures 34 and 35 show a graphical representation of the factorial effects data for both log and rank transformed data. Compared to the analysis using the raw data, the sign of the effects of the various factors remains largely unchanged with the exception of proppant concentration. However, their magnitudes relative to each other do change. For example, for the log transformed data, the positive effect of the presence of breaker is enhanced, the effect of polymer loading is stronger, the negative impact of temperature is diminished and proppant concentration has a positive effect. For the rank transformed data, the positive effect of the presence of breaker is also enhanced. Therefore, based on the foregoing, the question is of which one of these datasets we should base our ranking of the relative importance of these factors. To answer this question, we have to test the factorial effects computed using each dataset and determine which dataset offers the strongest conclusions. We undertake this task in the next section.

TABLE 18—MAIN AND INTERACTION EFFECTS BASED ON LOGARITHMIC AND RANK-TRANSFORMED DATA

Factor	Log-transformed factorial effects	Rank-transformed factorial Effects
A (Nitrogen Rate)	-0.6660	-4
B (Temperature)	-0.5550	-3.25
C (Polymer Loading)	-0.7605	-3
D (Presence of Breaker)	0.6459	3.25
E (Closure Stress)	-1.0131	-5.25
F (Proppant Concentration)	0.3577	1
CF, DE	0.5516	2
CE, DF	-0.2079	0.25
AF, BE	0.0375	1
AE, BF	0.0181	0.75
BC, AD	-0.0542	-0.25
AC, BD	-0.1684	-1.5
AB, CD, EF	0.2137	-0.25

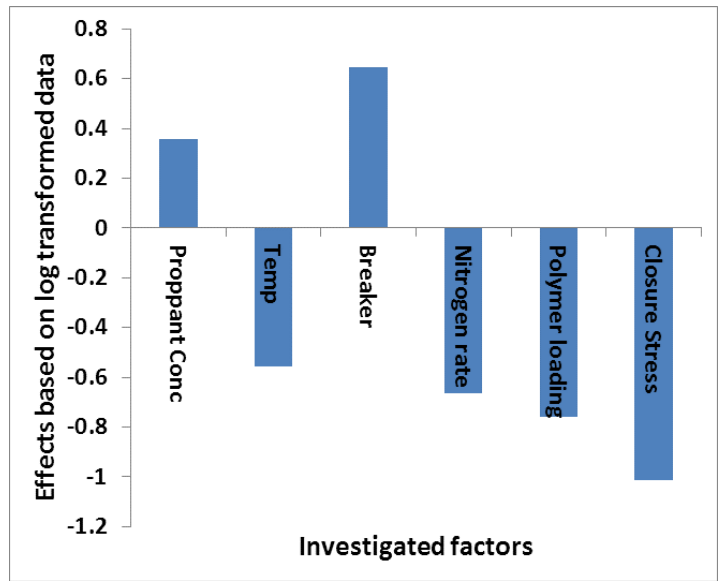


Figure 34—Factorial effects based on log transformed data.

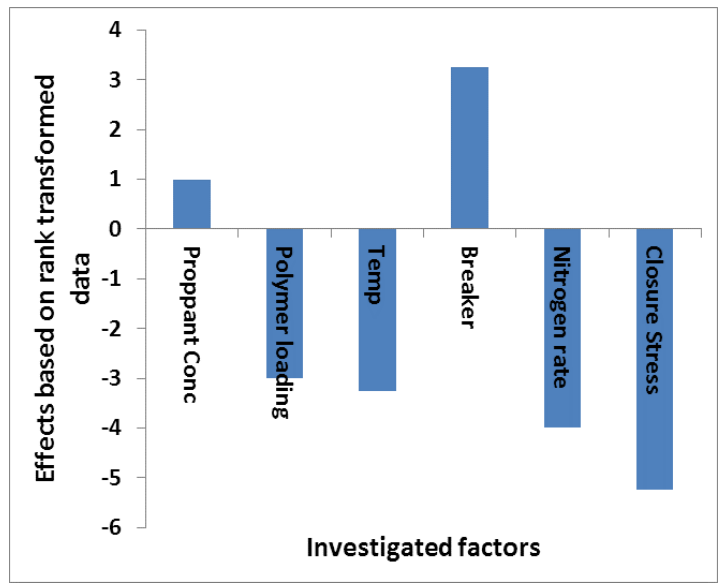


Figure 35—Factorial effects based on rank transformed data.

C.3.3 Tests of Effect Significance

Essentially, we have treated our experimental design as unreplicated. In order to test for effects significance in unreplicated experiments, two methods are commonly used in design of experiment literature. One of them is graphical in nature (half-normal plot) and the other is based on a formal test of significance (Lenth's test). The half normal plot is a plot of the ordered values of the absolute value of the effects estimates against coordinates based on the half-normal distribution. A line is thereafter fit to the points closest to zero and any effect whose corresponding point falls off the line is said to be significant.

Using the raw data, **Figure 36** shows that closure stress (factor E), temperature (factor B), nitrogen rate (factor A) and the interaction between polymer loading and closure stress (factor CE) are significant. If there is a slight shift in the slope of the line, polymer loading (factor C) too might be significant. The half-normal plot is qualitative in nature and it is subjective because it depends on the slope of the line. A more quantitative estimation of the significance or otherwise of the effects is obtained by using the Lenth's test. In the Lenth test, an effect is declared to be significant when its statistic exceeds a given critical value. The effects and the corresponding test-statistics are shown in **Table 19**. The procedure for computing the statistic and the table of critical values is given in **Appendix A**. For subsequent analysis of data, we will be using the Lenth test because of its less subjective nature compared to the half-normal plot.

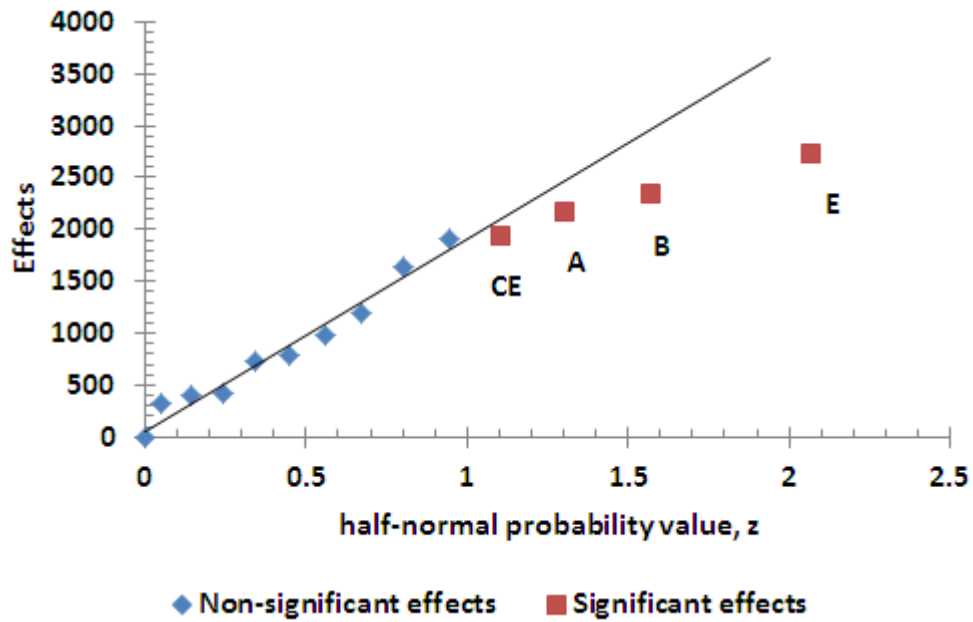


Figure 36—Half-Normal plot of the factorial effects using raw data. Significant effects are highlighted.

TABLE 19—TEST STATISTIC OF ORDERED EFFECTS (RAW DATA)

Factor	Effect	Test-statistic
AC	325	0.18
D	401	0.22
F	426	0.24
CF	735	0.41
AB	780	0.43
BC	977	0.54
AE	1204	0.67
AF	1642	0.91
C	1906	1.06
CE	1923	1.06
A	2162	1.20
B	2341	1.30
E	2722	1.51

As shown in **Table 20**, the number of effects declared to be significant is related to the significance level, α . The significance level α , is also referred to as the probability of type I error. This is defined as the probability of rejecting the null hypotheses (in this case that none of the effects is significant) when it is true. At $\alpha=0.05$, the probability that we wrongly conclude that an effect is significant is 0.05. As we can deduce, this requirement is too stringent for our dataset and none of the effects is deemed significant at this level. However at $\alpha=0.2$, closure stress and temperature are deemed to be significant. This result though comes at a cost. The probability of our erroneously concluding that one of these effects is significant is 0.2.

TABLE 20— FACTORIAL EFFECTS AT VARYING LEVELS OF SIGNIFICANCE (RAW DATA)

Level of significance, α	Significant effects
0.05	None
0.1	None
0.2	Closure stress (E), Temperature (B)
0.3	Nitrogen rate (A), CE, Polymer loading (C),

Tables 21 and 22 present the results of the analysis of the log transformed data using the Lenth's test. **Tables 23 and 24** present the results of the same procedure for the rank transformed data.

TABLE 21—TEST STATISTIC OF ORDERED EFFECTS (LOG TRANSFORMED DATA)

Factor	Effect	Test-statistic
AE	0.0181	0.03
AF	0.0375	0.07
BC	0.0542	0.10
AC	0.1684	0.31
CE	0.2079	0.39
AB	0.2137	0.40
F	0.3577	0.67
CF	0.5516	1.03
B	0.5550	1.03
D	0.6459	1.20
A	0.6660	1.24
C	0.7605	1.42
E	1.0131	1.89

TABLE 22— FACTORIAL EFFECTS AT VARYING LEVELS OF SIGNIFICANCE FOR LOG TRANSFORMED DATA

Level of significance, α	Significant effects
0.05	None
0.1	Closure Stress (E)
0.2	Polymer Loading (C), Nitrogen Rate (A)
0.3	Presence of breaker (D), Temperature (B), CF

TABLE 23—TEST STATISTIC OF ORDERED EFFECTS (RANK TRANSFORMED DATA)

Factor	Effect	Test-statistic
CE	0.25	0.11
BC	-0.25	0.11
AB	-0.25	0.11
AE	0.75	0.33
F	1	0.44
AF	1	0.44
AC	-1.5	0.67
CF	2	0.89
C	-3	1.33
B	-3.25	1.44
D	3.25	1.44
A	-4	1.78
E	-5.25	2.33

TABLE 24—FACTORIAL EFFECTS AT VARYING LEVELS OF SIGNIFCANCE FOR RANK TRANSFORMED DATA

Level of significance, α	Factorial effects
0.05	Closure Stress (E)
0.1	Nitrogen Rate (A)
0.2	Temperature (B), Polymer Loading (C), Presence of breaker (D)
0.3	None

We summarize the above analysis in **Table 25**. The remaining question is which one of these conclusions we should accept.

TABLE 25—COMPARISON OF RESULTS FOR ANALYSIS ON RAW AND TRANSFORMED DATA

Raw data	Log transformed data	Rank transformed data
Closure stress ($0.1 < \alpha < 0.2$)	Closure stress ($0.05 < \alpha < 0.1$)	Closure stress ($0 < \alpha < 0.05$)
Temperature ($0.1 < \alpha < 0.2$)	Polymer loading ($0.1 < \alpha < 0.2$)	Nitrogen rate ($0.05 < \alpha < 0.1$)
Nitrogen rate ($0.2 < \alpha < 0.3$)	Nitrogen rate ($0.1 < \alpha < 0.2$)	Presence of breaker ($0.1 < \alpha < 0.2$)
Polymer loading ($0.2 < \alpha < 0.3$)	Presence of breaker ($0.2 < \alpha < 0.3$)	Temperature ($0.1 < \alpha < 0.2$)
Proppant concentration (> 0.3)	Temperature ($0.2 < \alpha < 0.3$)	Polymer loading ($0.1 < \alpha < 0.2$)
Presence of breaker (> 0.3)	Proppant concentration (> 0.3)	Proppant concentration (> 0.3)

To help us answer this question, we check for the normality of the raw and transformed conductivity values. This is because the normality of the dataset is an implicit assumption for most of the analysis techniques that we use to analyze the data. We know that in a normal distribution, the data-points should be on or at least close to the straight line on a normal plot. **Figure 37** is the normal plot for the raw and transformed conductivity data. In this figure, we see that the raw data is clearly not normally distributed and that the log and rank transformed datasets are closer to being normally distributed. Therefore, we will focus on the log and rank transformed datasets.

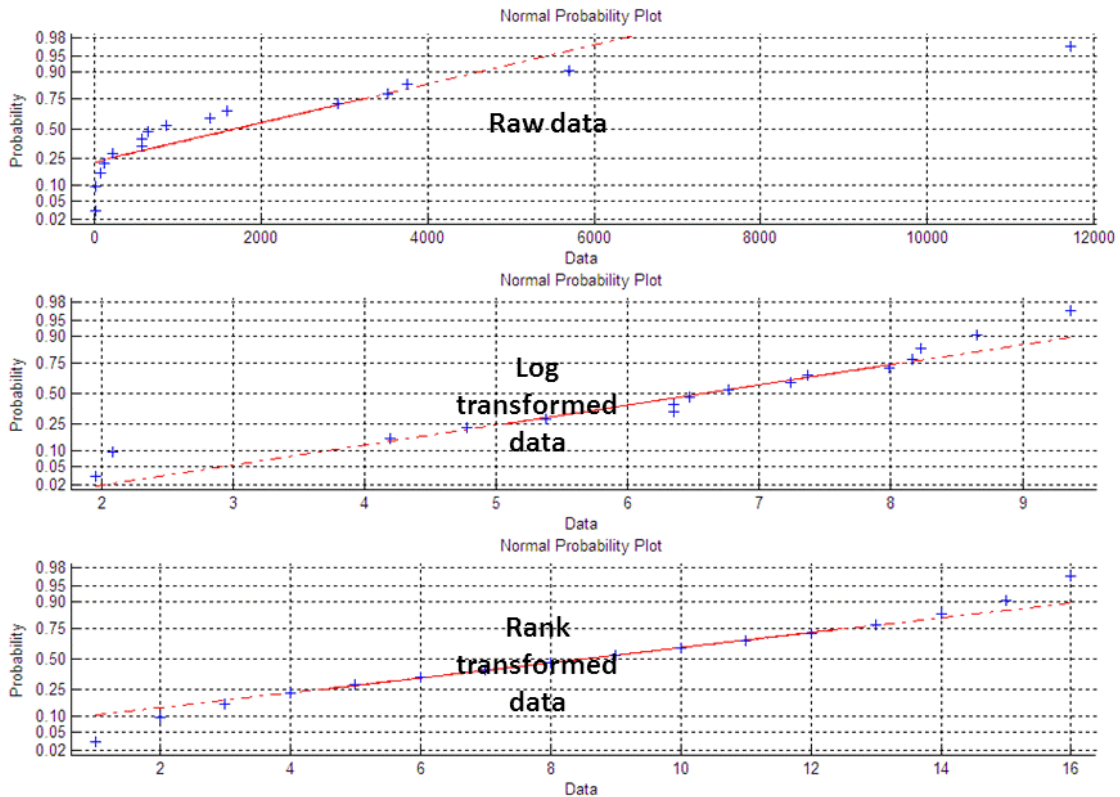


Figure 37—Normal plots for raw, logarithm and rank transformed conductivity data.

As we mentioned previously, another criterion is that we accept the analysis that offers the strongest conclusions. Based on the α -values, the analysis based on the rank transformed data provides the strongest conclusions. This fact is balanced by the observation that using rank transformed data is not a practice that is common in petroleum engineering. Therefore, we will have to consider that dataset that provides the next strongest set of conclusions—which is the log transformed dataset. Another justification for basing our analysis and hence conclusions on the log-transformed dataset is that permeability in petroleum engineering is known to be log-normally distributed. Therefore, for subsequent analysis except for the purposes of illustration, we will be using the log transformed dataset.

Discussion of Results

C.3.4 Effect of Closure Stress

Closure stress is observed to have a detrimental effect on fracture conductivity (negative slope, **Figure 38**). The estimate of fracture conductivity at 2000 psi is the average of all logarithmically transformed conductivity measurements at this closure stress. The average conductivity at 6000 psi is calculated in a likewise manner. This effect is attributed to the reduction in fracture width as closure stress is increased (**Table 26**). In Table 26, the average fracture width is reduced by a factor of 3 and 1.5 at 0.5 ppg and 2 ppg proppant concentration respectively.

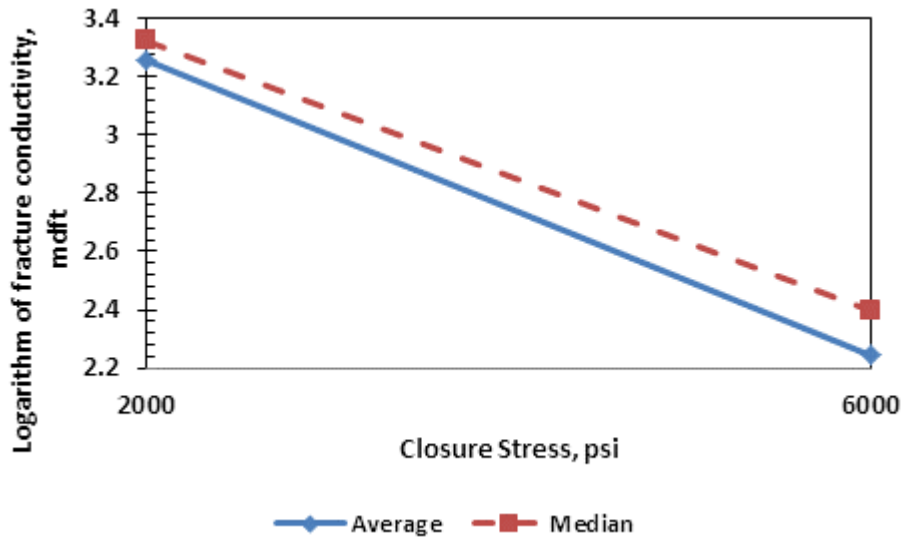


Figure 38—Dependence of fracture conductivity on closure stress.

TABLE 26—VARIATION OF LABORATORY FRACTURE WIDTH WITH CLOSURE STRESS

Proppant concentration, ppg	Closure stress, psi	Average fracture width, inches	Standard deviation of fracture width, inches
0.5	2000	0.0305	0.0237
	6000	0.0116	0.0115
2	2000	0.0691	0.0322
	6000	0.0448	0.0098

C.3.5 Effect of Reservoir Temperature

Fracture conductivity was observed to decrease with an increase in the system temperature from 150°F to 250°F. This result is counter-intuitive because our original expectation was that an increase in temperature should improve cleanup (gels have lower viscosities at higher temperatures), thereby improving fracture conductivity. What we observed though was the formation of a dense proppant-polymer cake that severely reduced conductivity at high closure stress and high temperature (**Figure 39**). The extent of the reduction in conductivity as temperature is increased is shown in **Figure 40**. An important question that needs to be answered is whether this effect occurs in field-scale fractures or whether it is a laboratory artifact unlikely to be a significant phenomenon in hydraulic fracture treatments.



Figure 39—Dehydrated polymer-proppant cake.

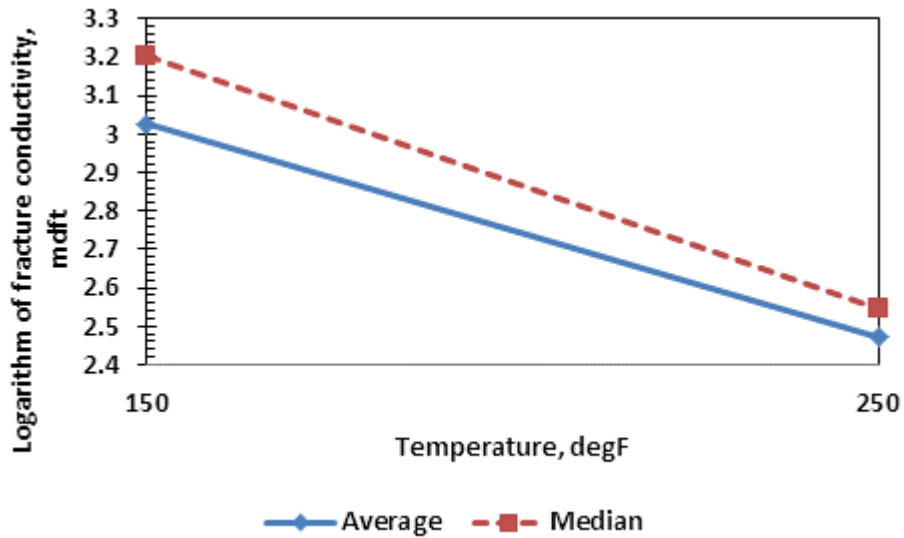


Figure 40—Dependence of fracture conductivity on temperature.

In relation to the above question, we understand that the dehydration phenomenon might not be a factor during the shut-in phase after the hydraulic fracture treatment in the reality. This is because pressure elevates the evaporation point of water. The reservoir temperatures required for evaporation to occur at the bottomhole pressures experienced by polymer fluids are extremely excessive—almost unrealistic (**Figure 41**).

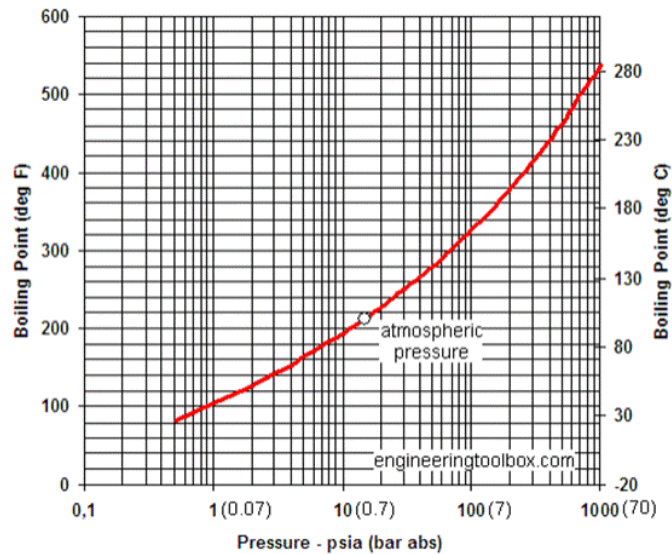


Figure 41—Boiling point of water vs. pressure (engineeringtoolbox.com).

However, during production, there is usually a pressure drawdown of several thousand psi between the reservoir and the wellbore. As a result, gas expands and the water-carrying capacity of the gas increases (**Figure 42**). This process can lead to the dehydration of polymer fluid in the fracture. We flew wet gas in all our experiments. We make the following observation from our study: the negative temperature effect can affect the performance of field-scale fractures and should be considered while designing fracture treatments.

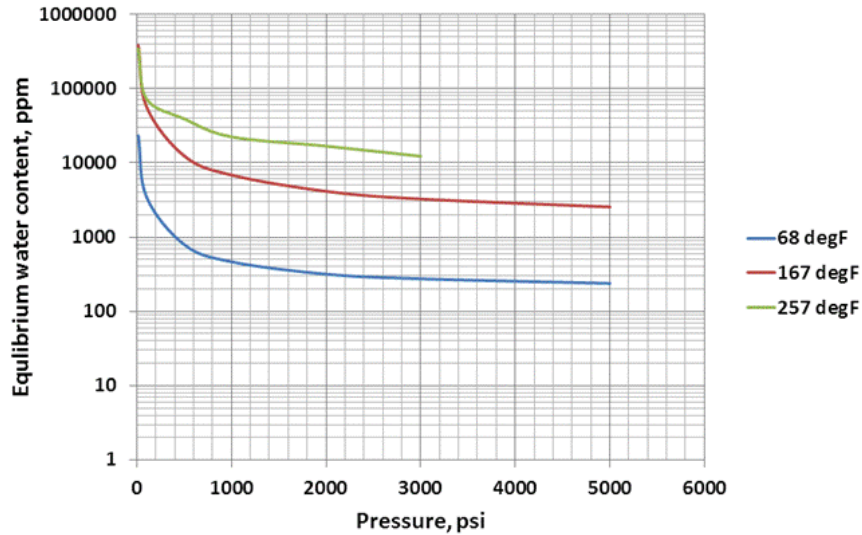


Figure 41—Equilibrium water content of methane gas vs. pressure (data plotted from Downs, 2009).

C.3.6 Effect of Nitrogen Rate

Based on our results, we see that an increase in nitrogen rate leads to a drastic reduction in conductivity (**Figure 43**). We believe this result is related to the explanation for the negative effect of temperature; that is, the dehydration of polymer fluid due to evaporation induced by gas expansion. Mahadevan et al. (2005) reported that fracture cleanup in gas reservoirs is primarily because of two mechanisms, namely, displacement and evaporation of water due to gas expansion. In their study, evaporation had a beneficial effect as it reduced the water saturation in the wellbore region. Le and Mahadevan (2011) presented their work on the productivity loss experienced in gas wells as a result of salt deposition. They pointed out that in some wells, the production of gas can result in drying of the near wellbore region. The cause of the dehydration was gas expansion.

Currently, the predominant narrative for explaining fracture cleanup or lack thereof is that at some point in a long fracture, the pressure gradient across the fracture face will be insufficient to overcome the yield stress of the unbroken fluid in the fracture. From that point to the fracture tip, the fracture fluid essentially stays immobile. This narrative essentially describes a displacement process.

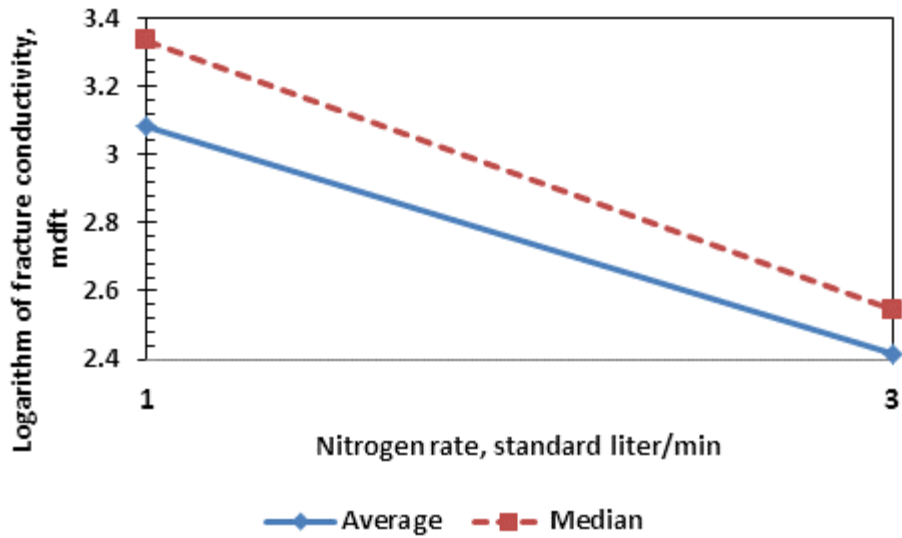


Figure 43—Dependence of fracture conductivity on nitrogen rate.

What our experiments suggested is that fracture fluid displacement by gas might not be the only mechanism operating during the cleanup of gas wells. Evaporation as a result of gas expansion might also be a factor affecting the cleanup of fractures in gas reservoirs. It is noted that the evaporation process in fractures will be detrimental to fracture conductivity. This is because the dehydrated polymer will reduce the porosity, and, by extension, the permeability of the proppant pack in the fracture. We further explain this hypothesis by the use of **Figure 44**.

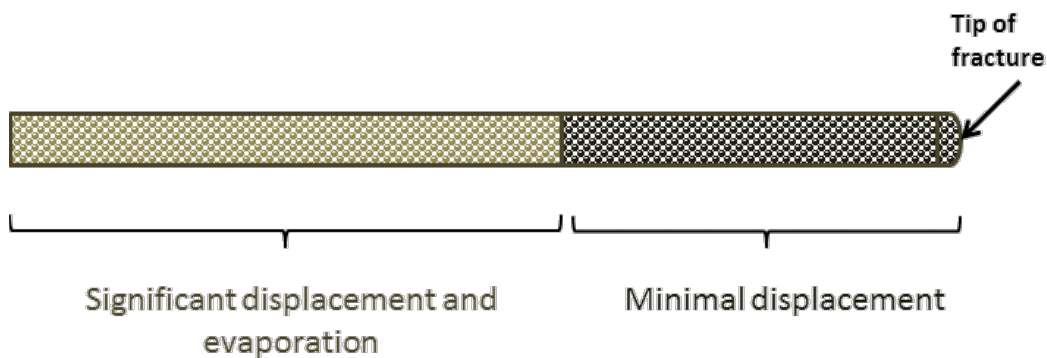


Figure 44—Representation of fracture with potential mechanisms that can affect cleanup.

In Figure 44, we hypothesize that the section of the fracture that contains high yield stress fracture fluid will experience minimal displacement. This is because the pressure gradient is below the critical value required to overcome the yield stress. However, the portion of the fracture that is cleaning up will experience both displacement and evaporation. This is because the pressure drop is large enough to overcome the yield stress of the fluid. Also, because of the pressure drop (as stated above), gas expands and evaporation occurs. Our fracture cleanup paradigm thereby changes from a purely displacement based process to one that is based on both displacement and evaporation.

In the filter cake cleanup section, we discussed that a critical flow rate exists for filter cake displacement. The results indicated that higher flow-rates generally lead to higher cleanup efficiencies. However, our conclusion from this part of the study is in disagreement with the conclusion from the filter cake cleanup section. We believe that the gas flowback rate is an important factor in fractured well performance. It is not a simple “the higher, the better” matter. Aggressive flow-back rate schedules might have a negative effect on conductivity and this should be investigated in field practices.

C.3.7 Effect of Polymer Loading

An increase in polymer loading predictably reduced the conductivity of the proppant pack. This is no surprise as this has been reported by investigators from Cooke (1975) to Wang et al. (2010). The extent of reduction is shown in **Figure 45**. As discussed in previous cases, both the mean and median were used as measures of central tendency at the low and high ends of polymer loading.

C.3.8 Effect of the Presence of Breaker

Increased conductivities are obtained when breaker is added to the fracturing fluid as shown in **Figure 46**. The effect of breaker is less noticeable in some cases at high temperatures because of polymer dehydration.

C.3.9 Effect of Proppant Concentration

If our analysis is based on the mean of the raw conductivity data, we see that conductivity increases with decrease in proppant concentration (**Figure 47**). The result

however, should be viewed in the light of the following facts; (1) The amount of proppant in the cell varies for the same slurry due to issues related to the transport properties of the fluid and the back-pressure imposed at the pump (**Table 27**) and (2) approximately 80% of the experiments run at the low loading of 0.5 ppa contain channels and void spaces that are more conducive while only approximately 20% of the experiments run at the high loading of 2 ppa contain channels and void spaces. **Figure 48** depicts an example of this phenomenon. Given that only high strength proppant was tested in this study, these results show that channels are more likely to develop in experiments run at low proppant loading (consistent with the partial monolayer concept). If strong proppants are used, conductivities from treatments run at low proppant concentrations might exceed those run at high proppant concentrations.

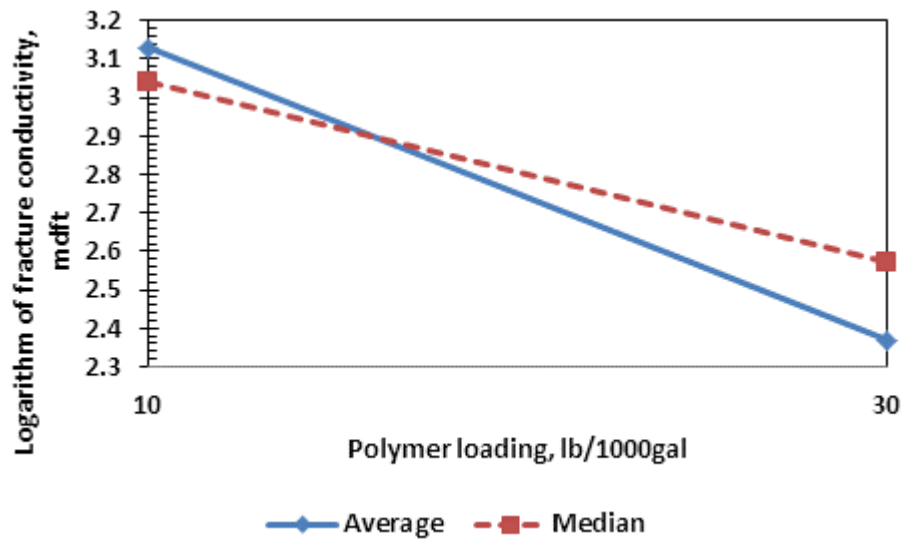


Figure 25—Dependence of fracture conductivity on polymer loading.

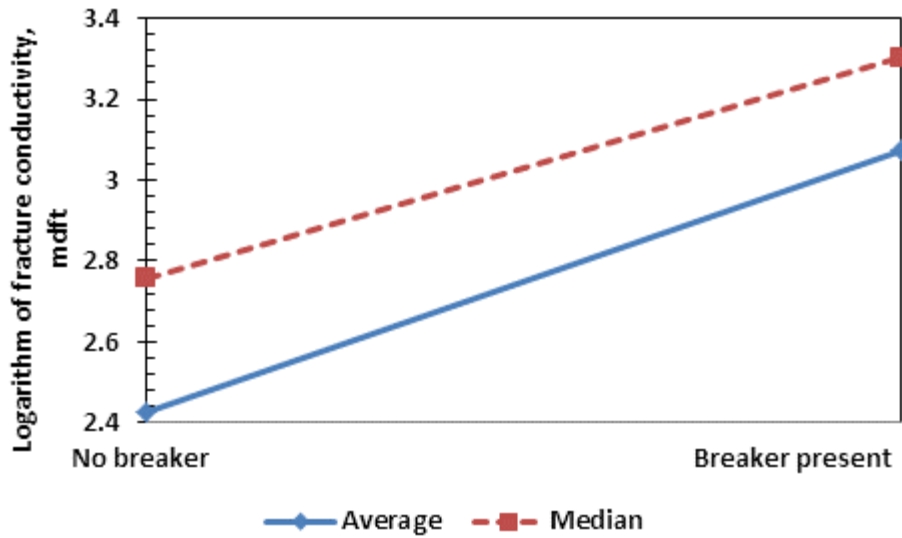


Figure 46—Dependence of fracture conductivity on the presence or absence of breaker.

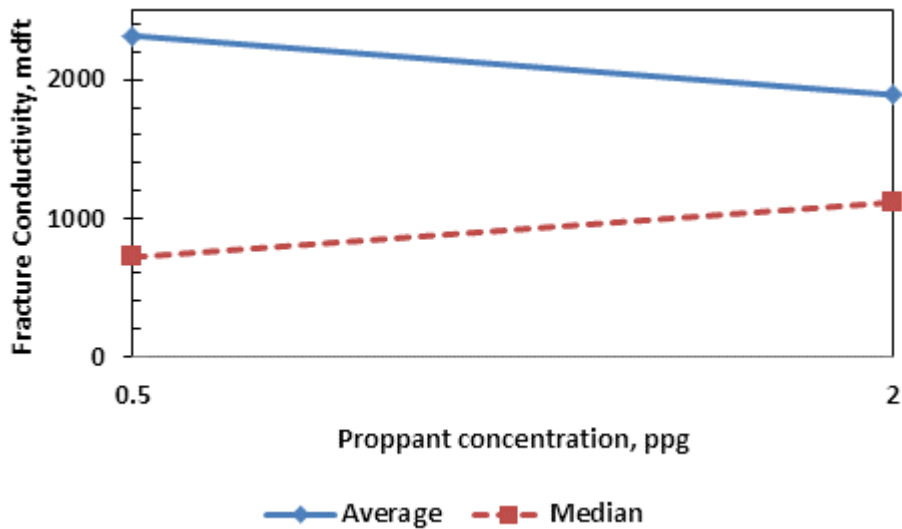


Figure 47—Dependence of fracture conductivity on proppant concentration, using raw conductivity data.

However, if the analysis is done using the mean/median of the logarithm transformed data or even the median of the raw data, fracture conductivity has a proportional relationship with proppant concentration as expected (Figure 49).

TABLE 27—VARIATION OF PROPPANT MASS IN CONDUCTIVITY CELL

Proppant concentration, ppg	Number of experiments used in analysis	Average mass per square area, lb/ft ²	Standard deviation of mass per square area, lb/ft ²
0.5	9	0.156	0.082
2	10	0.402	0.163

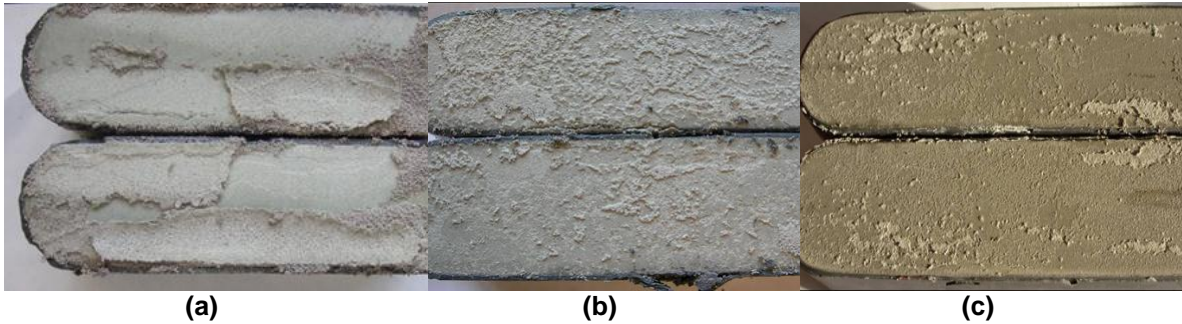


Figure 48—No channels, high closure stress and temperature, conductivity ~ 60 md-ft, 2ppa (a). No channels, high closure stress and temperature, conductivity ~ 10 md-ft, 0.5 ppg (b). Void spaces present, high closure stress and temperature, conductivity ~ 2500 md-ft, 0.5 ppg(c).

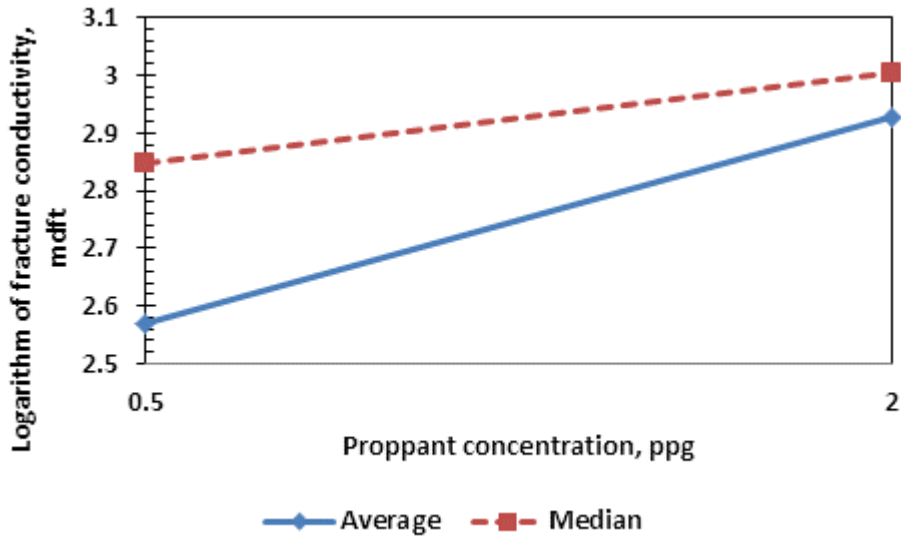


Figure 49—Dependence of fracture conductivity on proppant concentration.

C.3.10 Using Proppant Concentration as a Blocking Variable

While discussing the effect of proppant concentration, we established that conductivity measured from experiments run at 0.5 ppa are dominated by channels and

have high porosities reminiscent of partial mono-layer packs, while those run at 2 ppa do not have these channelized features. This leads to question if our general conclusions would still hold if we separated our dataset into two blocks and thereafter, analyzed the two blocks of experimental data separately. In design of experiment terms, this is analogous to using proppant concentration as a blocking variable. **Tables 28 and 29** are the experimental data at 0.5 ppa and 2 ppa, respectively.

TABLE 28—RESULTS FOR EXPERIMENTS RUN AT LOW PROPPANT CONCENTRATION

Treatment #	Number of replications	Mean Conductivity, mdft	Standard deviation, mdft
2	3	3757	2046
4	1	8	Not Applicable
5	2	868	818
7	3	571	569
9	1	216	Not Applicable
11	1	7	Not Applicable
14	3	1385	1038
16	2	11730	2376

*Not Applicable implies treatment had only one replicate

TABLE 29—RESULTS FOR EXPERIMENTS RUN AT HIGH PROPPANT CONCENTRATION

Treatment #	Number of replications	Mean Conductivity, mdft	Standard deviation, mdft
1	2	570	57
3	4	3521	830
6	2	643	294
8	1	66	Not Applicable
10	1	118	Not Applicable
12	2	5700	43
13	1	1587	Not Applicable
15	1	2927	Not Applicable

*Not Applicable implies treatment had only one replicate

Using the logarithm of the conductivity data, we computed the effects estimate for these 2 blocks of data. The results are presented in **Figures 50 and 51**.

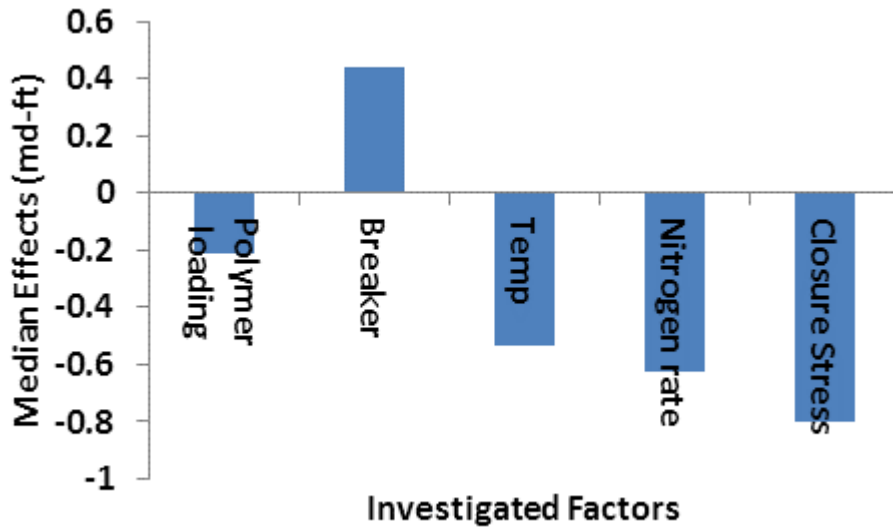


Figure 50—Effect of investigated factors at high proppant concentration.

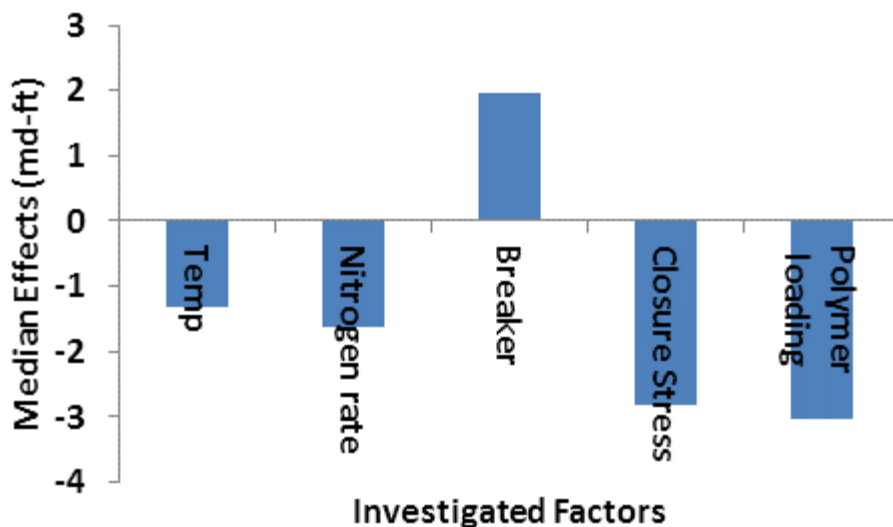


Figure 51—Effect of investigated factors at low proppant concentration.

As Figure 50 shows, at high proppant concentrations, the three most important effects are closure stress, nitrogen rate and temperature. This conclusion is similar to the conclusion reached if blocking was not applied. However, at proppant loadings of 0.5 ppa (Figure 51), the polymer loading and the presence of breaker supplants nitrogen rate and temperature as the most important factor. This underlines the importance of effective breaker design especially in fracturing operations with low proppant concentrations and also provides support for slickwater fracturing.

C.3.11 Interaction Effects

An example interaction effect is the one between the polymer loading and the proppant concentration as shown in **Figure 52**. An interesting feature that we noticed is that at high proppant concentrations, polymer loading seems to have minimal effect on conductivity. However at low proppant concentrations, we see that polymer loading has more significant effect on fracture conductivity. **Table 30** details the interaction effects we consider to be important and why we think so. These reason(s) are related to experimental design principles and our engineering judgment. Three-factor interactions and higher are ignored in this analysis. For the sake of completeness, we will include plots of all the interaction effects for the log transformed data in **Appendix B**.

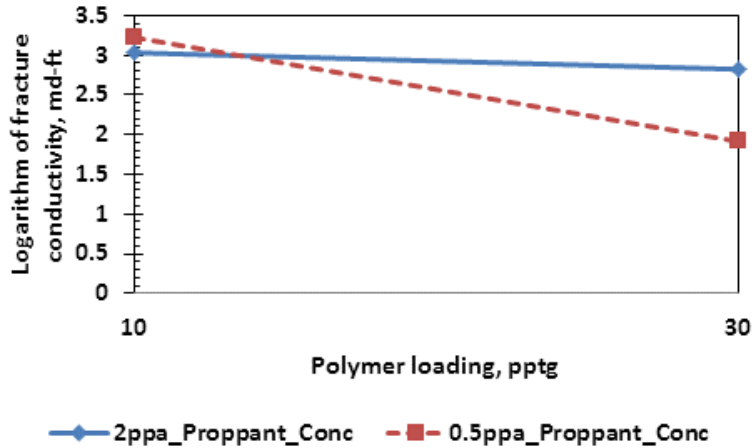


Figure 3—Interaction effect between polymer loading and closure stress.

TABLE 30—CRITERIA FOR IGNORING INTERACTION EFFECTS

Alias Combination	Selected Interaction effect	Reason(s)
CF, DE	CF	The polymer loading affects the proppant transport characteristics of the polymer. It makes more engineering sense for there to be interaction between them than between the presence of breaker and closure stress.
CE, DF	*CE	The combination of polymer loading and closure stress is of higher relative importance when compared with the combination of the presence of breaker and proppant concentration.
AF, BE	*BE	The combination of both temperature and closure stress is of higher relative importance when compared with the combination of nitrogen rate or proppant concentration.
AE, BF	*AE	The combination of nitrogen rate and closure stress is of higher relative importance when compared with the combination of proppant concentration and temperature.
BC, AD	BC	It makes more engineering sense for both temperature and polymer loading to interact.
AC, BD	*AC	The combination of nitrogen rate and polymer loading is of higher relative importance when compared with the combination of the presence of breaker and temperature.
AB, CD, EF	*CD	The combination of the polymer loading and presence of breaker is of higher relative importance when compared with either the nitrogen rate/temperature combination or the closure stress/ proppant concentration combination.

*by the effect heredity principle

Summary—Dynamic Fracture Conductivity Experiments

In previous sections, we have analyzed the raw, logarithm and rank transformed datasets. We decided to focus on the results from the log transformed dataset set because:

1. The logarithm of the conductivity dataset is normally distributed, which satisfies a major requirement of the analysis techniques we use in this study.
2. It makes physical sense because permeability is log-normally distributed and conductivity is a function of permeability. Therefore, we expect conductivity to be log-normally distributed.

The signs of the factorial effects do not change for both the raw and log-transformed datasets. However, the relative importance of the factors is seen to depend on the dataset analyzed. For this work, we think the analysis results from the log-transformed data hold more weight. As such, the effects of the investigated factors arranged in order of decreasing impact on conductivity are closure stress, polymer loading, flow back rate, presence of breaker, temperature and proppant concentration.

Over the last 30 years, industry has worked towards the consistent measurement of fracture conductivity. The API standard was developed based on that notion. In the static measurement of fracture conductivity, the proppant is carefully placed according to a standard concentration ($2\text{lb}/\text{ft}^2$) in most cases. For the purposes of evaluating proppant, this is the best practice. In this study, in order to simulate field treatment conditions, we flow slurry through a laboratory fracture instead of placing the proppant in a static manner. The results from the dynamic experiments show the stochastic nature of fracture conductivity data. This study provided critical insights necessary for us to be able to evaluate current methods of conductivity measurement. Observations such as channel formation and filter cake dehydration are issues that might have great relevance in field practice. Gel damage is a dynamic phenomenon, and the methodology developed in this study provided for researchers the ability to be able to examine the interacting effects of multiple parameters under conditions that attempt to mimic field operating conditions.

D. Results and Discussion—Theoretical Methods

It is common knowledge that hydraulically fractured tight-gas wells do not perform up to their potential because of slow or incomplete fracture fluid cleanup. A number of papers have been written to address individual factors related to fracture-fluid cleanup, but many questions as to which factors mostly affect gas production from such wells remain unanswered. Numerical reservoir simulation is one of the methods to study the fracture-fluid-cleanup problem and we used reservoir simulation to analyze systematically the factors that affect fracture fluid cleanup and gas recovery from tight-gas wells. We first developed a comprehensive data set for typical tight gas reservoirs and then ran single-phase-flow cases for each reservoir and fracture scenario to establish the idealized base-case gas recovery. We then systematically evaluated the following factors: multiphase gas and water flow, proppant crushing, polymer filter cake, and, finally, yield stress of concentrated gel in the fracture. The gel in the fracture is concentrated because of fluid leakoff during fracture treatments. We evaluated these factors additively in the order listed. We found that the most important factor that reduces fracture-fluid cleanup and gas recovery is the gel strength of the fluid that remains in the fracture at the end of the treatment. This part of the work illustrates the complexity of the fracture-fluid cleanup problem and points out the need to use reservoir simulation and to include all the pertinent factors to model fracture-fluid cleanup rigorously. The procedures presented can provide a useful, systematic guide to engineers in conducting a numerical simulation study of fracture-fluid cleanup. The following sub-sections (**D.1.1 to D.1.6**) are a summary of our work. For sub-section D.2, we developed a micro pore-scale model to mimic the real porous structure in a proppant pack. The relationship between pressure gradient and superficial velocity was investigated under the influence of primary parameters such as yield stress, power-law index, consistency index, and the proppant diameter. The Herschel-Bulkley model was used with an appropriate modification proposed by Papanastasiou (1987) to mitigate numerical difficulties.

D.1 Modeling Fracture-Fluid Cleanup in Tight-Gas Wells

D.1.1 Effect of Two-Phase Flow

The information presented under this section is not novel; however, this step is needed because subsequent analysis requires it. The assumption is that a hydraulic fracture has been created and the fracture-fluid filtrate that leaks off into the formation has the same properties as formation water. Therefore, after a fracture treatment, the region surrounding the fracture is saturated by the water phase. The presence of this region temporarily inhibits the gas from flowing into the fracture. There is a time lag before maximum production is reached because of the cleanup process. **Figure 53** shows the gas-production rate vs. time after a fracture treatment for different fracture conductivities for the two-phase flow scenario, where $L_f = 528$ ft, $p_r = 3,720$ psi, $k = 0.1$ md, $S_{wi} = 0.4$, and $h = 25$ ft. We can see that the gas-production rate increases for a period of time before it reaches a maximum value, which corresponds to the cleanup time. For a dimensionless fracture conductivity of 0.1, which is a very-low-conductivity fracture, the gas-production rate is much lower during the first 3 years of production. **Figure 54** shows cumulative gas production vs. time for the same scenario. We can see that cumulative gas production will be higher if the fracture conductivity is higher. If the fracture conductivity can be increased from 0.1 to 10, the cumulative gas production will increase by 36% in 10 years, which is approximately 0.325 Bcf for a well on 160-acre spacing. Thus, strong proppants and high fracture conductivity are critical to the success of fracture treatments and long-term gas production. However, from a production point of view, a proppant that can provide dimensionless fracture conductivity of 10 is good enough when only two-phase flow is considered and the fracture fluid-filtrate viscosity is the same as the formation water. The assumption that the filtrate viscosity is the same as formation water is quite reasonable. This is because laboratory tests have confirmed this assumption.

Figure 55 shows the gas-production rate vs. time at different values of fracture conductivity after a fracture treatment when $L_f = 528$ ft, $p_r = 1,860$ psi, $k = 0.1$ md, $S_{wi} = 0.4$, and $h = 25$ ft. The difference here from the prior example is that the reservoir pressure is only 1,860 psi. We can see that the gas-production rate increases for a period

of time before it reaches a maximum value, corresponding to the cleanup time. For this low-pressure case, one can clearly see the effect of fracture conductivity upon fracture fluid cleanup. We normally try to design for a C_r of 10 or better. In Figure 54, the early gas-flow rate for a C_r of 10 is approximately 2,000 Mscf/D and peaks at approximately 4,000 Mscf/D after 1 day. For the infinite-fracture-conductivity case ($C_r = 100$), the gas-flow rate starts at 8,000 Mscf/D, and declines to approximately 5,000 Mscf/D after 1 day. Thus, after a few days, $C_r = 10$ and $C_r = 100$ behave very similarly. The cleanup for this scenario in Figure 54 is similar to the higher-pressure scenario in Figure 52, but, at the same fracture conductivity, the cleanup time is longer and the gas-flow rate is lower. This implies that reservoir energy is a very important factor in analysis of fracture-fluid cleanup.

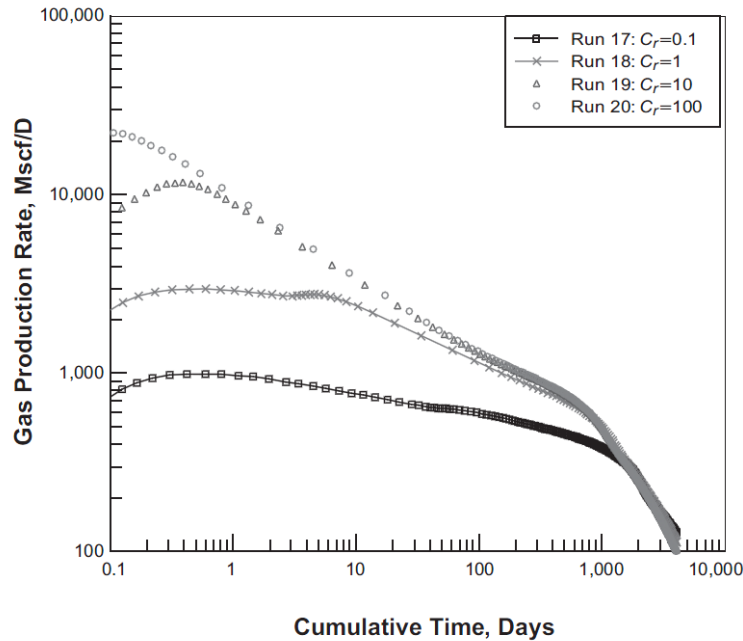


Figure 53—Gas-production rate at different fracture conductivity, where $L_f = 528$ ft, $p_r = 3,720$ psi, $k = 0.1$ md, $S_{wi} = 0.4$, and $h = 25$ ft.

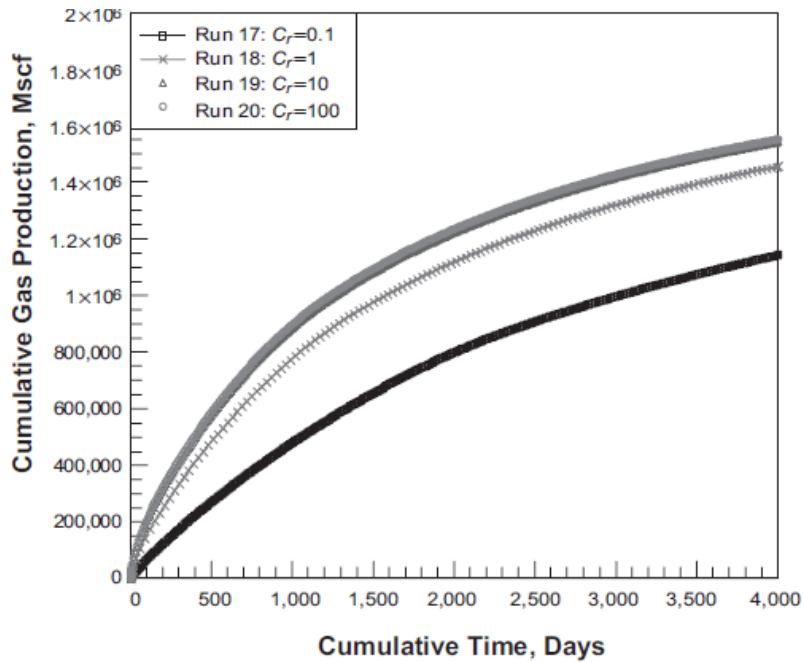


Figure 54—Cumulative gas production at different fracture conductivity, where $L_f = 528$ ft, $p_r = 3,720$ psi, $k = 0.1$ md, $S_{wi} = 0.4$, and $h = 25$ ft.

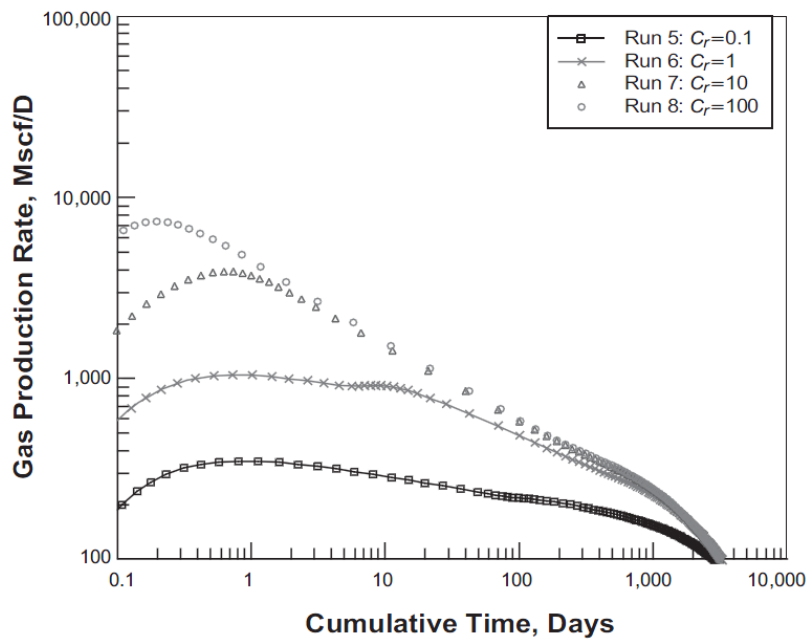


Figure 55—Gas-production rate at different fracture conductivity, where $L_f = 528$ ft, $p_r = 1,860$ psi, $k = 0.1$ md, $S_{wi} = 0.4$, and $h = 25$ ft.

D.1.2 Effect of Proppant Crushing

In this section, we build upon the results from the previous computer runs for two-phase gas/water flow by adding the effect of proppant crushing. It is well known that the value of fracture conductivity will decrease as the closure pressure on the proppant increases. We can model these effects, and we generally call this “proppant crushing.” When we include proppant crushing, the effect is additive, and our analysis of cleanup becomes more complex and more realistic. Proppant crushing was simulated by incorporating the stress dependence of proppant permeability into the reservoir simulator. **Figure 56** shows the gas production rate vs. time for different values of fracture conductivity after a fracture treatment with $L_f = 528$ ft, $p_r = 3,720$ psi, $k = 0.1$ md, $S_{wi} = 0.4$, and $h = 25$ ft. For a fracture conductivity of 0.1, the gas-production rate is much lower during the first 3 years of production. We normally try to design for a C_r of 10 or larger. In **Figure 55**, the early gas-flow rate for a C_r of 10 is approximately 4,000 Mscf/D and peaks at approximately 8,000 Mscf/D after 1 day. For the infinite-fracture-conductivity case ($C_r = 100$), the gas-flow rate starts at 20,000 Mscf/D and declines to approximately 10,000 Mscf/D after a few days. Thus, after a few days, $C_r = 10$ and $C_r = 100$ behave very similarly. **Figure 57** shows cumulative gas production vs. time for the same scenario. Cumulative gas production will be higher if the fracture conductivity is higher. However, the cumulative gas production does not differ much once the fracture conductivity is greater than 10. If the fracture conductivity can be increased from 0.1 to 10, the cumulative gas production will be increased by 50% in 10 years, which is approximately 0.5 Bcf for one well on 160-acre spacing. For a lower-reservoir-pressure scenario ($p_r = 1,860$ psi), the production performances are similar to **Figure 56** and **57**. The early gas-flow rate for a C_r of 10 is approximately 1,400 Mscf/D and peaks at approximately 3,000 Mscf/D after 1 day. For infinite fracture conductivity ($C_r = 100$), the gas-flow rate starts at 4,500 Mscf/D, increases to 7,000 Mscf/D, and then declines to approximately 4,000 Mscf/D after 1 day. Thus, after a few days, $C_r = 10$ and $C_r = 100$ behave very similarly. If the dimensionless fracture conductivity can be increased from 0.1 to 10, the cumulative gas production will increase by 68% in 10 years, which is approximately 0.08 Bcf for one well on 160-acre well spacing. Thus, strong proppants and high fracture conductivity are critical to the success of fracture treatment and long-

term gas production for high and low reservoir pressures. At the same fracture conductivity, the cleanup time is longer, the gas rate is lower, and the cumulative gas production is lower for the lower reservoir pressure. This means that reservoir energy is a very important factor in analysis of fracture-fluid cleanup, as one would expect.

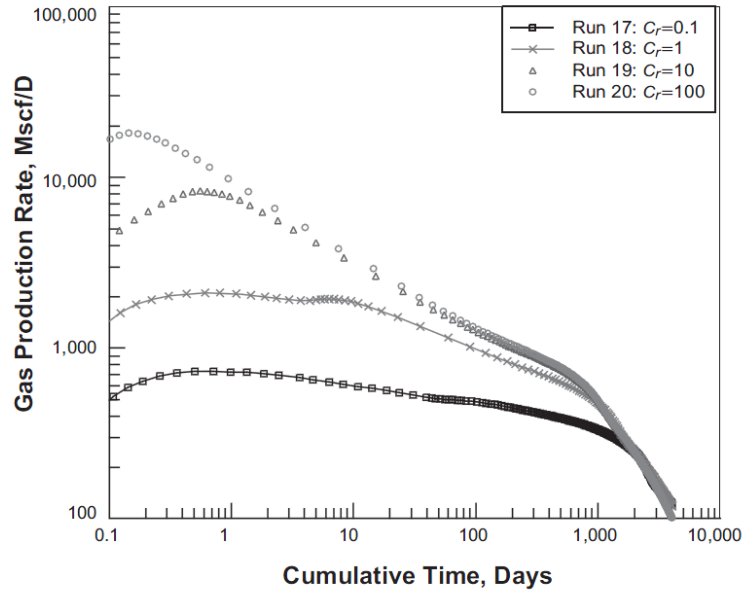


Figure 56—Gas-production rate at different fracture conductivity, where $L_f=528$ ft, $p_r=3,720$ psi, $k=0.1$ md, $S_{wi}=0.4$, and $h=25$ ft-effect of proppant crushing.

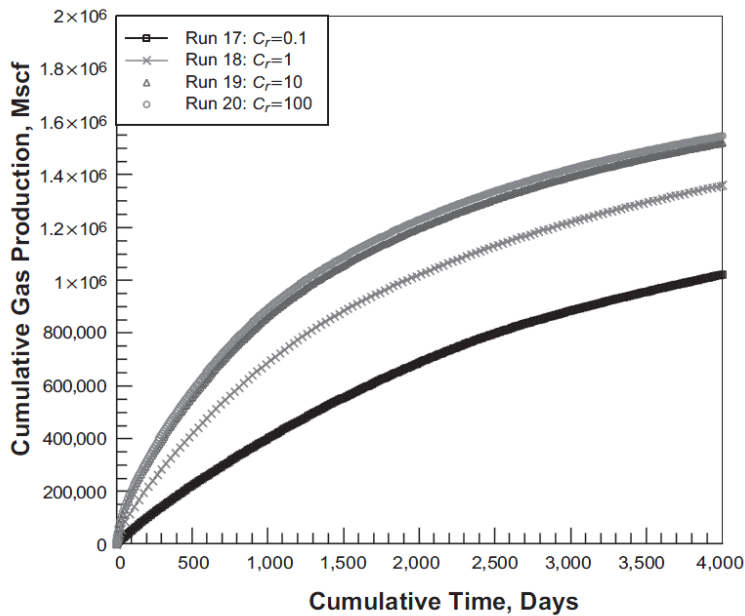


Figure 57—Cumulative gas production at different fracture conductivity, where $L_f=528$ ft, $p_r=3,720$ psi, $k=0.1$ md, $S_{wi}=0.4$, and $h=25$ ft-effect of proppant crushing.

D.1.3 Effect of Polymer Filter Cake

In this section, we add the effect of a polymer filter cake inside the fracture pack to the previous simulations of two-phase, gas/water flow with proppant crushing. The filter-cake properties, such as porosity and permeability, are assumed to be constant with time, which would be the case for filter cake not being removed during cleanup. The presence of the filter cake in our simulation is modeled as equivalent to a reduction of fracture width, which, in turn, directly reduces fracture conductivity.

Figure 58 shows the gas-production rate vs. time for different cases after a fracture treatment for Run 18 and Cases 1 through 5, where $L_f = 528$ ft, $p_r = 3,720$ psi, $k = 0.1$ md, $C_r = 1$, $S_{wi} = 0.4$, and $h = 25$ ft. We can see that the effect of filter cake does reduce the gas-production rate during early time. After 30 days, there is not much difference between the curves with and without filter cake. If the filter-cake thickness is minimal ($< 25\%$), the effect on gas production will be minimal. The filter cake does not make much difference on the cumulative gas production compared to the Case 3 without filter cake for this scenario.

Figure 59 shows gas-production rate vs. time at different fracture conductivities for Case 4 and Runs 17 through 20, where $L_f = 528$ ft, $p_r = 3,720$ psi, $k = 0.1$ md, $S_{wi} = 0.4$, and $h = 25$ ft. The fracture cleans up faster if the fracture conductivity is higher, but, after approximately 3 years, there is not much difference between the cases except for $C_r = 0.1$. For a dimensionless fracture conductivity of 0.1, the gas-production rate is much lower during the first 3 years of production. Cumulative gas production will be higher if fracture conductivity is higher but does not differ much once the dimensionless fracture conductivity is greater than 10 (**Figure 60**).

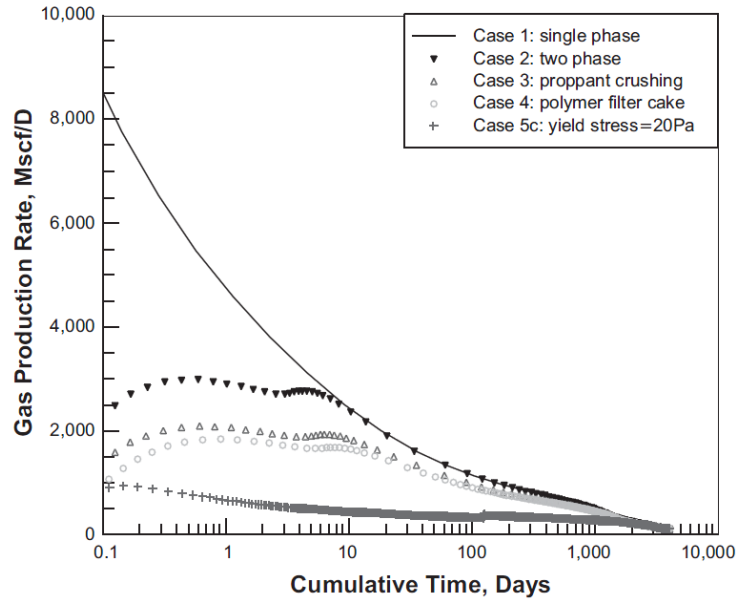


Figure 58—Gas-production rate for different cases for $C_r=1$, where $L_f=528$ ft, $p_r=3,720$ psi, $k=0.1$ md, $S_{wi}=0.4$, and $h=25$ ft-effect of polymer filter cake.

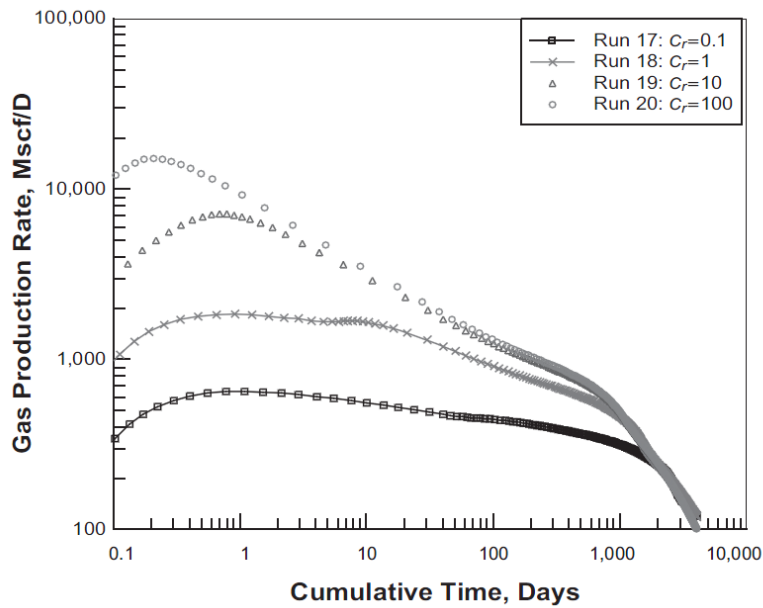


Figure 59—Gas-production rate at different fracture conductivity, where $L_f=528$ ft, $p_r=3,720$ psi, $k=0.1$ md, $S_{wi}=0.4$, and $h=25$ ft-effect of polymer filter cake.

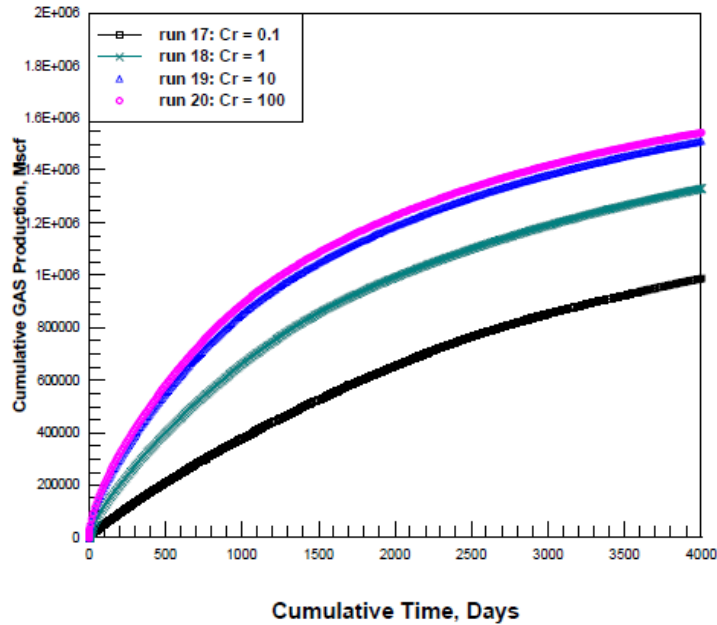


Figure 60—Cumulative gas production for different fracture conductivities, where $L_f = 528$ ft, $p_r = 3,720$ psi, $k = 0.1$ md, $S_{wi} = 0.4$, and $h = 25$ ft-effect of polymer filter cake.

D.1.4 Effect of Gel Damage

We now model three phases: gas, formation water, and unbroken fracture fluid. The fracture fluid that leaks off is considered to be the same phase as the formation water. The gel remaining in the proppant pack is the third phase. The reservoir is assumed to have gas and water phases initially, and the third phase—fracture fluid in the proppant pack—is injected during the fracture treatment. The simulation results have been compared to those in Cases 1 through 5 to see the effects of gel damage on fracture-fluid cleanup and gas recovery. Our simulator also enables the study of gel damage by considering static yield stress, flowing yield stress, fracture plugging by polymer residue, and formation of filter cake. To model polymer residue, the ratio of the damaged to original fracture permeability is correlated to the fraction of pore space occupied by the residue, which is gel saturation. For each grid block, the fracture permeability and porosity were recalculated using this correlation.

Figure 61 shows the gas rate vs. time for Cases 1 through 5 for $L_f = 528$ ft, $p_r = 3,720$ psi, $k = 0.1$ md, $C_r = 1$, $S_{wi} = 0.4$, and $h = 25$ ft. The gas-production rate becomes lower as additional factors have been considered from Case 1 to Case 5. If the gel has a yield stress of 20 Pa or more, the gas-flow rate never peaks and remains much lower compared to Cases 1 through 4. For Case 2 (two-phase flow), gas rate takes

approximately 10 days, and, for Case 3 (proppant crushing), it takes approximately 1,000 days to reach single-phase flow. So, when more factors are considered, the cleanup process takes longer and results should be more realistic. These concepts should help both researchers and engineers better understand how the cleanup process occurs in real wells. The cleanup process is highly dependent on the conductivity of the hydraulic fracture. The conductivity of the fracture on the other hand, depends heavily on the yield stress of the broken fracture fluid. The most important learning point from this section of the work is that engineers should design the breaker schedules not only based on the polymer concentration in the fracture fluid, but based on the polymer concentration in the filter-cake.

Figure 61 shows the cumulative gas production vs. time for the same scenario as Figure 57. Over 10 years, proppant crushing reduces the cumulative gas production to 93% of the ideal case, the addition of filter cake does not make much difference, but the inclusion of gel yield stress of 20 Pa in the fracture will reduce cumulative gas production to 63% of the ideal single-phase case. **Figure 62** shows the effect of yield stress on cumulative gas production.

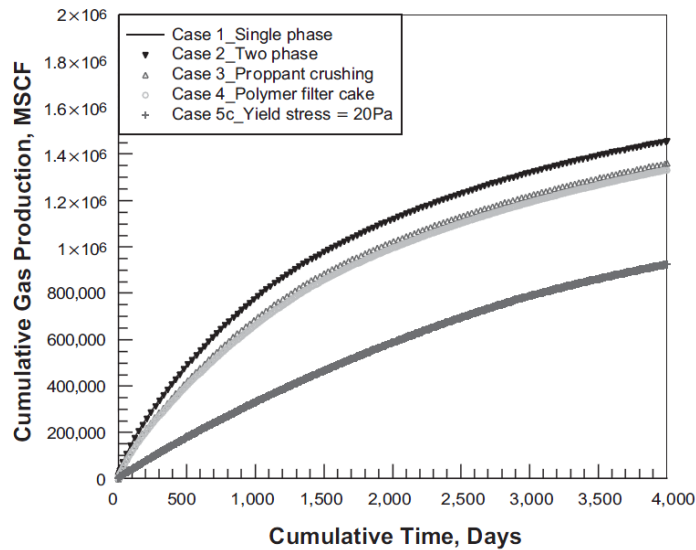


Figure 61—Cumulative gas production for different cases for $C_r=1$, where $L_f=528$ ft, $p_r=3,720$ psi, $k=0.1$ md, $S_{wi}=0.4$, and $h=25$ ft-effect of gel damage.

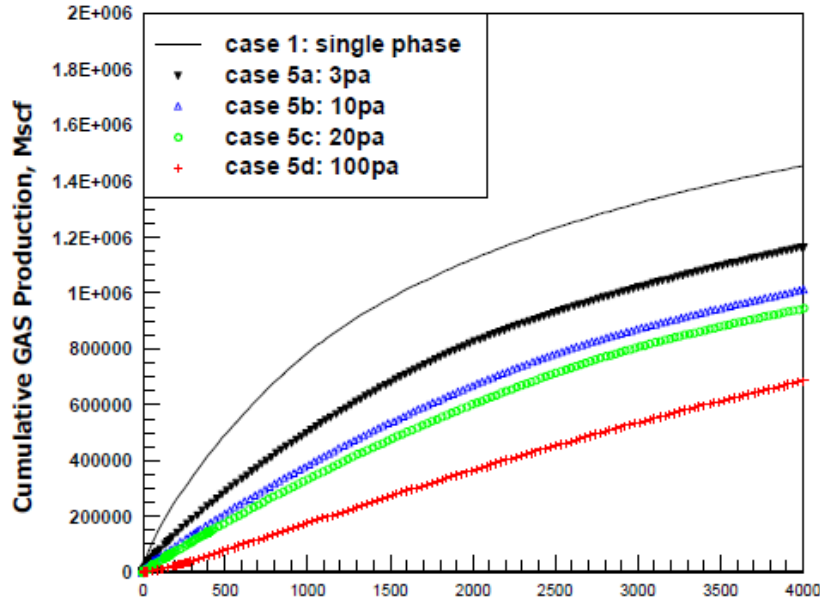


Figure 62—Cumulative gas production for different cases for $C_r=1$, where $L_f=528$ ft, $p_r=3,720$ psi, $k=0.1$ md, $S_{wi}=0.4$, and $h=100$ ft—effect of varying yield stress.

D.1.5 Effect of Yield Stress of Fracture Fluid

Yield stress is simulated in an identical manner to gel damage. Fractures clean up faster and gas-flow rates are higher for a lower value of yield stress (**Figures 61 through 63**). Even a small yield stress of 3 Pa reduces the gas production rate. From our laboratory experiments, polymer concentrations in the filter cakes range from about 400 lbm/1000gal to approximately 700 lb/1000gal. However, we have yield stress data for fracture fluids up to 200lbm/1000gal loading only. Still, at this loading, the yield stress is between 0 and 5 Pa depending on the efficacy of the breaker schedule. For $L_f = 528$ ft, $p_r = 3,720$ psi, $k = 0.1$ md, $C_r = 1$, $S_{wi} = 0.4$, and $h = 25$ ft, cumulative gas production will increase by 0.5 Bcf for a well on 160-acre spacing in 10 years if the yield stress is reduced from 100 to 3 Pa. For a similar scenario with lower reservoir pressure ($p_r = 1,860$ psi), the incremental cumulative gas production is 0.2 Bcf per well in 10 years. Gel damage with a yield stress of 20 Pa reduces the cumulative gas production to 63% and 50% of the ideal single-phase production for these two scenarios (reservoir pressure of 3,720 psi and 1,860 psi), respectively (Figure 62). Fracture fluid with yield stress that remains in the fracture will require much reservoir energy to clean up. Gel remaining in the fracture is probably the most important problem affecting fracture-fluid cleanup. We recommend for the industry to design and begin using fracturing fluids that can degrade

effectively, ideally to a Newtonian fluid, so that fractures can clean up effectively and productivities of fractured wells can be increased.

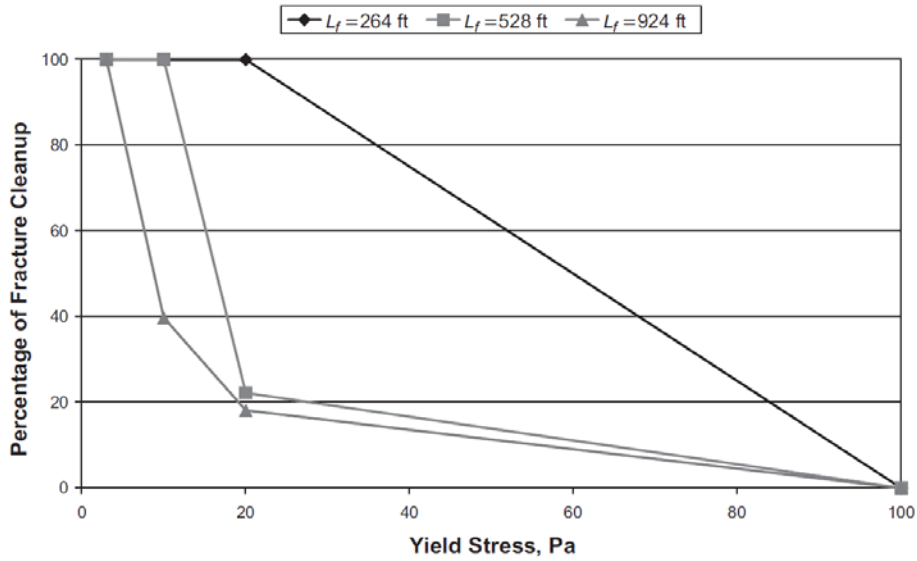


Figure 63— Percentage of fracture that cleans up 1 year after a fracture treatment vs. different yield stress at different L_f , where $p_r = 3,720$ psi, $k = 0.1$ md, $C_r=10$, $S_{wi}=0.4$, and $h = 25$ ft.

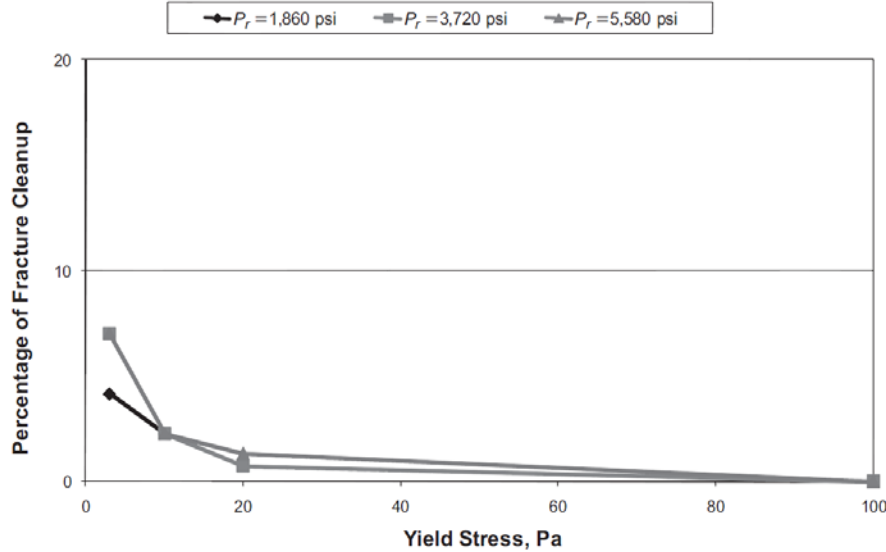


Figure 64— Percentage of fracture that cleans up 1 year after a fracture treatment vs. yield stress at different reservoir pressures, where $L_f = 528$ ft, $k = 0.1$ md, $C_r = 0.1$, $S_{wi}=0.4$, and $h = 25$ ft.

Note that in Figure 64, the cleanup even at low yield stress is low because the fracture is less conductive than the reservoir. In essence, instead of a high-permeability pathway, we

have a choke. In Figure 65, the fracture is 10 times more conductive than the reservoir, hence the better cleanup.

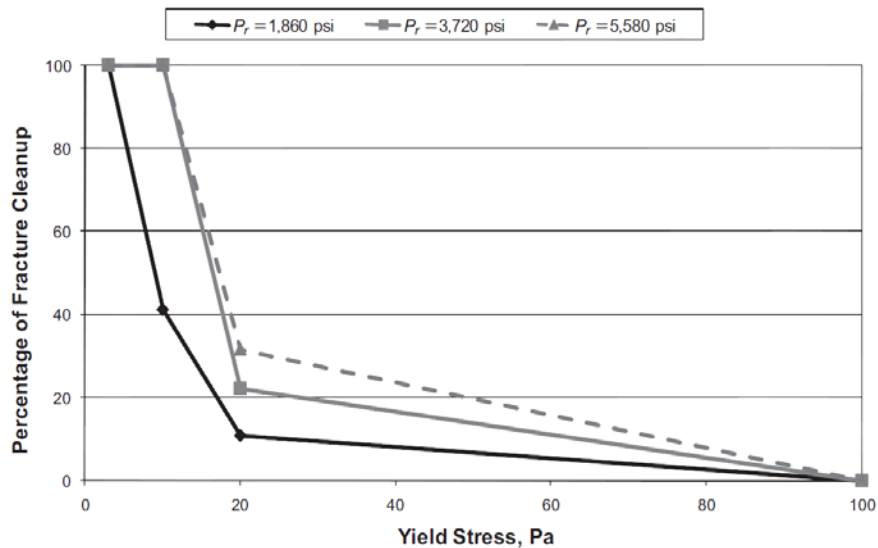


Figure 65— Percentage of fracture that cleans up 1 year after a fracture treatment vs. yield stress at different reservoir pressures, where $L_f = 528$ ft, $k = 0.1$ md, $C_r = 10$, $S_{wi} = 0.4$, and $h = 25$ ft.

D.1.6 Effect of Fracture Length

Applying a 30%-gas-saturation cutoff to simulation results, we determined the percentage of the fracture that has cleaned up 1 year after the treatment for each simulation run with gel damage. The percentage of fracture that cleans up is the ratio of effective-fracture length to propped-fracture length. In the cleaned up portion of the propped fracture, the gel has been recovered and gas is flowing. However, the remaining portion of the propped fracture length is still plugged by gel. It is difficult to find a physical reason for why the percent cleanup versus yield stress profile is different for each fracture length. The important issue however is to recognize that the percent cleanup decreases with increasing fracture length. This makes sense especially if the fracture does not have infinite conductivity.

Figure 63 shows the percentage of the fracture that cleans up vs. yield stress for different fracture lengths, where $p_r = 3,720$ psi, $k = 0.1$ md, $C_r = 10$, $S_{wi} = 0.4$, and $h = 25$ ft. Based on the percentage of fracture cleanup, the optimal fracture should be $L_f = 924$ ft for yield stress of 3 Pa, $L_f = 528$ for yield stress of 10 Pa, and $L_f = 264$ ft for yield stress of 20 Pa or more. If $C_r = 0.1$, the percentage cleaned up becomes lower. This means that

fracture-fluid cleanup is very important. If the fracture is not effectively cleaned up, the effort on fracture-treatment design and field operation is practically worthless. Ultimately, a fracture that is not effectively cleaned up will have poor dimensionless conductivity. The effect of poor dimensionless conductivity is to reduce the ultimate recovery from the reservoir system (see Figures 54, 57 and 60).

D.2 Modeling Flow of Herschel-Bulkley Fluid in Porous Media

D.2.1 Description of Geometry of the Computational Domain

To replicate the real porous structure, micro pore-scale modeling is applied to describe the computational domain. The micro pore-scale model consists of a pore which is surrounded by grains and connected to other pores. Geometry is established by GAMBIT, commercial software for generating geometry and mesh. A full numerical simulation for flow in a porous media including all proppants is impractical, because of computational capacity limits. The calculation region includes two half proppants in the Y and Z directions with ten proppants in the X direction. The computational domain also includes an entrance region and an exit region. The computational domain is shown in Figure 19. The packed bed is assumed to be periodic in the width direction.

D.2.2 Choosing the Optimal Grid Size

The unstructured grids are generated using GAMBIT. The sensitivity of the results to mesh resolution is examined to assure the accuracy of numerical simulation. Usually, using the smaller grid size in computational domain leads to better results, but might cause numerical instability and need more calculating time. We wanted to find a suitable grid size to save computational time, but also have exactly numerical results. So we compare the result from different grid sizes. The grid size in the x, y, and z-directions was decreased from 0.3 to 0.15mm, and the total grid number increased from approximately 350,000 to 1.5 million grids, as shown in **Table 31**. A diagram of the different grid elements on the proppant surface is shown in **Figure 66**. For pressure gradient, the numerical results using the grid size of 0.15 was approximately 1% higher than the grid size of 0.2, 2% higher than the grid size of 0.25 and 5% higher than grid size

of 0.3. The results show that there is minimal loss of accuracy resulting from the use of the larger grid sizes. The grid size of 0.2 has been chosen for all numerical simulations to keep a balance between numerical accuracy and computational cost. The computational result using grid size of 0.2 is acceptable and don't have any instability problem.

TABLE 31—MAXIMUM GRID EDGE SIZE AND TOTAL NUMBER OF GRIDS	
Maximum Grid Edge Size (mm)	Total Number of Grid
0.015	1529144
0.020	800284
0.025	517116
0.030	349712

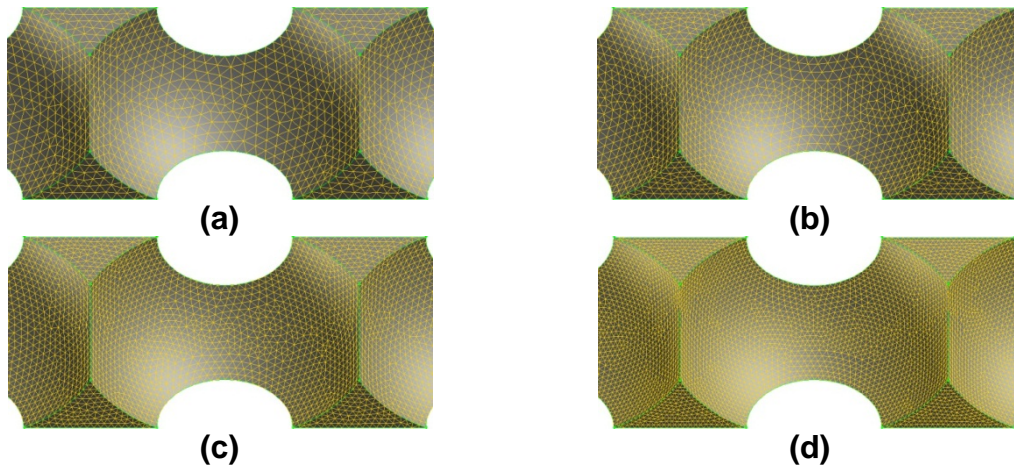


Figure 66—Representation of gridding on proppant surfaces using different grid sizes, grid size = 0.03mm (a). Grid size = 0.025mm (b). Grid size = 0.02mm (c). Grid size = 0.015mm (d).

D.2.3 Effect of the Yield Stress on the Pressure Gradient

From the numerical results, for a fluid that has yield stress, the value of apparent viscosity is infinite if the pressure gradient is less than a critical value. **Figure 67** plots the pressure gradient vs. velocity at different initial yield stress. As seen in Figure 67, the Bingham fluid can flow only after the pressure gradient exceeds a critical value. **Figure 68** reveals that the flow initiation pressure gradient increases linearly with the yield stress. The yield stress can influence the flow behavior of the non-Newtonian fluids in two ways. First, for fluids with yield stress, a certain critical pressure drop value needs to be exceeded for flow to be initiated. Second, for yield stress fluids, there is a plug flow

region of constant velocity in the center of flow channel. For Newtonian fluids, that don't have yield stress, the velocity profile is parabolic. So the yield stress reduces the mean velocity of non-Newtonian fluid in porous media. **Figure 69** shows the dimensionless velocity profile of the yield stress fluid in the pore throats of the porous pack. The yield stress has significant influence on the value of the critical pressure gradient required to initiate flow.

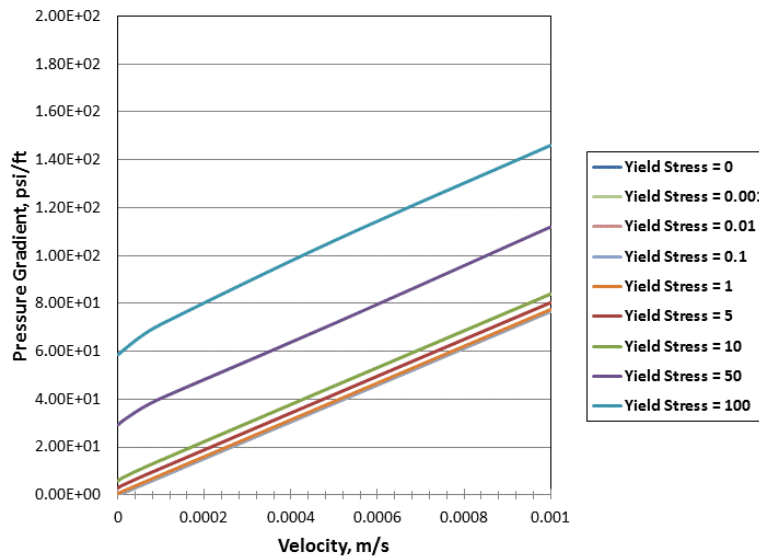


Figure 67—Pressure gradient vs. superficial velocity for Bingham fluids.

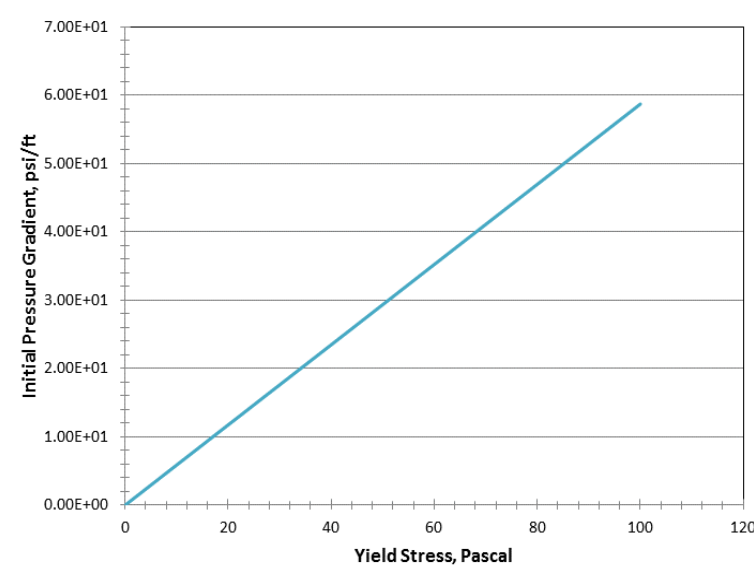


Figure 68—Flow initiation gradient vs. yield stress for Bingham fluids.

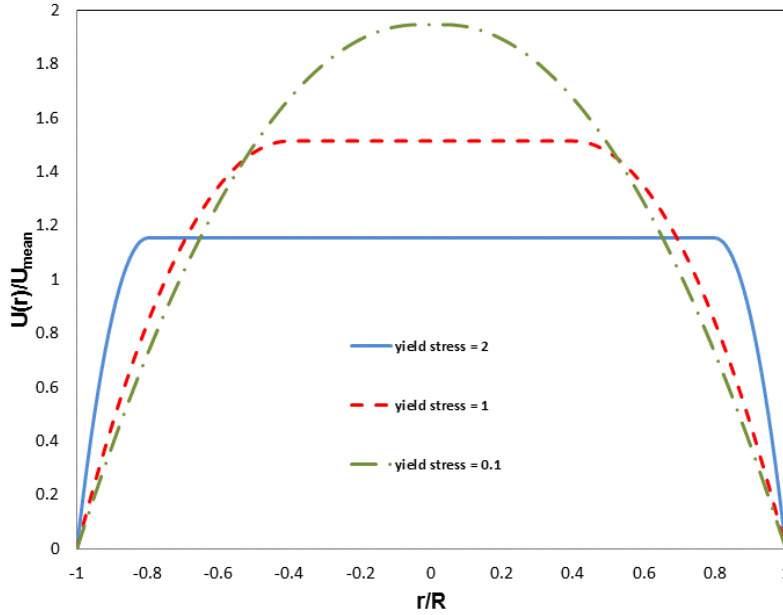


Figure 69— Dimensionless velocity profiles for the fluids with different yield stress.

D.2.4 Effect of the Power-Law Index

Figure 70 shows pressure gradient vs. Herschel-Bulkley fluid flow velocity at different power-law index. The power-law index has a significant impact on pressure gradient, especially at high superficial velocities. At high velocity, the shear-thickening fluids ($n > 1$) will cause an acute increase in pressure gradient. The interesting discovery is that the pressure gradient is inversely proportional to the power-law index at very low velocity, as shown in **Figure 71**. This can be explained from relationship for power-law fluid flow in porous media, shown below.

$$U_{Darcy} = \frac{1}{3 + \frac{1}{n}} \left(\frac{\Delta PR}{2cL} \right)^{\frac{1}{n}} R\Phi \quad (24)$$

where U_{Darcy} is the Darcy velocity in meters/second; n is the power-law index; ΔP is the pressure drop in Pa; R is the effective pore throat radius in meters; c is the consistency index; L is the pore throat length and Φ is porosity. At low superficial velocity, if the term $\left(\frac{\Delta PR}{2cL} \right)$ is smaller than 1, smaller n ($0.6 < n < 1.4$) leads to smaller value of the term $\left(\frac{\Delta PR}{2cL} \right)^{\frac{1}{n}}$. Therefore, for a fixed velocity at low value zone, the small power-law index n

needs a large pressure gradient. From Figures 70 and 71, it is observed that in pore throats, increasing power-law index sharpens the velocity profile and decreasing power-law index flattens the velocity profile.

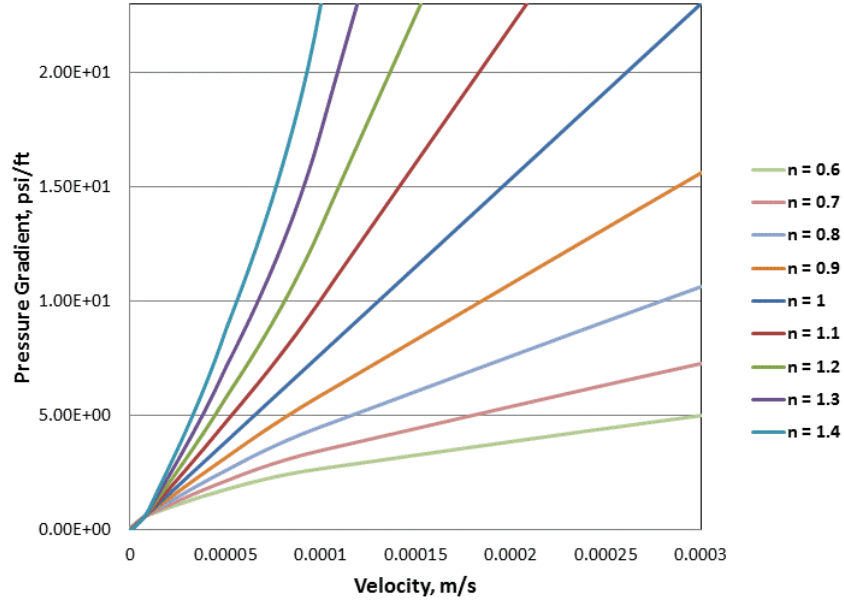


Figure 70— Pressure gradient vs. superficial velocity for power-law fluids at high velocities.

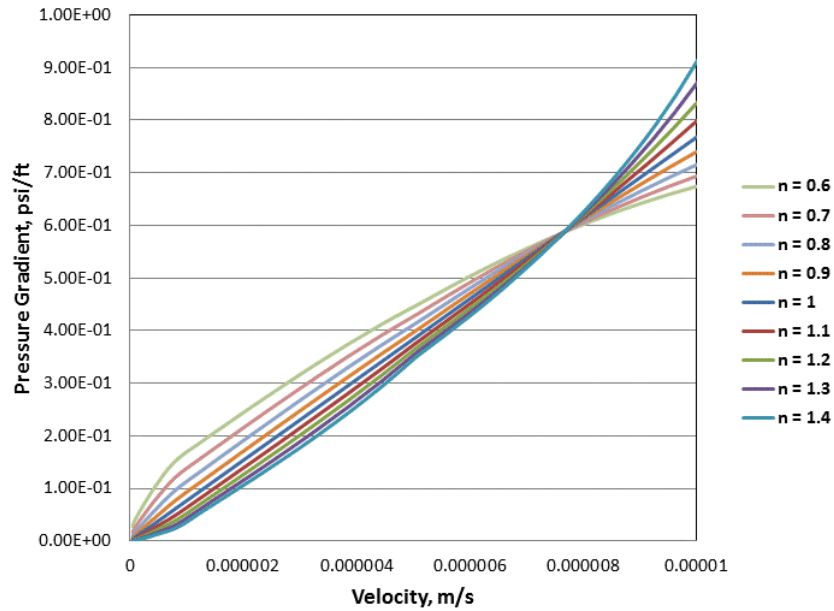


Figure 71— Pressure gradient vs. superficial velocity for power-law fluids at low velocities.

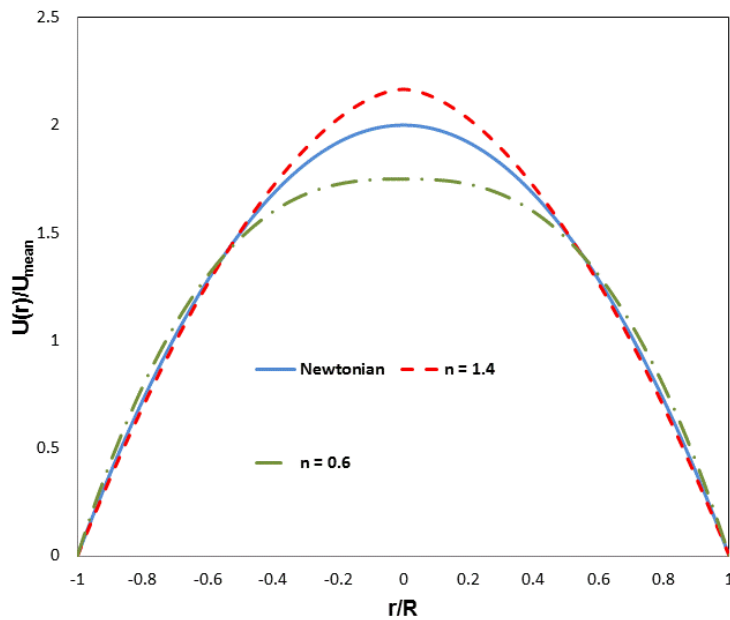


Figure 72— Dimensionless velocity profiles for power-law indices.

D.2.5 Effect of Proppant Diameter

The arrangement of the proppant pack in the present work is a simple cubic geometry. We considered the four typical values of mesh size, 20, 40, 70 and 100 mesh; and the corresponding proppant diameters are 0.84, 0.42, 0.21, 0.149 mm. **Figure 73** reveals that the proppant diameter has large influence on the permeability of the proppant pack. The permeability will be approximately multiplied by a factor of four, if the proppant diameter doubles. **Figure 74** shows the influence of flow initiation pressure gradient on yield stress of non-Newtonian fluid flowing in packs of varying proppant diameter. The result shows that the flow initiation pressure gradient has an inverse relationship with proppant diameter.

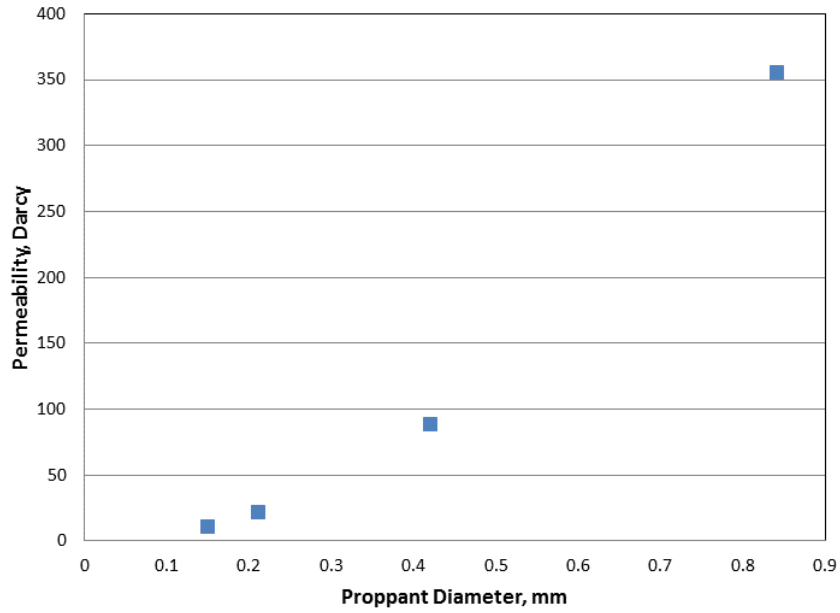


Figure 73—Permeability vs. Mesh Size.

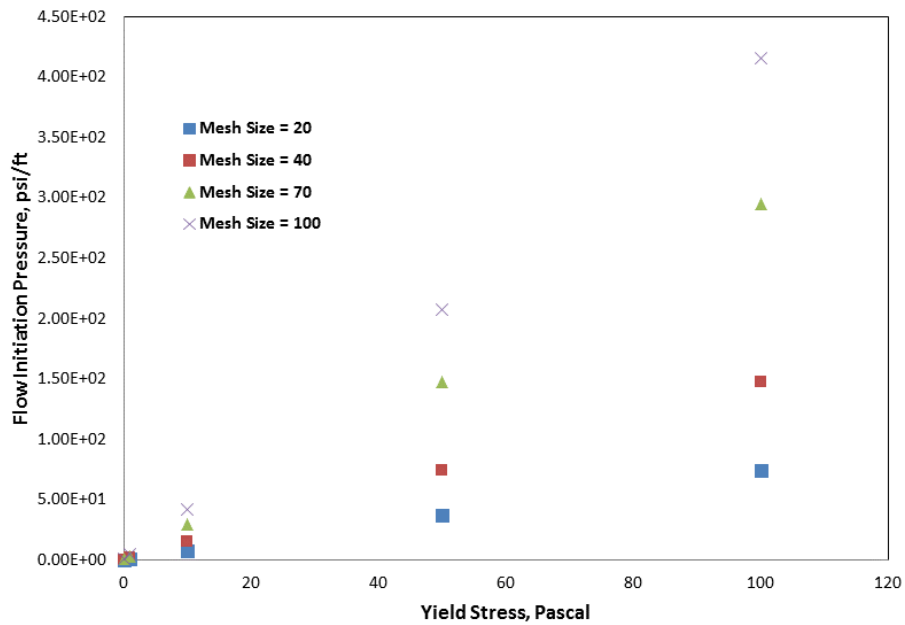


Figure 74— Flow initiation pressure gradient vs. yield stress for varying proppant mesh sizes.

E. Tight Gas Advisor for Completion and Stimulation

E.1 Background

In the literature, several authors have proposed various methods to mine and use published data to solve problems. Mohaghegh et al. (2003) proposed a two-level data-mining process. Level one is descriptive data-mining; that is an explanatory process, attempting to find high-impact parameters (HIP) mostly determining well performance. Second, his process searches for patterns existing among treatment parameters (stimulation fluid type, amount of proppant, injection pressure, etc.) and well/reservoir characteristics (saturation, depth, pressure, stresses, etc.) on one side and subsequent well performance on the other. Level two is a predictive process that is a consequent step, trying to make recommendations and forecasts based on the trends derived in the descriptive stage. Methods applied to extract practical knowledge from existing well and reservoir data varied from early 3-dimensional maps (Ameri et al. 1987) and combinations of generic algorithm and artificial neural network (Mohaghegh et al. 2000) to 3-dimensional, 3-phase reservoir simulators (Ederhard et al. 2000) and sophisticated fusion of forward selection and backward elimination and hard/fuzzy clustering (Mohaghegh et al. 2001). Also various approaches were proposed to control the quality of datasets and fix erroneous and missing data (Popa et al. 2003). Furthermore, Mohaghegh (2003) proposed to incorporate a data-driven model and expert knowledge into a comprehensive data-mining process. All the methods described above were built using sophisticated, statistical analysis of data collected during completion, stimulation and production. All of the analysis methods require large datasets and their optimization applicability is limited to the area where the data were collected. However, data in the public domain often do not contain the detailed information needed to do a data-driven analysis. Xiong et al. (1999) used published case histories where new and existing technologies were used successfully to complete and stimulate TGSs to develop a decision-making process. They studied the petroleum literature and interviewed experts to determine the high impact factors for well stimulation. Based on their findings, they developed an expert system, which is able to propose optimal detailed treatment design

based on input data. They found that a fuzzy logic system can be a suitable approach to capture the complexity of relations between the stimulation, reservoir parameters and subsequent well response (Xiong et al. 1994, 1995, 1996). We have used a similar approach to identify high impact factors using public domain and expert's opinions. Also, we have adopted some of the identified high impact factors and relations among them published by Xiong et al. (1999).

E.2 Approach

To place all the decision making steps in a logical order, we had to develop a workflow on how all decisions are made concerning the drilling, completion and stimulation of a well in a TGS reservoir (**Figure 75**). Using all available information about a well and a reservoir (input data), an engineer should be able to determine the volume of the total gas-in-place per layer and which layers can be produced economically. The engineer can then proceed to design a completion for the layers containing gas in commercial accumulation. On the left hand side of Figure 75, the size of the casing required for the subject well is evaluated on the basis of how we plan to complete the well. We have to consider the optimum choice for perforation, a diversion technique if multistage hydraulic fracture treatments are to be pumped. The diversion method and the perforation technique dictate the minimum production casing diameter. On the right hand side of Figure 75, we decide what size casing is required to accommodate the expected production rates from the well. In some cases, we will need large casing and tubing not to restrict very high flow rates. In other cases, we will need small tubing to continuously remove liquids from the wellbore. If artificial lift is planned, such as rod pumps or plunger lift, we need to design these systems ahead of time to know the optimum casing and tubing diameters to produce the well. Thus, we can compute another estimate of the production casing diameter, on the basis of our needs when producing the well once it is put to sales. An iteration process should be used to determine the smallest size casing that will be acceptable if conflicting values for optimal casing diameter are determined using the methods described in Figure 75. Once the production casing diameter satisfies both the completion and production purposes, the stimulation design is initiated. For a stimulation treatment, we will require a certain

minimum casing diameter, so we can pump the chosen fracture fluid at the chosen injection rate. As such, the iteration processes are required to determine optimal way to complete, stimulate and produce a TGS well. The last stage of the well design is a drilling design. We are using a modular architecture to program the software that we call TGS Advisor. Most modules are stand-alone subroutines programmed to provide advice in a limited domain, such as perforation design and proppant selection. We used the petroleum literature to determine the most important parameters for perforation design and proppant selection. We also looked for best-practices to discover correlations between reservoir properties and the best applicable technologies. When possible, we summarized our results graphically in decision charts, trying to capture the thought process of a subject matter expert making a decision. We sent our decision charts to experts and asked for their advice and suggestions. Then we programmed subroutines to automate the decision processes. The subroutines consider input well and reservoir parameters and give recommendations based on the decision charts and fuzzy logic models that were developed in this research.

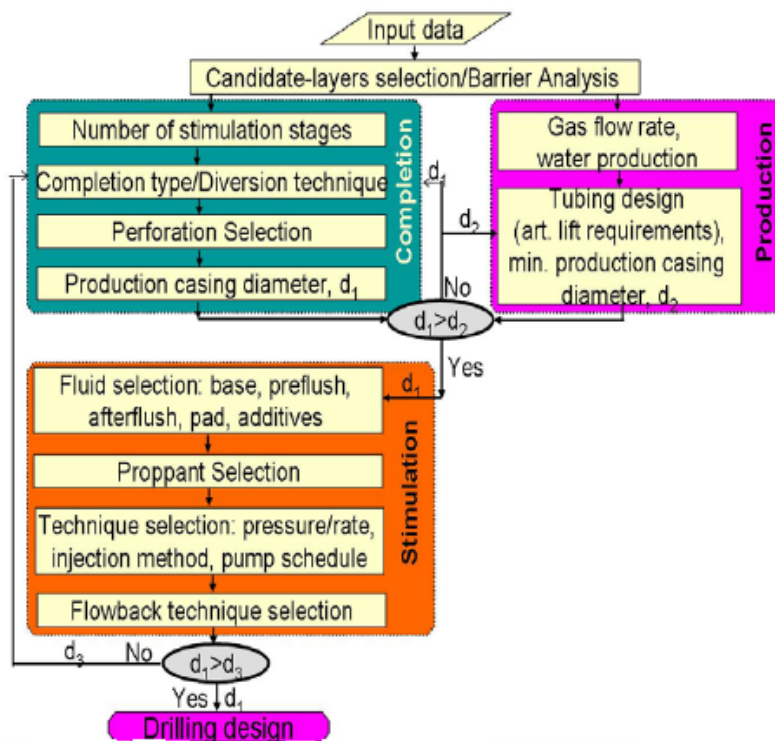


Figure 75—Major decision points in the completion and stimulation of tight gas sands. Every independent level requires making a critical decision that affects all levels below it.

E.3 Applications

The advisor described above has been applied in several field scenarios. A review of these scenarios can be found in the following publications: Holditch et al (2008) for perforation design and proppant selection, Wei et al. (2009a) for estimates of optimal fracture half-length, Wei et al. (2009b) for proppant selection, slurry pumping schedule and fracturing fluid selection and Wei et al. (2010) for production tubing and casing size determination. The tight gas sand advisor is one component in a suite of software applications called the Unconventional Gas Reservoir (UGR) advisory system (**Figure 76**).



Figure 76—Starting window for the UGR advisory system. Red arrow points to the TGS application.

E.4 Program Installation Instructions

1. Navigate to the UGR folder.
2. Click on the setup.exe executable and install program as an administrator.
3. Create folder C: \Windows\Microsoft
4. Modify permission for all users (give users permission to read, write and delete the created folder). All users on the machine will be able to run the software.
5. Navigate to the location of the UGR Express Panel icon and run the program.

F. Summary of Findings

This section will be organized in a similar fashion as the executive summary. The findings during this project are grouped under the following headings:

1. Yield stress and filter-cake investigations
2. Dynamic fracture conductivity investigations
3. Modeling of fracture fluid clean up in tight gas reservoirs
4. Modeling flow of Herschel-Bulkley fluids in proppant packs
5. Tight gas expert system

Yield stress and filter-cake investigations

- Concentrated guar polymer solutions, such as those in the filter cake created by leakoff from a fracture, exhibit a yield stress that increases with polymer concentration. A gel with concentration of 200 lbm/1,000 gal has a yield stress greater than 60 Pa with no breaker added.
- When sufficient breaker is added to the fracture fluid, the yield stress decreases to near zero.
- From measurements of the filter-cake thickness, gel concentrations ranging from 400 to 700 lbm/1,000 gal were created when filtrate leaked off from the fracture fluids.
- The filter cake thickness increases as leak off volume increases at various shear rates tested. However, it was found that at higher shear rates, filter cake thickness growth is slower. High shear rate impedes the growth of the filter cake as some of the polymer solids deposited are eroded. The relationship between filter cake thickness and leak off volume was found to be a quadratic.
- A model for the filter cake thickness and properties was developed and can be used in a reservoir simulation model to capture the effects of gel damage.
- The filter cake properties established for different pumping conditions can be used to design filter cake clean up by flowing back formation fluids at a shear

stress that exceeds the yield stress of the filter cake. A theoretical model developed was tested using water as the flow back fluids.

Dynamic fracture conductivity investigations

- Based on the log transformed dataset, the effects of investigated factors arranged in order of decreasing impact on conductivity are closure stress, polymer loading, flow back rate, presence of breaker, reservoir temperature and proppant concentration.
- In order to have a better understanding of the cleanup process in laboratory fractures, both displacement and evaporation processes need to be considered. We provided experimental support for this assertion by presenting data that showed the deleterious effect of increases in flow back rate on fracture conductivity. In the laboratory, aggressive cleanup schedules are seen not to be beneficial for fracture conductivity development. Whether this observation can be generalized to field scale hydraulic fractures will require more work. In the interim, if there is no compelling engineering reason for aggressive well cleanup schedules, it is advisable that flowback rates be limited to the critical value required to efficiently displace the broken polymer fluid from the fracture.
- At low proppant concentrations, we have presented evidence that channelized features are formed in proppant packs. Also, we have presented data to show that it is possible for the proppant concentrations in laboratory fractures to be in the partial mono-layer range. We think this is the reason why conductivities at low proppant concentrations (in the worst case scenario) are as good as those from multi-layer proppant packs.
- We also conducted an analysis using proppant concentration as a blocking variable. We concluded that at high proppant concentrations, the three most important effects are closure stress, nitrogen rate and temperature. This conclusion is similar to the conclusion reached if blocking was not applied. However, at proppant loadings of 0.5ppa, the polymer loading and the presence of breaker supplants nitrogen rate and temperature as the most important factor. This underlines the importance of effective breaker design especially in fracturing

operations with low proppant concentrations and also provides support for slickwater fracturing.

- At high temperatures and closure stresses, we presented physical evidence of the formation of a polymer-proppant cake that reduces conductivity development in laboratory fractures.

Modeling fracture clean up in tight gas reservoirs

Important factors affecting fracture-fluid cleanup have been identified, and a systematic investigation has been carried out by varying formation permeability, reservoir pressure, fracture length, fracture conductivity, flowing bottomhole pressure, and values for yield stress. The steps outlined in this paper provide an easy-to-follow procedure for any engineer to study fracture-fluid cleanup for water or gel fracturing in tight-gas wells. The main conclusions are as follows:

- Important factors affecting how a gas well will clean up after a fracture treatment are multiphase flow, fracture-proppant crushing, and gel remaining in the fracture that does not break back to small molecules resulting in a low viscosity.
- To properly analyze a well that has been fracture treated, one should measure not only everything that is pumped during the fracture treatment but also what is produced back after the treatment, including flowing pressures, gas-flow rates, water-flow rates, and polymer concentration in the produced water.
- To analyze post-fracture performance data correctly, one may need to use a multiphase reservoir model that is capable of simulating non-Newtonian flow behavior of the gel in the fracture after fracture closure.
- If the fracture fluid breaks down to a low viscosity and behaves as a Newtonian fluid, then a dimensionless fracture conductivity of 10 or greater is all that is required to optimize fracture-fluid cleanup and gas production.
- If the fracture fluid does not break completely and retains yield stress of 3–100 Pa, then fracture fluid will either clean up slowly or never clean up when the dimensionless fracture conductivity is 10 or less.
- We recommend that the industry design and begin using fracturing fluids that can degrade effectively, ideally to a Newtonian fluid, after the treatment so that

fractures can be cleaned up effectively and productivities of fractured wells can be optimized.

Modeling flow of Herschel-Bulkley fluids in proppant packs

- Non-Newtonian fluid flow in porous media was investigated numerically by solving the Navier-Stokes equation directly. In the present work, variable physical properties for non-Newtonian fluid and different proppant diameters are considered. The numerically predicted flow initiation pressure gradient rises rapidly with the increasing of the yield stress. The yield stress affects the Darcy velocity through two physical mechanisms. Compared with the shear-thinning fluid, the shear-thickening fluid requires much higher pressure gradient to attain the same Darcy velocity. Permeability has a quadratic relationship with proppant diameter, and the flow initiation pressure gradient is inversely proportional to proppant diameter. The pore scale study provides detailed observation of flow phenomenon and fundamental understanding of the mechanism of non-Newtonian fluid flow in porous media. We recommend that the influence of proppant arrangement on non-Newtonian fluid flow in porous media should be investigated in the future.

Tight Gas Expert System

- A combination of a fuzzy logic approach and an “IF-THEN” expert system methodology is an excellent way to program practical knowledge derived from critically evaluated publicly available data and information coupled with opinions from subject-matter experts. TGS Advisor can be developed into a permanent, practical, applicable depository of industry knowledge and experience.
- TGS Advisor produces consistent recommendations that should assist decision making while developing TGS reservoirs, as well as to facilitate development and improve the economics of developing TGS reservoirs.
- Using TGS Advisor to capture the best practices in completion and stimulation activities will be extremely useful for new frontier TGS developments and exploration wells, especially when an operator does not have much experience in the application of the technology.

- The recommendations from TGS Advisor as part of the initial version of the software can be further modified and improved with time as the operator gains more information, knowledge and experience in a particular basin, field or formation.
- Young engineers can derive benefits from using TGS Advisor, while they make completion and stimulation decisions. First, TGS Advisor should prevent inexperienced engineers from making unreasonable decisions and focuses them on a few potentially applicable solutions. Second, TGS Advisor can be used as a training tool to help inexperienced engineers.

G. Impact to Producers

The main goal of this work is to improve hydraulic fracturing practices in tight gas reservoirs. The central role of hydraulic fracturing in enabling economic production from unconventional gas reservoirs makes it clear that advances in the economic application of hydraulic fracturing will add substantial unconventional gas reserves to the nation's future gas supply. The focus on gel damage in this work in particular could have a major impact on gas reserves in tight gas reservoirs. When a substantial part of a hydraulic fracture remains plugged with unbroken gel, the effective length of the fracture is reduced. The small effective length of such a fracture in turn reduces the area drained by the well in a reasonable length of time, proportionately reducing recoverable reserves. The results from this project have underlined the importance of proper hydraulic fracturing process design to optimum productivity of a well drilled in a tight gas reservoir.

H. Technology Transfer Efforts

Technology transfer is an important component of this project. During the period of three years, we have used the conferences, workshops and publications to transfer the findings to the industry, and also to seek the comments, guidelines and recommendations from the industry. We have participated SPE ATCE, SPE Hydraulic Fracture Technology Conference and Crisman Research Institute review meeting every year, presented the results on these conferences. We also participated in RPSEA workshops in related subject areas, and presented the research progress at the workshops. These conferences and workshops made the technology transfer possible for the project. We have published several MS thesis/PhD dissertation works (Correa, 2010, Pieve La Rosa, 2010, Xu, 2010, Yango, 2011, Romero, 2012, Awoleke, 2012), and 4 SPE papers (Awoleke, Romero, Zhu and Hill, 2011, Ouyang, Yango, Zhu, and Hill, 2011, Xu, Wang, Hill, and Zhu, 2011, Cheng, Wu and Holditch, 2011).

I. Conclusions and Recommendations

Experimental and theoretical studies have been carried out to evaluate gel damage problem in tight gas sand fracturing. Yield stress measurements were made to relate the damage potential of fracturing fluids. Experiments to measure filter-cake thickness were carried out to develop correlations between filter-cake thickness and leak-off under both static and dynamic conditions. The analytical model developed for the displacement of gel/filter-cake at lab-scale was validated with experimental work. A systematic experimental investigation was completed to consider, in a holistic sense, the important parameters such as reservoir properties, fracture fluid/proppant characteristics, and operational considerations (proppant schedule and flow-back rate). The effect of two-phase flow, proppant crushing, gel damage, yield stress and fracture length on long term gas productivity was investigated using a 3-D, 3-phase reservoir simulator. Also, the flow of Herschel Bulkley fluids through a proppant pack was studied. Lastly, a tight gas advisor was developed to improve hydraulic fracture design practices.

All the studies agree that the yield stress of the broken fracture fluid is a key indicator of the optimal productivity or otherwise of a hydraulic fracture. It was noted that when breaker is added to the fracture fluid, the yield stress decreases to a near-zero value, hereby aiding cleanup. In static experiments, filter-cake thickness has a direct relationship with the leak-off volume. In dynamic experiments, the shear rate impedes the growth of the filter-cake and there is a quadratic relationship between the filter-cake thickness and leak-off volume.

Based on the log transformed dataset, the effects of investigated factors arranged in order of decreasing impact on conductivity are closure stress, polymer loading, flow back rate, presence of breaker, reservoir temperature and proppant concentration. Increases in closure stress, flow back rate, temperature and polymer loading were observed to have deleterious effects on fracture conductivity. In particular, at high closure stresses and high temperatures, fracture conductivity was severely reduced due to the formation of a dense proppant-polymer cake. Dehydration of the residual gel in the

fracture appears to cause severe damage to the proppant conductivity at higher temperatures. Also, at low proppant concentrations, there is the increased likelihood of the formation of channels resulting in high fracture conductivities.

Simulation runs made to test the important factors that affect cleanup in tight gas reservoirs reached similar conclusions regarding the high importance of proppant crushing (effect of closure stress) and gel damage. It was also concluded that if the fracture fluid does not break completely and retains yield stress of 3-100Pa, then the fracture fluid will either cleanup slowly or will never cleanup when the dimensionless fracture conductivity is 10 or less.

The advisory system developed in this project is a valuable reference for future fracturing design. With the information from extensive literature research and rich experiences from the PIs, the guideline from the advisory system will help to optimization fracture treatment in tight gas sand reservoirs.

References

- Aguirre-Torres, V., Perez-Trejo, M.E. 2007. Outliers and the Use of the Rank Transformation to Detect Active Effects in Unreplicated 2^f Experiments. *Communications in Statistics-Simulation and Computation* **30** (3): 637–663. <http://dx.doi.org/10.1081/SAC-100105084>
- Ameri, S., Aminian, K. and Yost II, A.B. 1987. Data Base for Eastern Gas-Bearing Formations: Development and Application. Paper SPE 17065 presented at the SPE Eastern Regional Meeting, Pittsburg, Pennsylvania, and 21-23 October. <http://dx.doi.org/10.2118/17065-MS>
- Awoleke, O.O., Romero, J., Zhu, D., and Hill, A.D. 2012. Experimental Investigation of Propped Fracture Conductivity in Tight Gas Reservoirs Using Factorial Design, Paper SPE 151963 presented at the SPE Hydraulic Fracturing Technology Conference, The Woodlands, Houston, Texas, 6–8 February. <http://dx.doi.org/10.2118/151963-MS>
- Ayoub, J.A., Hutchins, R.D., and van der Bas, F., et al. 2006. New Findings in Fracture Cleanup Change Common Industry Perceptions. Paper SPE 98746 presented at the International Symposium and Exhibition on Formation Damage Control, Lafayette, Louisiana, USA, 15–17 February. <http://dx.doi.org/10.2118/98746-MS>.
- Balhoff, M.T. 2005. Modeling the flow of non-Newtonian fluids in packed beds at the pore scale. PhD dissertation, Department of Chemical Engineering, Louisiana State University and Agricultural & Mechanical College, Baton Rouge, Louisiana (August 2005).
- Cheng, K., Wu, W., and Holditch, S.A. 2011. Integrated Management and Visualization of Unconventional Resource Evaluation Data. Paper SPE 143822 presented at SPE Digital Energy Conference Exhibition, 19-21 April 2011, The Woodlands, Texas, USA.
- Cooke, C.E. 1975. Effect of Fracturing Fluids on Fracture Conductivity. *SPE Journal of Petroleum Technology* 27 (10). <http://dx.doi.org/10.2118/5114-PA>
- Coulter, G., R., Benton, E., G., and Thomson, C., L. 2004. Water Fracs and Sand Quantity: A Barnett Shale Example. Paper SPE 90891 presented at the SPE Annual Technical Conference and Exhibition, Houston, Texas, 26-29 September. <http://dx.doi.org/10.2118/90891-MS>.
- Downs, J.D. 2009. Observations on Gas Permeability Measurements Under HPHT Conditions in Core Materials Exposed to Cesium Formate Brine. Paper SPE 121649 presented at the SPE European Formation Damage Conference, Scheveningen, The Netherlands, 27–29 May. DOI: 10.2118/121649.
- Eberhard, M. J., Mullen, M. J., Seal, C. A. et al. 2000. Integrated Field Study for Production Optimization: Johan Field – Sublette County, Wyoming. Paper SPE 59790 presented at the SPE/CERI Gas Technology Symposium, Calgary, Canada, 3-5 April. <http://dx.doi.org/10.2118/59790-MS>
- Grieser, B., Hobbs, J., Hunter, J. and Ables, J. 2003. The Rocket Science Behind Water Frac Design. Paper SPE 80933 presented at the SPE Production and Operations Symposium, Oklahoma City, OK, 23-25 March. <http://dx.doi.org/10.2118/80933-MS>
- Holditch, S. A. and Ely, J.: 1973. Successful Stimulation of Deep Wells Using High Proppant Concentrations. *J. Pet Tech* **25** (8): 959–964. SPE-4118-PA. <http://dx.doi.org/10.2118/4118-PA>.

- Holditch, S.A, Xiong, H., Rueda, J. *et al.* 1995. Using an Expert System to Select the Optimal Fracturing Fluid and Treatment Volume. Paper SPE 26188 presented at the SPE Gas Technology Symposium, Calgary, Canada, 14-17 November. <http://dx.doi.org/10.2118/26188-MS>.
- Holditch, S.A. and Bogatchev, K.Y. 2008. Developing Tight Gas Sand Adviser for Completion and Stimulation in Tight Gas Sand Reservoirs Worldwide. Paper SPE 114195 presented at the CIPC/SPE Gas Technology Symposium Joint Conference, Calgary, Alberta, Canada, 16-19 June. <http://dx.doi.org/10.2118/114195-MS>.
- Le, D., Mahadevan, J. 2011. Productivity Loss in Gas Wells Caused by Salt Deposition. *SPE J.* **16** (4): 908—920. SPE 132606-PA. DOI: 10.2118/132606-PA.
- Mahadevan, J., Sharma, M. 2005. Factors Affecting Cleanup of Water Blocks: A Laboratory Investigation. *SPE J.* **10** (3): 238—246. SPE 84216-PA. DOI: 10.2118/84216-PA.
- Marpaung, F., Chen, F., Pongthunya, P., Zhu, D., and Hill, A.D. 2008. Measurement of Gel Cleanup in a Propped Fracture With Dynamic Fracture Conductivity Experiments. Paper SPE 115653 presented at the SPE ATCE, Colorado, Denver, 21—24 September. <http://dx.doi.org/10.2118/115653-MS>.
- Mayerhofer, M. J., Richardson, M. F., Walker, R. N., Jr., Meehan, D. N., Oehler, M. W., and Browning, R. R., Jr. 1997. Proppants? We Don't Need No Proppants. Paper SPE 38611 presented at the SPE Annual Technical Conference and Exhibition, San Antonio, Texas, 5-8 October. <http://dx.doi.org/10.2118/38611-MS>.
- Mohaghegh, S., Revees, S. and Hill, D. 2000. Development of an Intelligent System Approach for Re-stimulation Candidate Selection. Paper SPE 59767 presented at the 2000 SPE/CERI Gas Technology Symposium, Calgary, Canada, 3-5 April. <http://dx.doi.org/10.2118/59767-MS>.
- Mohaghegh, S.D., Gaskari, R., Popa, A. *et al.* 2001. Identifying Best Practices in Hydraulic Fracturing Using Virtual Intelligence Techniques. Paper SPE 72385 presented at the SPE Eastern Regional Meeting, Canton, Ohio, 17-19 October. <http://dx.doi.org/10.2118/72385-MS>.
- Mohaghegh, S. D. 2003. Essential Components of an Integrated Data Mining Tool for the Oil & Gas Industry, With an Example Application in the DJ Basin. Paper SPE 84441 presented at the SPE Annual Technical Conference and Exhibition, Denver, 5-8 October. <http://dx.doi.org/10.2118/84441-MS>.
- Ouyang, L., Yango, T., Zhu, D., and Hill, A.D. 2011. Theoretical and Experimental Modeling of Residual Gel Filter Cake Displacement in Propped Fractures, Paper SPE 147692 presented at the SPE Annual Technical Conference and Exhibition, Denver, Colorado, 30 October–2 November. <http://dx.doi.org/10.2118/147692-MS>.
- Papanastasiou, T.C. 1987. Flow of materials with yield. *J. Rheol.*, 31:385-404.
- Popa, A.S., Mohaghegh, S.D., Gaskari, R. *et al.* 2003. Identification of Contaminated Data in Hydraulic Fracturing Databases: Application to the Codell Formation in the DJ Basin. Paper SPE 83446 presented at the SPE Western Regional/AAPG Pacific Section Joint Meeting, Long Beach, California, 19-24 May. <http://dx.doi.org/10.2118/83446-MS>.
- Walker, Ray N., Jr., Hunter, *et al.* 1998. Proppants, We Still Don't Need No Proppants – A Perspective of Several Operators. Paper SPE 49106 presented at the SPE Annual

- Technical Conference and Exhibition, New Orleans, La., 27-30 September. <http://dx.doi.org/10.2118/49106-MS>.
- Wang, Y. 2008. Simulation of Fracture Fluid Cleanup and Its Effect on Long-term Recovery in Tight Gas Reservoirs. PhD dissertation, Texas A&M University, College Station, Texas.
- Wang, Y., Holditch, S.A., and McVay, D.A. 2008. Simulation of Gel Damage on Fracture Fluid Cleanup and Long-Term Recovery in Tight Gas Reservoirs. Paper SPE 117444 presented at the SPE Eastern Regional/AAPG Eastern Section Joint Meeting, Pittsburgh, Pennsylvania, USA, 11–15 October. <http://dx.doi.org/10.2118/117444-MS>
- Wang, J.Y., Holditch, S., and McVay, D. 2010. Modeling Fracture-Fluid Cleanup in Tight-Gas Wells. *SPE Journal* **15** (3). <http://dx.doi.org/10.2118/119624-PA>
- Wu, C.F.J., Hamada, M. 2010. *Experiments: Planning, Analysis, and Parameter Design Optimization*, New York City: John Wiley & Sons, Inc.
- Wei, Y.N. and Holditch, S.A. 2009. Computing Estimated Values of Optimal Fracture Half Length in the Tight Gas Sand Advisor Program. Paper SPE 119374 presented at the SPE Hydraulic Fracturing Technology Conference, The Woodlands, Texas, 19-21 January. <http://dx.doi.org/10.2118/119374-MS>.
- Wei, Y. N., Cheng, K. and Holditch, S.A. 2009. Computing Estimated Values of Optimal Fracture Half Length in the Tight Gas Sand Advisor Program. Paper SPE 124323 presented at the SPE Annual Technical Conference and Exhibition, New Orleans, Louisiana, 4-7 October. <http://dx.doi.org/10.2118/124323-MS>.
- Wei, Y. N., Cheng, K., Jin, X. et al. 2010. Determining Production Casing and Tubing Size by Satisfying Completion Stimulation and Production Requirements for Tight Gas Sand Reservoirs. Paper SPE 132541 presented at the SPE Tight Gas Completions Conference, San Antonio, Texas, USA, 2-3 November. <http://dx.doi.org/10.2118/132541-MS>.
- Xiong, H. and Rahim, Z. 1999. Using Stimulation Expert System to Design Hydraulic Fracturing Treatments – Field Examples. Paper SPE 52223 presented at the SPE Mid-Continent Operations Symposium, Oklahoma City, Oklahoma, 28-31 March. <http://dx.doi.org/10.2118/52223-MS>.
- Xiong, H. and Holditch, S.A. 1995. An Investigation the Application of Fuzzy Logic to Well Application Treatment Design. *SPE Comp App* **7**(1):18-24. SPE-27672-PA. <http://dx.doi.org/10.2118/27672-PA>.
- Xiong, H., Rahim, Z., Holditch, S.A. et al. 1996. A New Approach to Develop Petroleum Engineering Software. Paper SPE 36000 presented at the 1996 Petroleum Computer Conference, Dallas, 2-5 June. <http://dx.doi.org/10.2118/36000-MS>
- Xu, B., Wang, L., Hill, A.D., Zhu, D. 2011. Experimental Evaluation of Guar Fracture Fluid Filter Cake Behavior. *SPE Prod & Oper* **26**(4): 381-387. SPE-140686-PA. <http://dx.doi.org/10.2118/140686-PA>.
- Yango, Takwe. 2011. Characterization of Filter Cake Buildup under Dynamic Fluid Loss Conditions. MS Thesis. Texas A&M University, College Station, Texas (December 2011).
- Zhu, L., Sun, N., Papadopoulos, K., and Kee, D.D. 2001. A Slotted Plate Device for Measuring Static Yield Stress *J. Rheol.* **45** (5): 1105–1122. <http://dx.doi.org/10.1122/1.1392299>.

APPENDIX A

PROCEDURE FOR USING LENTH'S TEST

1. Compute the initial standard error, s_0 .

$s_0 = 1.5 \times \text{median}$, where the median is defined as the unsigned values of all the effects.

2. Compute the pseudo-standard error, PSE.

$PSE = 1.5 \times \text{median}$, where the median is the median of the effects, excluding effects greater than $2.5s_0$.

3. Compute the test statistic using the following relationship:

$$t_{PSE,j} = \frac{\text{effect}_j}{PSE}$$

where j is the number of factorial effects.

4. Look up the critical value in the table for critical values for the Lenth's method (Wu and Hamada 2010).
5. An effect is deemed significant if the $t_{PSE,j}$ value exceeds the critical value determined in step 4 for a given number of compared effects and level of significance, α .

APPENDIX B

INTERACTION EFFECTS—LOGARTHMIC TRANSFORMED DATA

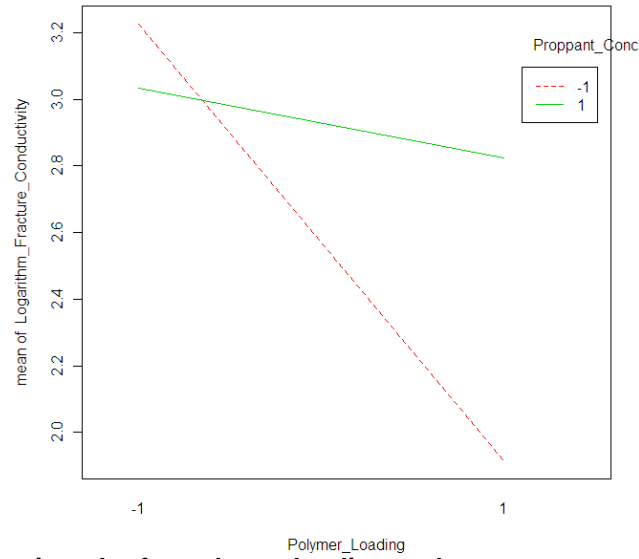


Figure A.1—Interaction plot for polymer loading and proppant concentration. The lines cross and this implies significant interaction between these two factors.

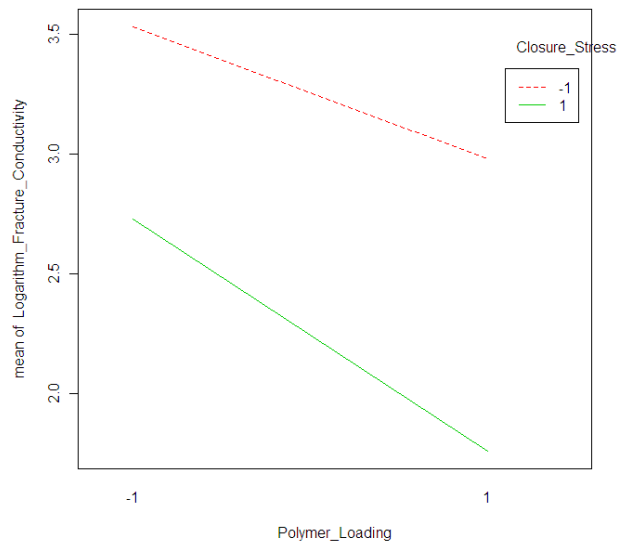


Figure A.2—Interaction plot for polymer loading and closure stress.

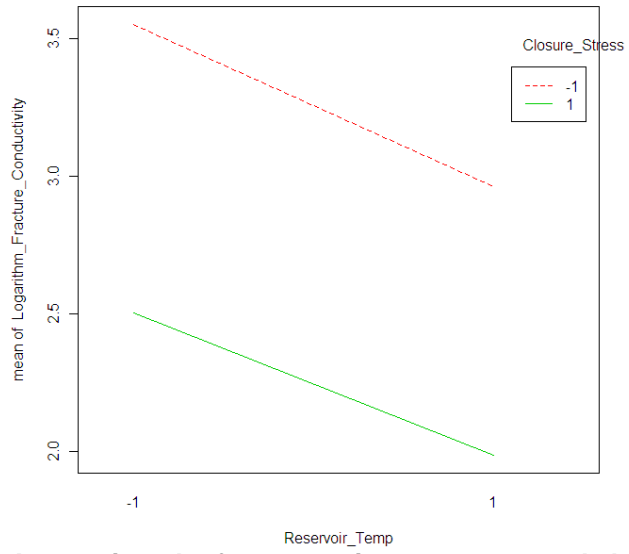


Figure A.3—Interaction plot for reservoir temperature and closure stress.

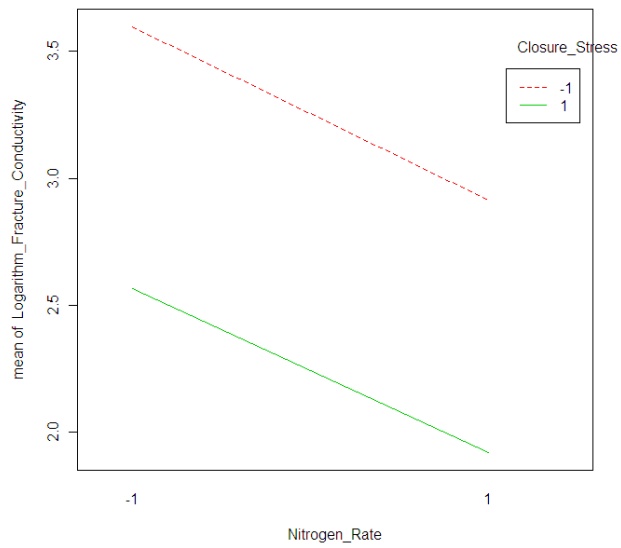


Figure A.4—Interaction plot for nitrogen rate and closure stress.

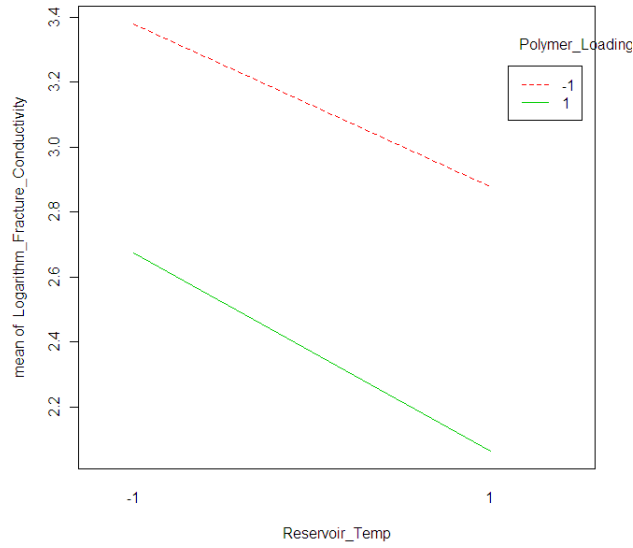


Figure A.5—Interaction plot for reservoir temperature and polymer loading.

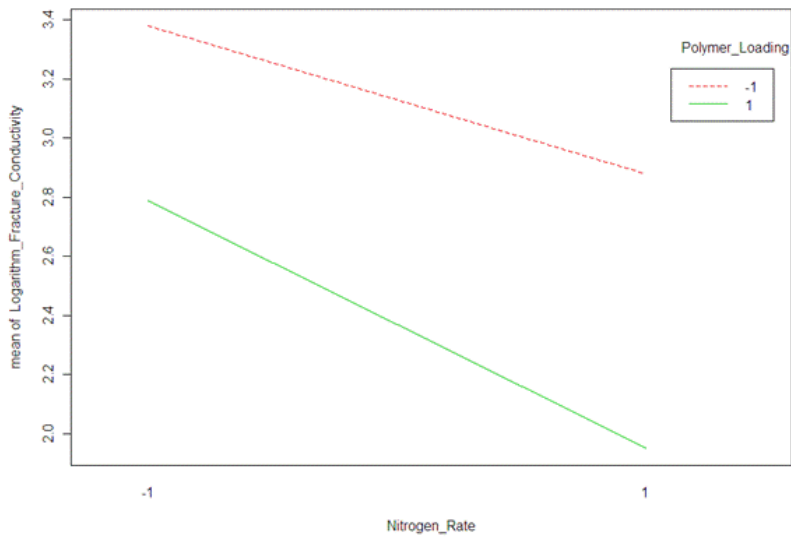


Figure A.6—Interaction plot for nitrogen rate and polymer loading.

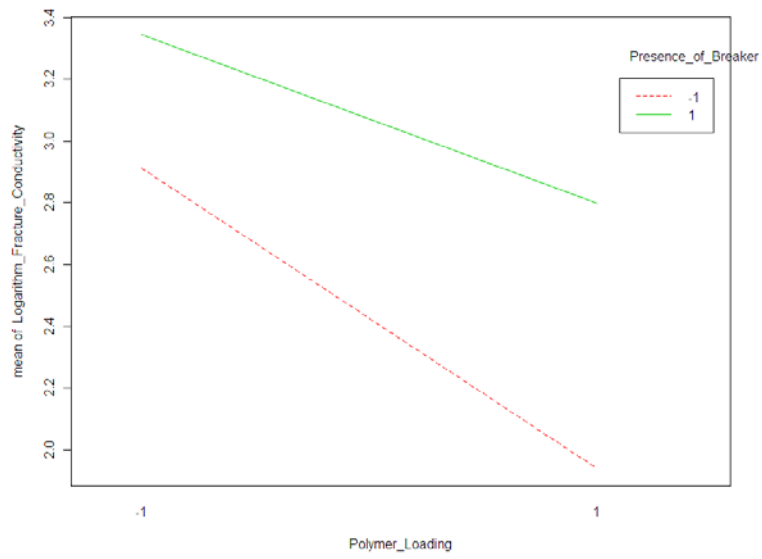


Figure A.7—Interaction plot for polymer loading and the presence of breaker.